


Summer 1-1-2017

Modeling the Binding of Neurotransmitter Transporter Inhibitors with Molecular Dynamics and Free Energy Calculations

Bernandie Jean
Duquesne University

Follow this and additional works at: <https://dsc.duq.edu/etd>

 Part of the [Biophysics Commons](#), and the [Other Biochemistry, Biophysics, and Structural Biology Commons](#)

Recommended Citation

Jean, B. (2017). Modeling the Binding of Neurotransmitter Transporter Inhibitors with Molecular Dynamics and Free Energy Calculations (Doctoral dissertation, Duquesne University). Retrieved from <https://dsc.duq.edu/etd/240>

This One-year Embargo is brought to you for free and open access by Duquesne Scholarship Collection. It has been accepted for inclusion in Electronic Theses and Dissertations by an authorized administrator of Duquesne Scholarship Collection. For more information, please contact phillipsg@duq.edu.

MODELING THE BINDING OF NEUROTRANSMITTER TRANSPORTER
INHIBITORS WITH MOLECULAR DYNAMICS AND FREE ENERGY
CALCULATIONS

A Dissertation

Submitted to the Bayer School of Natural and Environmental Sciences

Duquesne University

In partial fulfillment of the requirements for
the degree of Doctor of Philosophy

By

Bernandie Jean

August 2017

Copyright by
Bernandie Jean

2017

MODELING THE BINDING OF NEUROTRANSMITTER TRANSPORTER
INHIBITORS WITH MOLECULAR DYNAMICS AND FREE ENERGY
CALCULATIONS

By

Bernandie Jean

Approved April 18, 2017

Jeffrey D. Evanseck, Ph.D.
Professor of Chemistry
(Committee Chair)

Michael Cascio, Ph.D.
Associate Professor of Chemistry
(Committee Member)

M. Rita Mihailescu, Ph.D.
Professor of Chemistry
(Committee Member)

Christopher K. Surratt, Ph.D.
Professor of Pharmacology
Mylan School of Pharmacy
(Outside Reader)

Robert B. Lettan II, Ph.D.
Associate Professor of Chemistry
Chatham University
(Outside Reader)

Ellen Gawalt, Ph.D.
Chair, Department of Chemistry
Professor of Chemistry

Phillip P. Reeder, Ph.D.
Dean, Bayer School of Natural and
Environmental Sciences

ABSTRACT

MODELING THE BINDING OF NEUROTRANSMITTER TRANSPORTER INHIBITORS WITH MOLECULAR DYNAMICS AND FREE ENERGY CALCULATIONS

By

Bernandie Jean

August 2017

Dissertation supervised by Jeffrey D. Madura

The monoamine transporter (MAT) proteins responsible for the reuptake of the neurotransmitter substrates, dopamine, serotonin, and norepinephrine, are drug targets for the treatment of psychiatric disorders including depression, anxiety, and attention deficit hyperactivity disorder. Small molecules that inhibit these proteins can serve as useful therapeutic agents. However, some dopamine transporter (DAT) inhibitors, such as cocaine and methamphetamine, are highly addictive and abusable. Efforts have been made to develop small molecules that will inhibit the transporters and elucidate specific binding site interactions. This work provides knowledge of molecular interactions associated with MAT inhibitors by offering an atomistic perspective that can guide designs of new pharmacotherapeutics with enhanced activity.

The work described herein evaluates intermolecular interactions using computational methods to reveal the mechanistic detail of inhibitors binding in the DAT. Because cocaine recognizes the extracellular-facing or outward-facing (OF) DAT conformation and benztropine recognizes the intracellular-facing or inward-facing (IF) conformation, it was postulated that behaviorally “typical” (abusable, locomotor psychostimulant) inhibitors stabilize the OF DAT and “atypical” (little or no abuse potential) inhibitors favor IF DAT. Indeed, behaviorally-atypical cocaine analogs have now been shown to prefer the OF DAT conformation. Specifically, the binding interactions of two cocaine analogs, LX10 and LX11, were studied in the OF DAT using molecular dynamics simulations. LX11 was able to interact with residues of transmembrane helix 8 and bind in a fashion that allowed for hydration of the primary binding site (S1) from the intracellular space, thus impacting the intracellular interaction network capable of regulating conformational transitions in DAT.

Additionally, a novel serotonin transporter (SERT) inhibitor previously discovered through virtual screening at the SERT secondary binding site (S2) was studied. Intermolecular interactions between SM11 and SERT have been assessed using binding free energy calculations to predict the ligand-binding site and optimize ligand-binding interactions. Results indicate the addition of atoms to the 4-chlorobenzyl moiety were most energetically favorable.

The simulations carried out in DAT and SERT were supported by experimental results. Furthermore, the co-crystal structures of DAT and SERT share similar ligand-binding interactions with the homology models used in this study.

DEDICATION

I dedicate this work to my mother, Lise, whose unconditional love and support made it possible for me to pursue my doctoral degree. I also dedicate this work to my late research advisor, Dr. Jeffry D. Madura, who passed away unexpectedly on March 14, 2017. Thank you for encouraging me to reach for the stars.

ACKNOWLEDGEMENT

Thank you to everyone who helped to guide me through my education and made this research possible. I would like to thank Dr. Jeffrey D. Madura for accepting me into his computational research group and challenging me to reach my fullest potential in both my education and research. I am grateful for all that I was able to learn from him and am saddened that we will no longer have the opportunity to engage in thought-provoking scientific discussions. Dr. Madura was an excellent mentor who trained me to be independent and critical in my scientific approach, and he was determined to push me to be the best scientist I could be, and for that, I am forever grateful. My thanks will never be sufficient enough for his efforts.

I would like to extend my deepest gratitude to Dr. Christopher K. Surratt. From the beginning of my graduate career, Dr. Surratt has been a mentor and a friend. Thank you for training me and allowing me to work in your lab. I cannot thank you enough for your patience and support. I would like to express my appreciation to Drs. Jeffrey D. Evanseck and Ralph A. Wheeler for offering insightful suggestions to advance my research in our joint group meetings. I am much obliged to Dr. Jeffrey D. Evanseck for advising me through the final weeks of my graduate studies. I am thankful to my dissertation committee members, Drs. Michael Cascio, and Mihaela-Rita Mihailescu, for their assistance and encouragement. Special thanks to Dr. Robert B. Lettan II for synthesizing the SM11 analogs used in this project. I would also like to acknowledge Drs. Jonathan L. Katz and Weimin C. Hong for helpful discussions on DAT-inhibitor complexes.

To my current and past lab members, Riley Workman, Emily Benner, Matt Srnec, Mike Wasko, Kendy Pellegrine, and Drs. Kalyan Immadisetty and Tammy Nolan. I appreciate all the opportunities we had to have helpful scientific discussions. I thank you all for patiently listening to my research presentations and offering your valuable advice. Special thanks to Scott Boesch for maintaining the computational resources utilized in this project. Thank you to the faculty in the Department of Chemistry and Biochemistry, the administrative staff, especially Amy Stroyne, and Margaret Cowburn, academic advisor Heather Costello, Dean of BSNES Dr. Philip Reeder, and Assistant Dean Dr. Phillip D. Palmer. Thank you to the Duquesne University, Department of Chemistry and Biochemistry and the Center for Computational Sciences, and the Bayer School for Natural and Environmental Sciences for giving me this incredible opportunity to pursue my graduate studies. Thank you to the Chuck Cooper Foundation for their financial support in academic scholarships from 2014 to 2017.

I would like to give special thanks to my dear friend and mentor, Jefry Rosmarin. Indeed, I would not have completed this journey if not for the unconditional love and support of my family and most beloved friends. Though I was far from home, they were never far from my heart.

TABLE OF CONTENTS

	Page
Abstract.....	iv
Dedication.....	vi
Acknowledgement	vii
List of Tables	xii
List of Figures.....	xiii
List of Abbreviations	xvi
CHAPTER 1	1
ROLE OF MONOAMINE TRANSPORTERS	1
1.1 Neurotransmitter transporters as therapeutic targets	1
1.2 Computational study of DAT and SERT inhibitor binding.....	8
1.2.1 Modeling the binding of DAT inhibitors.....	8
1.2.2 Lead optimization of a novel SERT inhibitor	11
1.3 Computational methods for studying inhibitor binding.....	13
1.3.1 Binding free energy calculations	15
1.4 Conclusions	28
1.5 References	29
CHAPTER 2	42
METHODS	42
2.1 Modeling the binding of DAT inhibitors.....	42
2.1.1 DAT homology models.....	42
2.1.2 System preparation and simulation details	43
2.1.3 Solvent accessibility surface area analysis.....	45

2.2	Lead optimization of a SERT inhibitor.....	46
2.2.1	Relative free energy calculations of ethane to methanol.....	46
2.2.2	Free energy calculation of T4 lysozyme to FK5	48
2.2.3	Free energy calculation of LeuT substrates.....	51
2.2.4	Free energy calculation of fluoxetine in SERT	54
2.2.5	Free energy calculation of SM11 in SERT.....	57
2.2.6	Measuring the affinity of SERT inhibitors.....	62
2.3	References	64
CHAPTER 3		68
MODELING THE BINDING OF DAT INHIBITORS IN DISCRETE DAT CONFORMATIONS		68
3.1	Introduction	68
3.2	Results and Discussion	70
3.3	Conclusions	93
3.4	References	95
CHAPTER 4		97
LEAD OPTIMIZATION OF A NOVEL SERT INHIBITOR		97
4.1	Introduction	97
4.2	Results and Discussion	100
4.2.1	Validating the free energy calculations	100
4.2.2	Determining the SERT SM11 binding site.....	104
4.2.3	Measuring affinity of SERT inhibitors.....	106
4.2.4	Relative binding free energy calculations of SM11 analogs	108
4.3	Conclusions	115

4.4	References	116
CHAPTER 5	120
FUTURE DIRECTIONS	120
5.1	Modeling the binding of DAT inhibitors.....	120
5.2	Lead optimization of a SERT inhibitor.....	122
5.3	References	126

LIST OF TABLES

	Page
Table 3.1: DAT affinity for cocaine and two 3 β -aryltropane analogs.....	70
Table 4.1: ABFE calculations of T4 lysozyme bound to FK5.....	102
Table 4.2: ABFE calculations of leucine in LeuT	103
Table 4.3: ABFE calculations of R-fluoxetine in the S2 binding site in SERT.....	104
Table 4.4: ABFE calculations of SM11 in the S1 binding site in SERT	105
Table 4.5: ABFE calculations of SM11 in the S2 binding site in SERT	105
Table 4.6: RBEF results of SM11 analogs in SERT	111

LIST OF FIGURES

	Page
Figure 1.1: Mechanism of action of monoamine neurotransmitters	2
Figure 1.2: The tertiary structure of monoamine transporters (MAT) protein	4
Figure 1.3: Alternating access mechanism of substrate transport	6
Figure 1.4: DAT inhibitors, cocaine (COC) and benztropine (BZT)	9
Figure 1.5: The extracellular-facing and intracellular-facing MAT	10
Figure 1.6: Structures of DAT inhibitors, LX10 and LX11	11
Figure 1.7: Hypothesized interactions of SM11 in the S2 site of SERT	12
Figure 1.8: Structure-based drug design scheme of a hit-to-lead compound	13
Figure 1.9: Forming a protein and ligand complex	16
Figure 1.10: Alchemical transformation as a function of the coupling parameter (λ).....	17
Figure 1.11: Gibbs binding free energy calculation: the relative binding free energy (RBFEE) change.....	20
Figure 1.12: Gibbs binding free energy calculation: the absolute binding free energy (ABFE).....	22
Figure 1.13: Geometric restraints applied to the ligand with respect to the protein.....	24
Figure 2.1: Alchemical transformation of ethane to methanol	47
Figure 2.2: Structure of K506 (FK5) ligand from PDB entry 1FKJ	49
Figure 2.3: Reference frame defining the binding of leucine in LeuT	53
Figure 2.4: Binding interactions of R-fluoxetine within the S2 binding site of SERT....	55
Figure 2.5: SM11 in S2 of SERT overlapped with S-citalopram in SERT co-crystal	58
Figure 2.6: SM11 in S1 of SERT.....	59

Figure 2.7: Groups of atoms to define the reference frame of SM11 to SERT	61
Figure 3.1: The OF DAT and IF DAT structures	69
Figure 3.2: The Drosophila DAT superposed with the rat DAT homology model	71
Figure 3.3: RMSD measured for each DAT-inhibitor system after 100 ns MD	73
Figure 3.4: RMSF measured for C α of DAT inhibitor-bound OF and IF DAT	74
Figure 3.5: Distances measured for D79 and Y156 for the OF and IF DAT.....	75
Figure 3.6: Water molecules within the outer and inner cavities of OF and IF DAT	76
Figure 3.7: Distances measured for the external and internal gate residue pairs.....	78
Figure 3.8: SASA measurements for OF DAT and IF DAT	80
Figure 3.9: LX10 and LX11 in OF DAT	82
Figure 3.10: Inner gate R60-D435 disposition in the OF DAT-LX10 bound system	83
Figure 3.11: The number of water molecules analyzed in OF and IF DAT	84
Figure 3.12: Intracellular interaction network in OF DAT.....	86
Figure 3.13: Comparison of cocaine binding in OF DAT to LX10 and LX11.....	89
Figure 3.14: Comparison of OF APO DAT superposed with inhibitor-bound OF DAT	91
Figure 3.15: Binding site interactions in OF DAT superposed with IF DAT.	92
Figure 4.1: Schematic representation of SM11 binding in SERT	99
Figure 4.2: Free energy change for the transformation of ethane to methanol.....	101
Figure 4.3: Competitive membrane binding assay of citalopram in SERT	106
Figure 4.4: Competitive membrane binding assay of SM11 in SERT	107
Figure 4.5: 2D ligand interaction map of SM11 in SERT S2 binding site	108
Figure 4.6: SM11 analogs in the S2 binding site of SERT	109
Figure 4.7: Modifications proposed for the 4-chlorobenzyl moiety of SM11.....	110

Figure 4.8: Modeling the binding of BJ11 in SERT	112
Figure 4.9: Binding site interactions with BJ12 in the SERT S2 binding site.....	113
Figure 4.10: Binding site interactions with BJ13 in the SERT S2 binding site.....	114
Figure 4.11: Binding site interactions with BJ14 in the SERT S2 binding site.....	115
Figure 5.1: 2-substituted aryltropane cocaine analogs.....	121
Figure 5.2: Proposed modifications to SM11 for future analogs.....	124

LIST OF ABBREVIATIONS

5-HT serotonin

ABFE absolute binding free energy

APO apoprotein

BAR Bennett acceptance ratio

BZT benztropine

CGenFF CHARMM General Force Field

CHARMM Chemistry at HARvard Macromolecular Mechanics

CNS central nervous system

COC cocaine

COMT catechol-o-methyltransferase

DA dopamine

DAT dopamine transporter

dDAT *Drosophila melanogaster* dopamine transporter

FEP free energy perturbation

fs femtosecond

GCMC grand canonical Monte Carlo

HEK Human embryonic kidney

hSERT human serotonin transporter

IF inward-facing

LeuT leucine transporter

LeuT_{Aa} *Aquifex aeolicus* leucine transporter

LX10 2 β -Ph₂-COCH₂-3 β -4-Cl-Ph cocaine analog

LX11 2 α -Ph₂-COCH₂-3 β -4-Cl-Ph cocaine analog

MAO monoamine oxidase

MAT monoamine transporter

MD molecular dynamics

MOE Molecular Operating Environment

NAMD Nanoscale Molecular Dynamics

NE norepinephrine

NET norepinephrine transporter

NPT isobaric-isothermal

ns nanosecond

NSS neurotransmitter sodium symporters

OF outward-facing

PBC periodic boundary conditions

PDB Protein Data Bank

PME particle mesh Ewald

PMF potential of mean force

ps picosecond

RMSD root-mean-square deviation

RMSF root-mean-square fluctuation

SBP solvent boundary potential

SERT serotonin transporter

SLC6 solute carrier 6

SM11 6-((4-(4-chlorobenzyl)piperazin-1-yl)methyl)-1,3,5-triazine-2,4-diamine

SNRI Serotonin norepinephrine reuptake inhibitor

SSBP spherical solvent boundary potential

SSRI selective serotonin reuptake inhibitor

TCA tricyclic antidepressant

TI thermodynamic integration

TM transmembrane

US umbrella sampling

WHAM weighted histogram analysis method

XSEDE Extreme Science and Engineering Discovery Environment

CHAPTER 1

1 ROLE OF MONOAMINE TRANSPORTERS

1.1 Neurotransmitter transporters as therapeutic targets

The serotonin transporter (SERT), dopamine transporter (DAT) and norepinephrine transporter (NET) exist as integral membrane proteins that belong to the family of neurotransmitter sodium symporters (NSS).¹ These monoamine transporters (MATs) and other members of the solute carrier 6 (SLC6) transporter family are characterized by the Na⁺-dependent symport of their native substrates along with Cl⁻ across a biomembrane.²⁻⁷ MATs are regulated through several signal transduction mechanisms to maintain appropriate levels of neurotransmitter in the synaptic cleft (**Figure 1.1**).⁸ During signaling, the neurotransmitter is released into the synaptic cleft and binds to receptors found on the post-synaptic membrane. Following neurotransmission, the neurotransmitters are trafficked into the neuron via the transporters (**Figure 1.1**).⁹ MATs are also recognized for their role as therapeutic targets for treating neurologic disorders, including depression, anxiety, and attention deficit hyperactivity disorder (ADHD), and in the abuse of psychostimulants.⁹⁻¹² Specific inhibitors for these transporters exert their physiological effects by interfering with synaptic uptake and thus prolonging the actions of the monoamine.² The small molecules that inhibit these proteins can serve as useful and effective therapeutic agents; however, some inhibitors are highly addictive and possess an abuse potential, such as cocaine and amphetamine derivatives.¹³⁻¹⁵

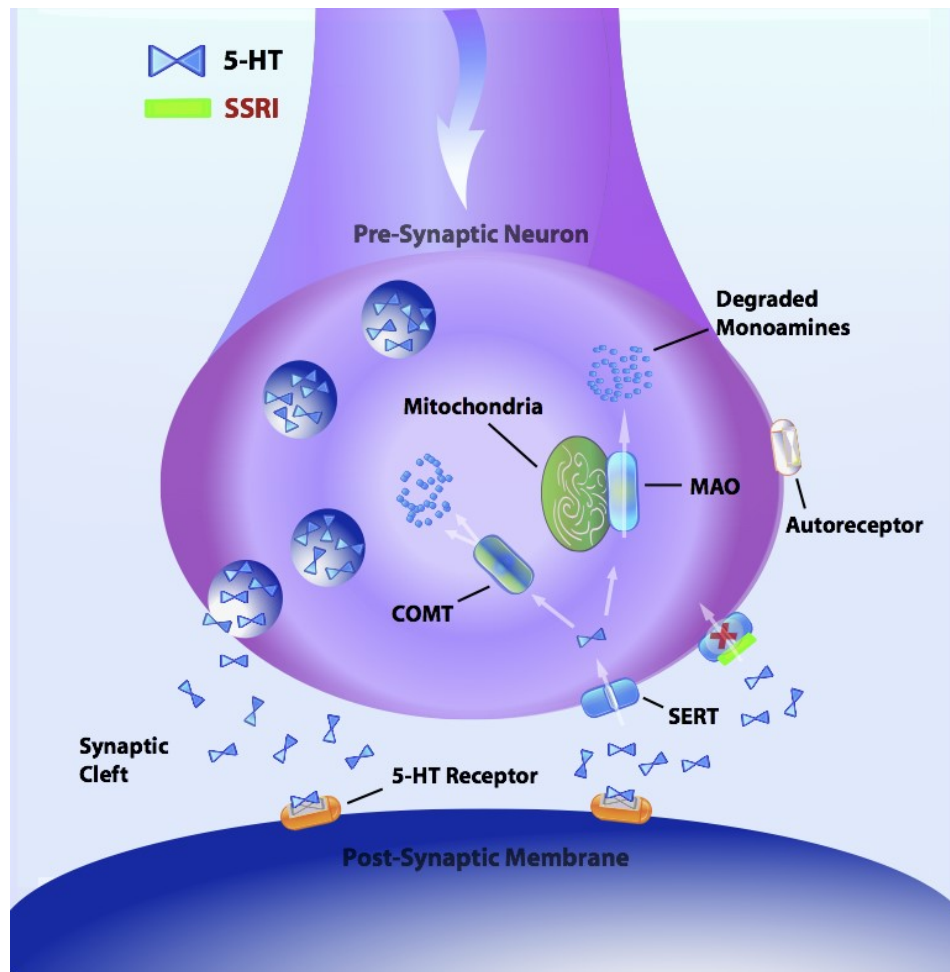


Figure 1.1: Mechanism of action of monoamine neurotransmitters.^{4, 7, 16} Signal propagated through pre-synaptic neuron allow for the release of neurotransmitter to synaptic cleft. The neurotransmitters are able to interact with post-synaptic receptors to continue chemical signaling. The transporter proteins located on the pre-synaptic membrane are responsible for the reuptake of the neurotransmitters into the pre-synaptic neuron. The serotonin (5-HT) transporter (SERT), dopamine transporter (DAT), and norepinephrine transporter (NET) are responsible for maintaining synaptic levels of neurotransmitters. Such inhibitors are capable of inhibiting the transporter proteins and preventing the reuptake of neurotransmitters. The pre-synaptic monoamine oxidase (MAO) and catechol-o-methyltransferase (COMT) are enzymes that degrade the monoamine neurotransmitters.

Most antidepressant medications currently prescribed for treating clinical depression are inhibitors of SERT. These inhibitors belong to the tricyclic amine (TCA) and selective serotonin reuptake inhibitor (SSRI) classes of antidepressants.¹¹ Molecules

that can selectively interact with two or more transporters and selectively interact with 5-HT receptors are of interest to improve the effectiveness of antidepressants and reduce the side effects.¹⁷⁻²² Adverse side effects may include sexual dysfunction, nausea, vomiting, weight gain, and sleep disturbance.^{12, 23-26} The selective serotonin-norepinephrine reuptake inhibitors (SNRIs) include venlafaxine (Effexor™), desvenlafaxine (Pristiq™), and duloxetine (Cymbalta™).^{11, 25, 27-30} There are FDA-approved medications that target NET and DAT to increase levels of NE and DA in the synapse.³⁰⁻³² Triple reuptake inhibitors such as tesofensine inhibit SERT, NET, and DAT.³³

Unfortunately, 30 to 40 % of depressed patients are unable to experience the full benefits of their antidepressant medications.^{11, 25, 34, 35} Understanding the mechanism of action of drugs inhibiting MATs is critical to adequately treating the neurological disorders associated with these systems.^{32, 35-39} Therefore, MATs remain a target for the development and design of novel small molecules that are capable of effectively inhibiting the uptake of monoamine neurotransmitters.

The MATs are characterized by 12 transmembrane (TM) helices with intracellular N- and C-termini.² There are at least two binding pockets present, the substrate/inhibitor primary binding pocket, or the S1 site, and an allosteric S2 binding pocket in the “extracellular vestibule”, the space between the S1 pocket and the outside of the cell (**Figure 1.2**).^{1, 2, 16, 40-45} The transport process is believed to follow an “alternating access” mechanism.^{2, 3, 46} The opening of an outer, relatively extracellular gate allows the ions and substrate to enter S1, a chamber central to the bilayer. Upon binding of substrate in S1, the outer gate closes, and an inner, relatively cytoplasmic gate

opens, allowing ions and substrate to exit S1 and enter the cell. Off-loading of ions and substrate allows the transporter protein to reset, shifting from an inward-facing conformation, which is open to the cytoplasm, back to an outward-facing conformation, open to the extracellular side of the synapse (**Figure 1.3**).^{2, 46, 47}

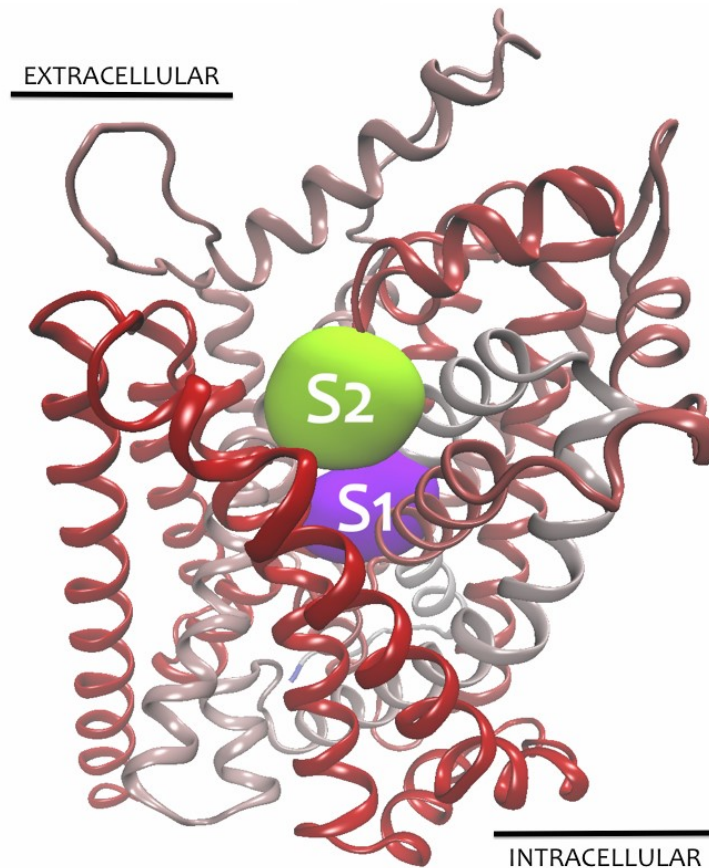


Figure 1.2: The tertiary structure of MAT protein. The 12 transmembrane helices are shown using ribbon rendering (red) with the primary binding site (S1) highlighted in purple and an allosteric binding site (S2) in green is highlighted.¹

Crystallization of the homologous *Aquifex aeolicus* bacterium leucine transporter (LeuT),^{2, 16, 40, 41, 48, 49} the *Drosophila melanogaster* dopamine transporter (dDAT),^{42, 44, 45} and recently the human serotonin transporter (hSERT)⁵⁰ has elucidated MAT topology and conformational states (**Figure 1.2**). The LeuT crystal structure 2A65² served as a

useful template for developing homology models of MAT 3-D structure despite only sharing 20-25% sequence identity with MATs.^{1, 51-56} Additional structures of LeuT in the substrate-free, inward-open, and outward-open conformations have offered insight into the mechanism of MAT translocation of substrates and its inhibition.^{16, 41}

A limitation of the available crystal structures, in general, is that the structures only offer a static image of the protein. Often mutations are made to the protein residues and detergents are used to facilitate crystal formation. To extract reasonable crystallographic structures, the temperature of the system may be reduced below physiological conditions to prevent atomic fluctuation.⁵⁷⁻⁵⁹ Despite advancements in uncovering MAT mechanism of transport, efforts continue to characterize the mechanistic aspects of these transporters, the structural changes that facilitate transport by allowing access to the central binding site, and the mechanism of drug inhibition.^{3, 8, 60-65}

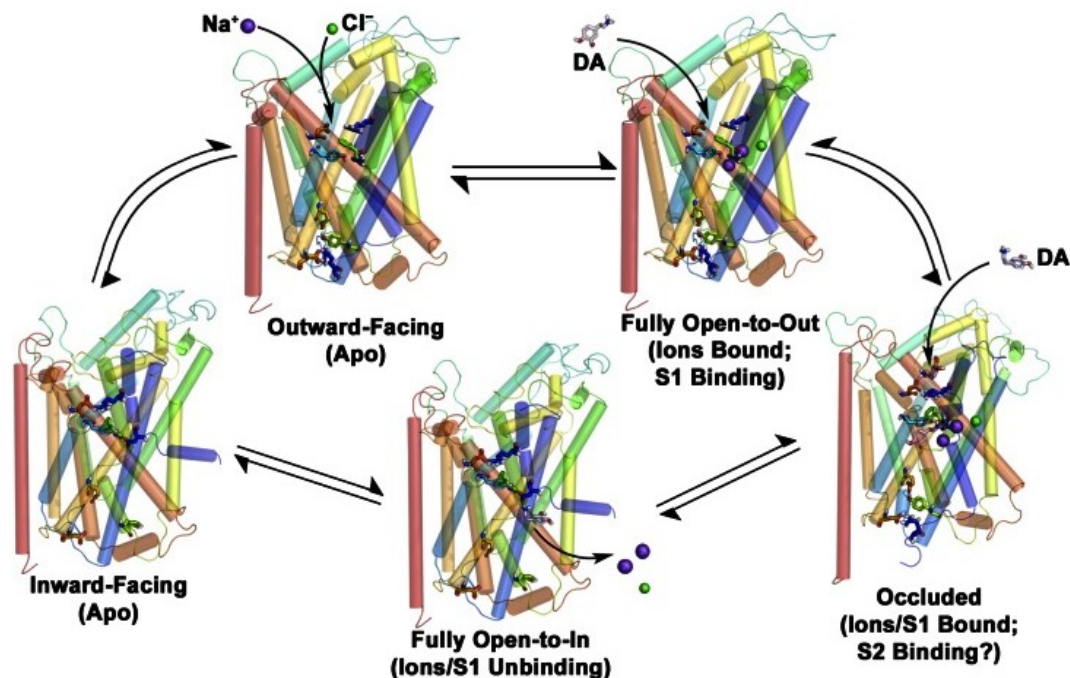


Figure 1.3: Figure adapted from Figure 3B from K.C. Schmitt, R.B. Rothman, and M.E.A. Reith (2013), Nonclassical Pharmacology of the Dopamine Transporter: Atypical Inhibitors, Allosteric Modulators, and Partial Substrates, *J Pharmacol Exp Ther*, 346(1):2-10; DOI: <https://doi.org/10.1124/jpet.111.191056> with permission from the American Society for Pharmacology and Experimental Therapeutics (ASPET). Alternating access mechanism of substrate transport.^{2, 16} MAT transition from extracellular-facing to intracellular-facing during substrate transport. First, the protein starts in an apoprotein (APO) state in the outward-facing conformation. Then ions and substrate will bind to the protein in the “fully open-to-out” conformation, where the binding site is accessible only from the extracellular space, creating an occluded conformation. The protein then transitions to a “fully open-to-in” conformation, where the binding site is accessible only from the intracellular space. The bound contents will be released into the cell at which point the protein will be in an APO inward-facing formation. The protein will then undergo a conformational shift that will allow for the reset of the transport mechanism.

Advancements in computing power and available computational tools afford the ability to study and characterize MAT interactions at physiologically relevant conditions *in silico*.^{55, 56, 66-72} Results from these simulations provide thermodynamic and kinetic information on the transporters and guide our understanding of how ligands interact with these transporters and modulate their function.^{5, 14, 68, 72-77} Characterization of competitive

and allosteric inhibitor binding sites have aided in designing new molecules to treat the disorders associated with the dysfunction of MATs.⁷⁷ The primary binding site (S1) and allosteric binding site (S2) have been the target of computational drug design strategies such as virtual screening and lead optimization.⁷⁸⁻⁸⁴ In several LeuT crystal structures, TCAs are bound in the allosteric S2 site formed by residues from TM1 (L25, L29, R30, V33, E37), TM3 (Y107, I111, W114), TM6 (F253), and TM10 (K398, L400, D401, D404).^{48, 85}

Even though binding of TCAs in the S2 site of LeuT may not fully support antidepressant binding in SERT based on later studies,⁸⁶ modeling the binding of antidepressants in the S2 site of SERT can reveal details about interaction in the allosteric binding site.⁸⁷ Moreover, the recent crystal structure of SERT with S-citalopram (PDB entry 5I73) shows two inhibitor molecules in the S1 and S2 binding sites of SERT,⁵⁰ supporting the likelihood for a second molecule to engage in the allosteric site in addition to occupying the primary binding site. Novel SERT ligands have been discovered by Manepalli *et al.* through a virtual screening of the ZINC database at the S2 site of a SERT homology model based on LeuT.⁷⁸ Research efforts have also been made by Larsen *et al.* and Topiol *et al.* to modify the structure of citalopram (CelexaTM), a high affinity S1 SERT inhibitor, to bind specifically in S2 with high-affinity.^{67, 88}

A second allosteric site in SERT was targeted by Mortensen and colleagues for the development of novel lead allosteric modulators of SERT that interact at a site previously referred to as A1, comprised of residues Q111, N112, I327, D328, A331, Q332, K490, E494, R564, Y568, and Y572.^{89, 90} A four-point receptor pharmacophore using the residues D328, K490, E494 and Y568 was developed based on molecular dynamics

(MD) simulations and comparative genomics techniques to identify the allosteric pocket outside the translocation pathway.⁸⁹

1.2 Computational study of DAT and SERT inhibitor binding

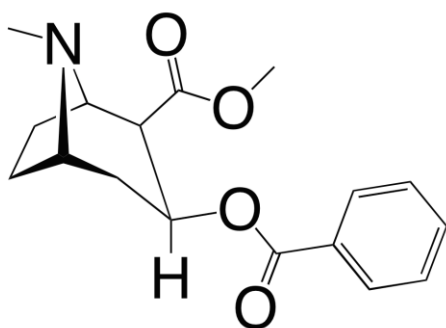
The work discussed herein studies the important interactions between novel inhibitors found to interact in DAT and SERT; specifically, studying the structural changes that occur upon inhibitors binding to the DAT and the interactions of an inhibitor in the allosteric (S2) site in SERT. This work intends to elucidate the appropriate drug binding pockets and improve the rational drug design by employing computational methods to study how the ligands are interacting with these proteins. Several computational tools were used to model protein and ligand binding and the conformational changes that occur in the protein. MD was used to simulate the physical movements of atoms and molecules to visualize the process of the ligands interacting with the protein residues. This allows the systems to equilibrate and sample a relatively small time frame for any changes in protein structure due to ligand binding. Free energy calculations were used as a quantitative tool to estimate the binding free energies of ligands in the protein and probe the significant interactions in the binding site. This approach reveals key interactions for MAT molecular recognition, toward developing more effective inhibitors.

1.2.1 Modeling the binding of DAT inhibitors

Illicit psychostimulants, such as cocaine, methamphetamine, and ecstasy target DAT.^{4, 44, 91} The non-abusable cocaine analogs benztropine and GBR12909 interact with

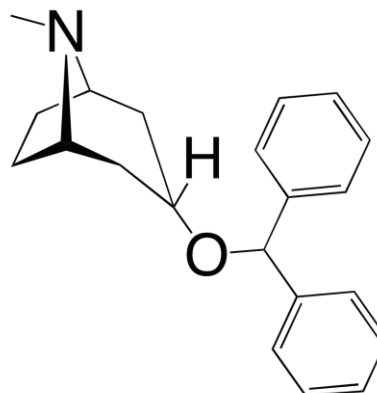
the DAT in a manner that differs from cocaine (**Figure 1.4**).^{92, 93} Experimental assays have determined cocaine and benztropine prefer different conformations of DAT, and the crystal structure of cocaine and DAT (4XP4) indicates cocaine can stabilize the outward-facing conformation (**Figure 1.5**).⁴⁴ Conformational studies on DAT-inhibitor complexes spawned the popular hypothesis that the non-abusable DAT inhibitors stabilize the inward-facing conformation of DAT (**Figure 1.5**).⁹⁴ The hypothesis is in doubt, as several analogs of cocaine and benztropine have been synthesized and shown to prefer the outward-facing DAT conformation in cysteine accessibility assays, yet mirror benztropine's lack of abuse potential.⁵³

cocaine (COC)



$$K_i = 98.1 \pm 6.6 \text{ nM}$$

benztropine (BZT)



$$K_i = 127 \pm 22 \text{ nM}$$

Figure 1.4: DAT inhibitors, cocaine (COC) and benztropine (BZT). Affinity (K_i) measured for DAT (mean \pm s.e.m.) obtained by displacement of the cocaine analog radioligand [³H]-WIN 35,428.⁵³

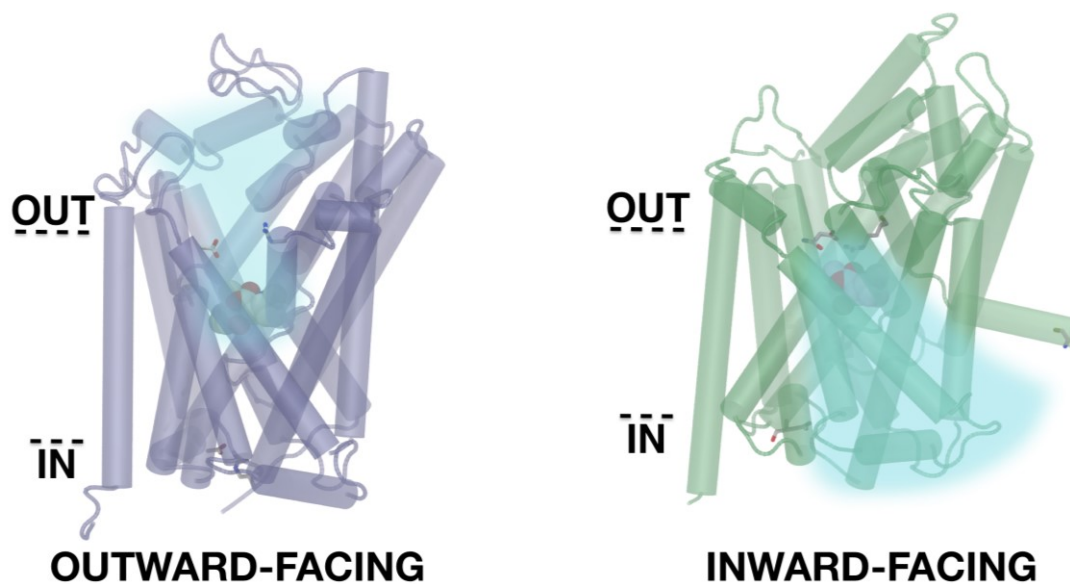


Figure 1.5: The extracellular-facing (outward-facing) and intracellular-facing (inward-facing) MAT conformation based on dDAT (PDB entry 4XP4)⁴⁴ and LeuT (PDB entry 3TT3).⁴¹ The molecule represented as van der Waals sphere within the central region of the protein represents a molecule bound in the S1 binding site. Regions highlighted in blue represent the pathway allowing access to the central binding site from either the extracellular pathway or the internally open intracellular pathway for the outward-facing or inward-facing conformation.

The binding of cocaine, benztropine and the cocaine analogs, LX10 and LX11 (**Figure 1.6**) were studied using a computational approach to assess ligand binding and structural changes in the protein in both the outward-facing and inward-facing conformations. Additional modifications to the diphenyl ether and chlorobenzyl moiety, such as the ones described by Hong *et al.*, can potentially reveal atomistic details of how the inhibitors can interact with the DAT binding site.

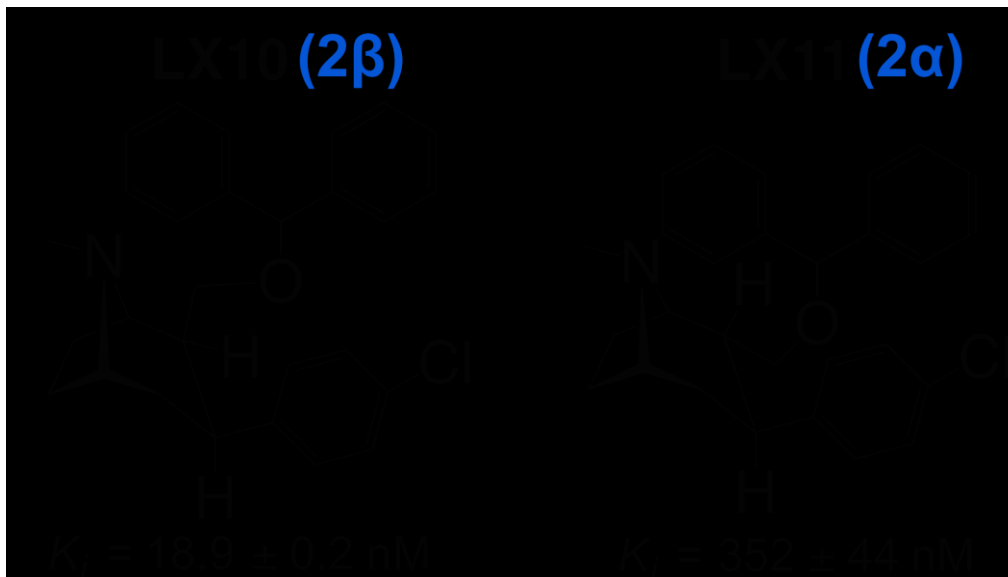


Figure 1.6: Structures of DAT inhibitors, the 3β -aryltropane cocaine analogs, LX10 (2β) and LX11 (2α). The analogs stereochemically differ at the tropane C-2 position. Affinity (K_i) measured for DAT (mean \pm s.e.m.) obtained by displacement of the cocaine analog radioligand [^3H]-WIN 35,428.⁵³

1.2.2 Lead optimization of a novel SERT inhibitor

A novel SERT inhibitor, SM11, was discovered through a virtual screening (docking) with the S2 allosteric binding site in the SERT.⁷⁸ SM11 was hypothesized to interact with the S2 binding site with observed interactions including hydrophobic with Trp103, Ile179, and Phe335 and hydrogen bond with Tyr107, Asp328, and Lys490 (**Figure 1.7**). The objective of this work involves a lead optimization of SM11 performed using free energy calculations to reveal critical interactions for probing ligand interactions in S2, and for developing more potent inhibitors with nanomolar SERT affinity.

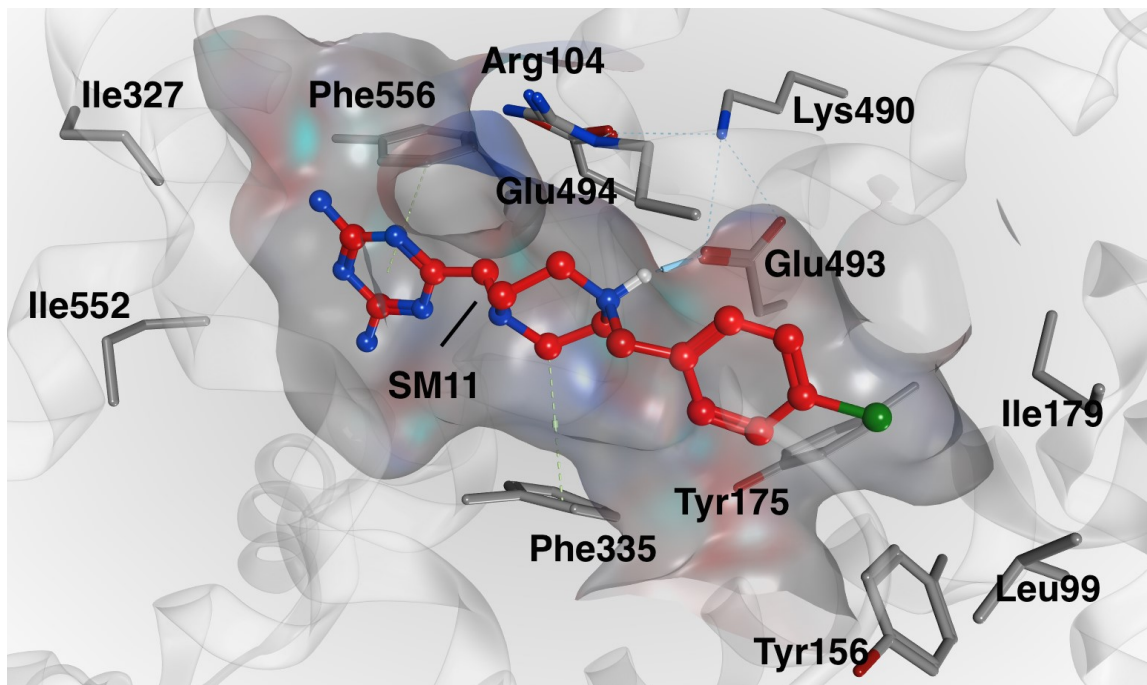


Figure 1.7: Hypothesized interactions of SM11 (red ball-and-stick) in the S2 site of SERT. The SM11 color scheme is as follows: red is for carbon, blue is for nitrogen, and green is for chlorine. The observed interactions between SM11 and SERT include hydrophobic with Trp103, Ile179, Phe335 and hydrogen bond with Tyr107, Asp328, Lys490.⁷⁸

The absolute binding free energy (ABFE) calculation of SM11 to SERT was performed for both the S1 and S2 binding sites (**Figure 1.2**); the latter site best matched experimental binding free energy calculations. Several analogs of SM11 were proposed based on binding site interactions in S2, and the analogs were subjected to relative binding free energy (RBFE) calculations to determine if the modifications would be energetically favorable.

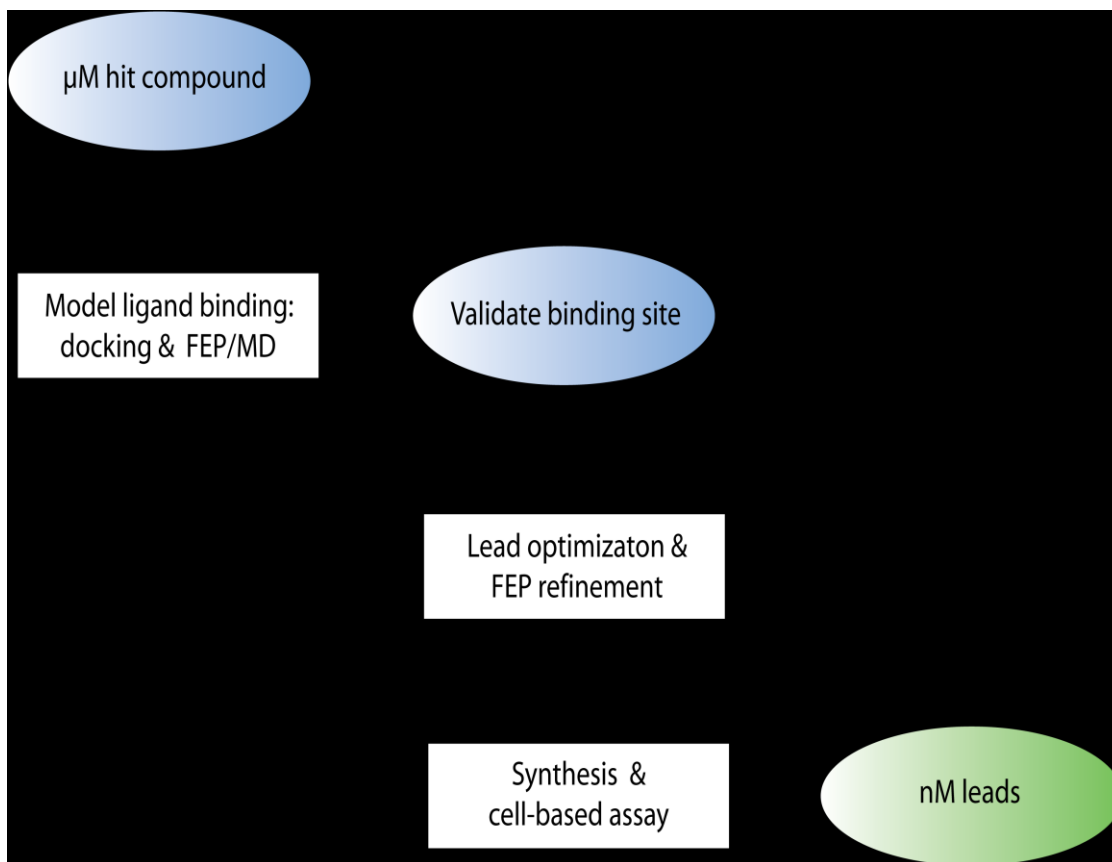


Figure 1.8: Structure-based drug design scheme of a hit-to-lead compound. The free energy perturbation (FEP) method was used to calculate the absolute binding free energy (ABFE) of a hit-to-lead compound, SM11, binding to SERT. The binding pose is determined based on the comparison of the ABFE calculation to the experimental measurement of the ligand affinity from a cell-based assay. Analogs of the lead compound are developed to probe drug recognition and optimize interactions within the transporter binding site.

1.3 Computational methods for studying inhibitor binding

The ability to predict the binding affinity of a ligand to a protein is an important computational tool in computer-aided drug design. Scoring functions are often used in virtual screening and docking simulations because this approach offers a quick estimate of the ligand binding affinity.⁹⁵ Scoring functions allow ligands to be compared and ranked based on an estimated free energy value⁹⁶⁻⁹⁸ beneficial for screening molecular

libraries containing millions of compounds. However, scoring of docked poses may not directly correlate with experimental affinity. A limitation of this approach is the treatment of the protein as a rigid system with implicit solvation.⁹⁹ This is a fast method, but it can produce an inaccurate prediction of binding affinity.¹⁰⁰ Explicit methods used for estimation of binding affinity account for specific properties of the protein-ligand complexes. Accurate calculations of binding affinity take into account protein flexibility and explicit solvent interactions, especially the interactions of water at the binding site.⁵⁵

101-105

Classical MD simulations calculate thermodynamic properties (*e.g.*, potential energy) based on the molecular forces acting on the system as a function of time. These simulations have helped to close the gap between the static images provided by experimentally acquired crystal structures and the dynamic nature of macromolecules. Classical MD is currently unable to simulate biological processes that occur on millisecond-to-second timescales, such as the time for transitions between MAT extracellular-facing and intracellular-facing conformations. It is difficult to overcome the large free energy barrier; however, supercomputers such as ANTON and those available at the Extreme Science and Engineering Discovery Environment (XSEDE) have expanded the ability to study biologically relevant timescales.^{106, 107}

Modifications of classical MD methods increase sampling of protein dynamics. MD has been paired with other computational methods to overcome the free energy barriers, toward reconstructing the free energy landscape from shorter timescale simulations. The thermodynamics calculation of Gibbs free energy uses statistical mechanics to determine the probability of finding the system in a given state.^{103, 108-111}

Free energy methods coupled with MD simulations account for the protein, ligand, and solvent interactions and more accurately estimate binding affinity because of the explicit treatment of the atomic force fields that drive molecular interactions.¹¹²

Challenges of this approach include the insufficient sampling of the degrees of freedom of a system.^{101, 103, 104, 109, 113-116} Several methods exist to improve estimation of the binding free energy. These methods include free energy perturbation (FEP)/thermodynamic integration (TI), and umbrella sampling (US).^{117, 118} The use of well-defined and polarizable force fields can increase the accuracy of free energy calculations.¹¹⁹⁻¹²² The application and limitations of these methods are reviewed below.

1.3.1 Binding free energy calculations

Helmholtz free energy and the partition function allow for thermodynamic calculations of the binding free energy. Gibbs free energy allows the use of Helmholtz free energy at constant volume and pressure

$$Z = \sum_i e^{-E_i/k_bT} \quad (1.1)$$

$$\Delta G = -k_bT \ln \left(\frac{Z}{Z_0} \right) \quad (1.2)$$

where Z represents the final bound state, and Z_0 presents the unbound state in bulk solvent. All configurations between these two states are taken into account in the calculations of Gibbs free energy.^{108, 123} The changes in equilibrium between these states is also dependent on changes in the heat, enthalpy and the disorder of the system:

$$\Delta G^0 = \Delta H^0 - T\Delta S^0 = -RT\ln(K_{eq}C^0) \quad (1.3)$$

At chemical equilibrium, ΔH^0 is the change in enthalpy, ΔS^0 is the change in entropy of the reaction, R is the gas constant, T is the temperature, and $C^0 = 1/1661 \text{ \AA}^3$ at 1 M standard concentration to account for the translational freedom of a single solute molecule in explicit solvent.^{103, 123, 124}

The free energy perturbation (FEP) method can be used to calculate Gibbs free energy and simulate processes of binding free energy to estimate the differences in the binding of a ligand. Applying FEP methods to the thermodynamic cycle allows for the efficient calculation of binding free energy change of a ligand to a protein (**Figure 1.9**).

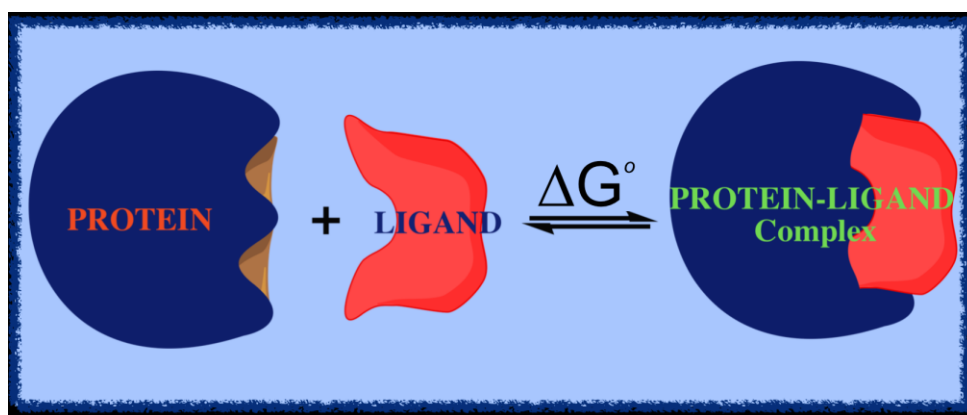


Figure 1.9: The binding free energy associated with forming a protein and ligand complex is determined through the thermodynamic calculation of Gibbs binding free energy (ΔG^0).

The accuracy of the computed binding free energy depends on the sampling strategy used to sample the configuration between the initial and final state of the system. The sampling is improved by including several intermediate states wherein the changes that take place between the initial state and the final state is controlled by introducing the coupling parameter, λ (**Figure 1.10**).^{119, 120, 125, 126} The free energy change of transforming

a system from state A ($\lambda=0$) to state B ($\lambda=1$) becomes a function of the coupling parameter so that the free energy change is measured between the initial state and final state as λ goes from 0 to 1.

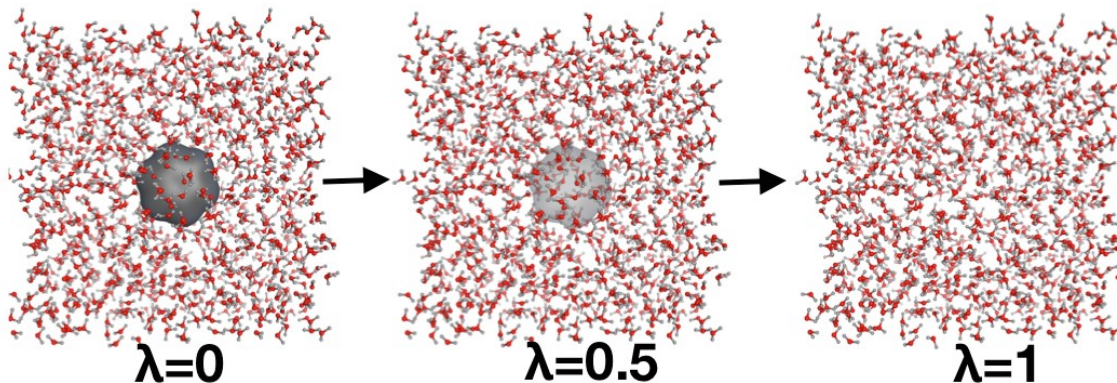


Figure 1.10: The alchemical transformation of a molecule in bulk water represented as a function of the coupling parameter (λ). As λ goes from 0 to 1, the molecule is perturbed from an initial state ($\lambda = 0$) to a final state ($\lambda = 1$).

The potential energy (U) of the bonds, angles, torsion and non-bonded terms is measured as a function of λ .

$$U(\lambda) = (1 - \lambda)U_0 + \lambda U_1 \quad (1.4)$$

The potential energy of the complex includes the energies of hydrogen bond formations, electrostatic interactions, dispersion, and charge-transfer interactions. An ensemble average of all the time steps is then used to measure the change in binding free energy,

$$\langle \Delta G_{\lambda \rightarrow \lambda + \Delta \lambda} \rangle = -k_B T \ln \left\langle \exp \left[-\frac{(U(\lambda + \Delta \lambda) - U(\lambda))}{k_B T} \right] \right\rangle_{\lambda} \quad (1.5)$$

where k_B is Boltzmann constant, T is the absolute temperature and $\langle \dots \rangle$ represents the ensemble average at the specified λ state. The convergence of the simulation must be monitored during the small changes between the two states ($\lambda_{0 \rightarrow 1}$). This will improve the

accuracy of the ensemble average by effectively sampling the degrees of freedom of the system.

1.3.1.1 Relative binding free energy calculations

The relative change in binding free energy ($\Delta\Delta G$) between two different ligands for the same protein is determined by applying FEP calculations to the thermodynamic cycle, where the two ligands can be represented as the initial and final states (**Figure 1.11**).^{109, 123} The relative binding free energy is given by

$$\Delta\Delta G = \Delta G_{\text{site}} - \Delta G_{\text{hydr}} = \Delta G_{\text{bind}}^y - \Delta G_{\text{bind}}^x \quad (1.6)$$

where ΔG_{bind}^x and ΔG_{bind}^y represent the change in binding free energy of the ligand in the protein, which is measured indirectly by taking the difference between ΔG_{hydr} and ΔG_{site} . The value of ΔG_{hydr} represents the change in hydration energy of the ligand in bulk solvent, and ΔG_{site} represents the change in binding energy of the ligand at the binding site of a solvated protein-ligand complex. The functional groups that are being modified are slowly perturbed as a function of the coupling parameter (λ). At State A ($\lambda=0$), only the interaction of the initial ligand L_x is being measured. Once the system reaches State B ($\lambda=1$), only the potential energy from the interactions of ligand L_y is measured. Outgoing atoms will see their electrostatic interactions with the environment dissociate during $\lambda = 0$ to 0.5 while the interactions involving incoming atoms are gradually introduced during $\lambda = 0.5$ to 1. The van der Waals (vdW) interactions of outgoing atoms are gradually decoupled during $\lambda = 0$ to 1 and the interactions of incoming atoms with the environment are incorporated during $\lambda = 1$ to 0.^{109, 113, 119, 120, 127}

The calculated relative binding free energy can be compared to experimental affinity measurements of both ligands,

$$\Delta\Delta G(L_x \rightarrow L_y) = RT \ln \left(\frac{K_i^{L_y}}{K_i^{L_x}} \right) \quad (1.7)$$

where $K_i^{L_x}$ and $K_i^{L_y}$ are the respective affinity measurements for each ligand to the target.

Relative binding free energy calculations were previously applied for the lead optimization of an anti-HIV agent.¹⁰⁹ The free energy calculations helped guide the molecular design of lead compounds to improve initial leads with activities at low-micromolar concentrations to low-nanomolar inhibitors.¹⁰⁹

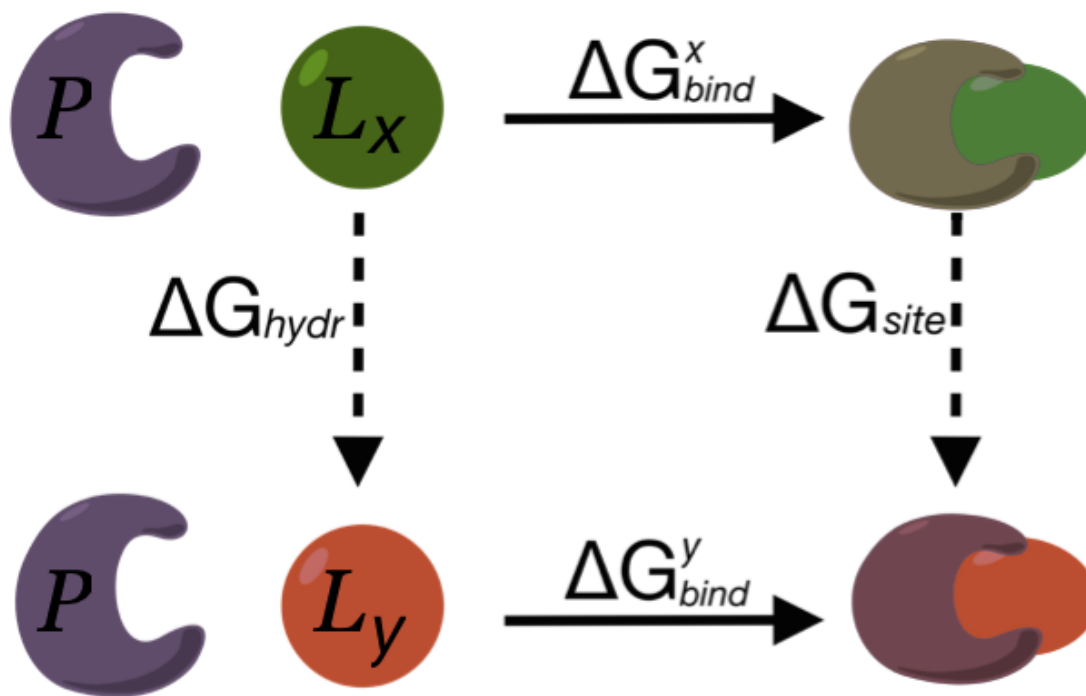


Figure 1.11: Gibbs binding free energy calculation applied to the thermodynamic cycle for calculating the relative binding free energy (RBFE) change between two ligand molecules (L_X and L_Y).^{123, 128} ΔG_{bind}^x represents the binding free energy associated with the binding of ligand X (L_X , green sphere) to a protein (P , violet) to form a protein-ligand complex. ΔG_{bind}^y represents the binding free energy associated with the binding of ligand Y (L_Y , orange sphere) to the same protein to form a new protein-ligand complex. The RBFE change ($\Delta\Delta G$) associated with the difference in ligand X and ligand Y binding to a protein can be determined through calculation of the hydration energy (ΔG_{hydr}), by mutating the ligands, L_X to L_Y , in bulk solvent. The binding site free energy (ΔG_{site}) is calculated by mutating the ligands in the protein binding site. The difference between the two calculations gives the RBFE ($\Delta\Delta G = \Delta G_{site} - \Delta G_{hydr} = \Delta G_{bind}^y - \Delta G_{bind}^x$).

The prominence of water in biological systems makes understanding the influence of water key to understanding the intermolecular forces that drive the interactions between a ligand and macromolecule.¹²⁹⁻¹³¹ Jorgensen *et al.* were able to replicate the experimental numbers for the free energy of hydration for the transformation of methanol to ethane.¹³² As a validation step, the relative FEP calculation conducted by Jorgensen *et*

al. was replicated to calculate the relative free energies of hydration for the transformation of methanol to ethane.

1.3.1.2 Absolute binding free energy calculations

The binding free energy (ΔG_{bind}) of a ligand (L) to a protein (P) is difficult to calculate directly.¹²³ Instead, the ABFE (ΔG_{abs}) calculations involve the ligand being mutated to a dummy molecule (D), which represents the alchemical annihilation transformation of the ligand to a molecule with no interactions with its environment (**Figure 1.12**). Two systems are used, wherein the first is a solvent water box with a ligand (L) that is replaced by a dummy molecule (D) to calculate the hydration energy of the ligand (ΔG_{hydr}). The second system includes a solvated protein-ligand complex ($P:L$), wherein the ligand (L) is replaced by a dummy molecule (D) to calculate the binding free energy (ΔG_{site}) of the ligand to the protein. The difference between the systems containing the perturbed dummy molecule in the bulk solvent and at the binding site has a binding free energy (ΔG_0) equal to zero with the assumption that the free energy difference is negligible between the bound and unbound dummy molecules.

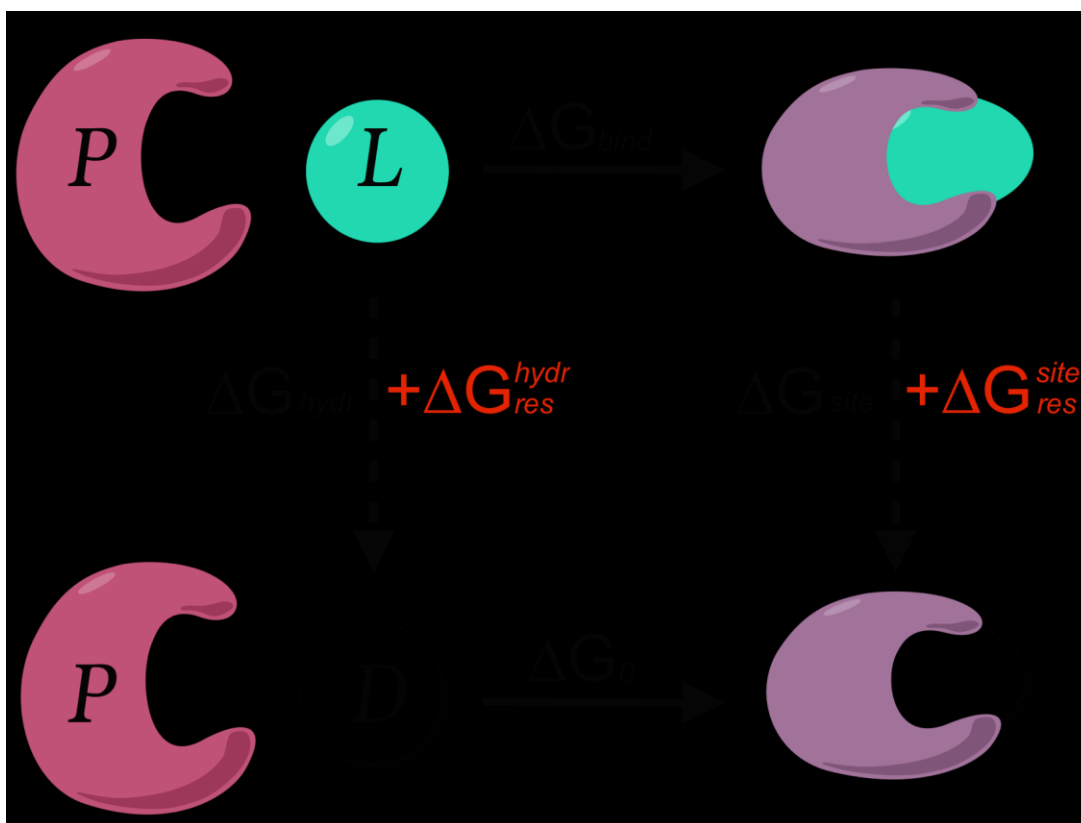


Figure 1.12: Gibbs binding free energy calculation applied to the thermodynamic cycle for calculating the absolute binding free energy (ABFE). ΔG_{bind} represents the binding free energy associated with the binding of a ligand (L , green sphere) to a protein (P , maroon) to form a protein-ligand complex (purple-green complex). ΔG_0 represents the binding free energy associated with the binding of a dummy ligand (D) to the same protein to form a new protein-ligand complex. The dummy ligand represents a placeholder molecule that lacks intermolecular interactions with the ligand's environment. The ABFE (ΔG_{abs}) associated with the ligand binding to the protein is determined indirectly by calculating the hydration energy (ΔG_{hydr}), by mutating the ligand to the dummy ligand in bulk solvent and the binding site free energy (ΔG_{site}), by mutating the ligand to a dummy ligand in the protein binding site. The difference between the two calculations gives the ABFE ($\Delta G_{abs} = \Delta G_{site} - \Delta G_{hydr} = \Delta G_0 - \Delta G_{bind}$). Geometric restraints are applied to the ligand to reduce the degrees of freedom of ligand with respect to the protein-binding pocket. The difference between the restraint free energies ($\Delta\Delta G_{res}$) associated with the harmonic restraints placed on the ligand in bulk solvent (ΔG_{res}^{hydr}) and in the solvated protein-ligand complex (ΔG_{res}^{site}) is included in the final ABFE calculation ($\Delta G_{abs} = \Delta G_{site} - \Delta G_{hydr} - \Delta\Delta G_{res}$).

1.3.1.3 Binding free energy calculations with harmonic restraints

Insufficient sampling during these calculations can lead to inaccurate estimation of loss of conformational freedom upon ligand binding.^{101, 108, 113, 114, 133, 134} This can be improved by limiting the degrees of freedom of the system by applying a series of geometrical restraints to improve the efficiency of sampling during simulations. The harmonic restraints act on a set of collective variables to reduce the conformational entropy of the system. The method proposed by Gumbart *et al.*¹¹⁰ was considered to prevent the ligand from wandering when the electrostatic and vdW interactions are scaled to zero (**Figure 1.12**).

Geometric restraints based on collective variables are applied to reduce the conformational, translational, and rotational entropies of the ligand (**Figure 1.13**). Harmonic restraints are applied to the translation (r, θ, ϕ), and the rotation (Θ, Φ, Ψ) of the ligand with respect to the protein (**Figure 1.13**).¹¹⁰ Groups of atoms are defined to form the reference structure of the ligand (L_1, L_2, L_3) and the protein (P_1, P_2, P_3) and harmonic restraints are applied to the root-mean-square deviation (RMSD) with respect to the native conformation of the protein-ligand complex. The thermodynamic cycle is utilized to calculate the ABFE (ΔG_{abs}^o) of a ligand to a protein with the energy associated with the harmonic restraint potentials (**Figure 1.12**).

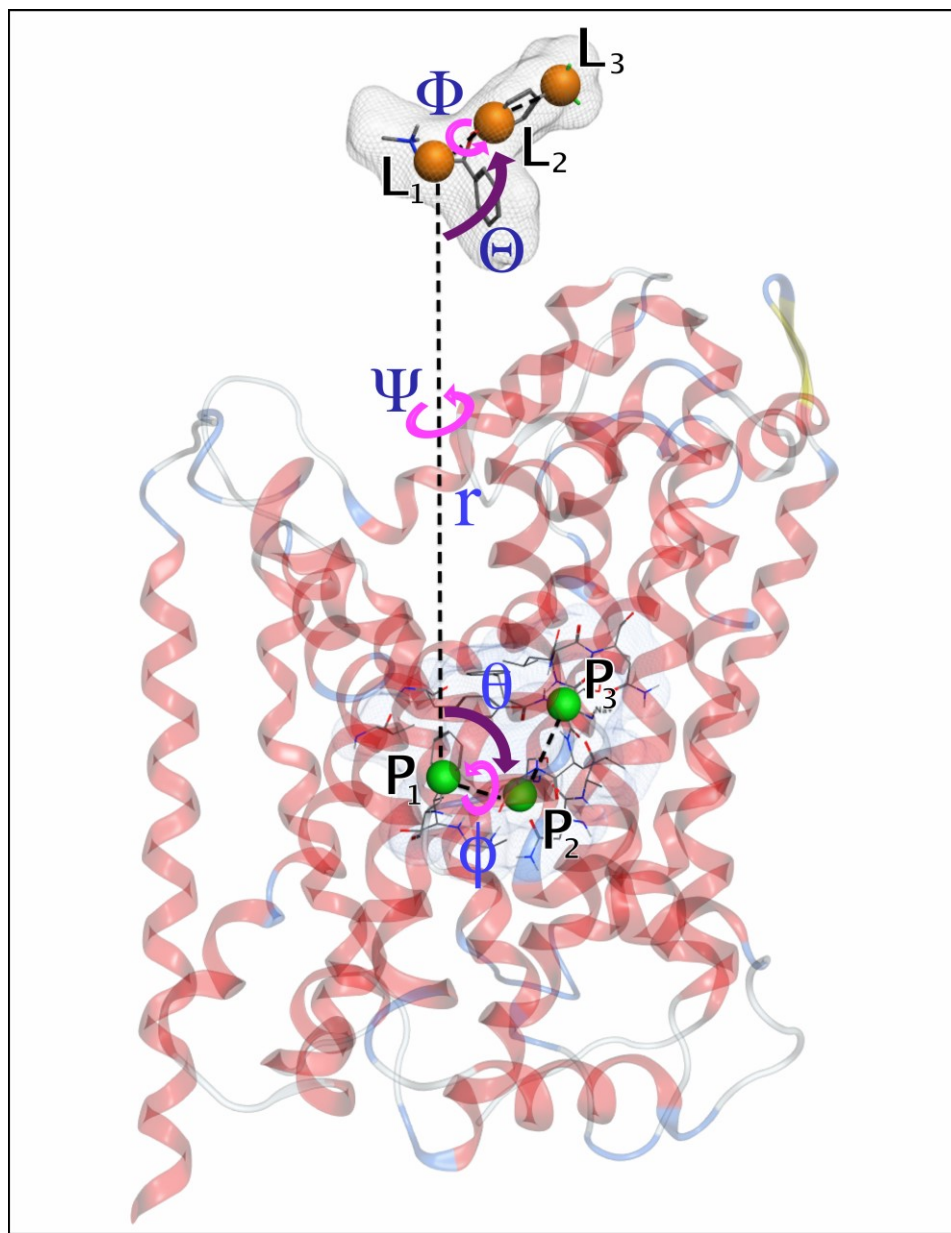


Figure 1.13: Geometric restraints used to reduce the conformational, translational (r, θ, ϕ), and rotational (Θ, Φ, Ψ) entropies of the ligand with respect to the protein.^{103, 110} Groups of atoms are defined to form the reference structure of the ligand (L_1, L_2, L_3) and the protein (P_1, P_2, P_3) and harmonic restraints are applied to the root-mean-square deviation (RMSD) with respect to the native conformation of the protein-ligand complex. For the translational restraints, r is the distance between P_1 and L_1 , θ is the angle formed by $P_2 - P_1 - L_1$, and ϕ is the dihedral angle of $P_3 - P_2 - P_1 - L_1$. For the rotational restraints, θ is the angle of $P_1 - L_1 - L_2$, Φ is the dihedral angle of $P_2 - P_1 - L_1 - L_2$, and Ψ is the dihedral angle of $P_1 - L_1 - L_2 - L_3$.

The calculations with harmonic restraints are applied in the bound state of ligand interacting in the protein binding pocket as well as the unbound state of the ligand interacting with its environment in bulk aqueous solvent. The translational restraint (U_t) is defined as

$$U_t = \frac{1}{2} [k_t(r - r_0)^2 + k_a(\theta - \theta_0)^2 + k_d(\phi - \phi_0)^2] \quad (1.9)$$

where r is the distance between P_1 and L_1 , θ is the angle formed by $P_2 - P_1 - L_1$, and ϕ is the dihedral angle of $P_3 - P_2 - P_1 - L_1$. The force constants applied for the distance, angle, and dihedral angle restraints are represented by k_t , k_a , and k_d , respectively. r_0 , θ_0 , and ϕ_0 are the reference restraint values taken from the equilibration simulation at the binding site. The rotational restraint (U_r) is defined as

$$U_r = \frac{1}{2} [k_a(\theta - \theta_0)^2 + k_d(\Phi - \Phi_0)^2 + k_d(\Psi - \Psi_0)^2] \quad (1.10)$$

where Θ is the angle of $P_1 - L_1 - L_2$, Φ is the dihedral angle of $P_2 - P_1 - L_1 - L_2$, and Ψ is the dihedral angle of $P_1 - L_1 - L_2 - L_3$.

The free energy contribution associated with the harmonic restraints are used to calculate the ABFE of the ligand bound to the protein where ΔG_{res}^{hydr} represents the binding free energy contributions from harmonic restraints placed on the conformational (ΔG_{conf}^{hydr}), translational and rotational ($\Delta G_{t,r}^{hydr}$) degrees of freedom of the ligand in bulk solvent with respect to the binding pose within the protein binding pocket (**Figure 1.12**). The same is applied to the binding site to give ΔG_{res}^{site} , which represents the free energy contribution from the removal of the harmonic restraint potentials placed on the ligand within the solvated protein binding pocket.^{103, 119, 123} The sum of all the free energy contributions (ΔG_i) is used to determine the equilibrium binding constant K_{eq} , where

$$K_{eq} = e^{-\beta[\sum\Delta G_i]} \quad (1.11)$$

and the final binding free energy (ΔG_{abs}^o) is given by,

$$\Delta G_{abs}^o = -RT\ln(K_{eq}C^o) \quad (1.12)$$

where R is the gas constant, T is the absolute temperature, and $C^o = 1/1661 \text{ \AA}^3$ at 1 M standard concentration to account for the translational freedom of a single solute molecule in explicit solvent.¹³⁵

Gumbart *et al.* performed the alchemical transformation of p41 (APSYSPPPPP) bound to Abl-SH3 to reproduce the experimental ABFE of $\Delta G_{exp} = -7.99 \text{ kcal/mol}$.¹¹⁰ This approach allows for improved sampling of the protein-ligand complex because of the reduced configurational degrees of freedom, especially for more dynamic systems. However, these calculations require a significant amount of setup, especially of the geometric restraints. Additionally, if the system is not properly equilibrated then the reference frame used to define the bound state will inaccurately capture the free energy associated with the binding interactions.

Implementing the ABFE calculations was simplified by the *Ligand Binder* web server, which provides standardized CHARMM (Chemistry at HARvard Macromolecular Mechanics) input files for performing ABFE calculations.^{105, 136} The ABFE is expressed in terms of specific intermediate steps in which the ligand-surrounding environment interactions, as well as the orientational, translational, and conformational sampling of the ligand, is reduced.

Jo *et al.* tested this method with the ABFE calculation of three nonpolar aromatic ligands to the L99A mutant of T4 lysozyme and three FK506-related ligands to FKBP12. The protein-ligand systems were prepared using the *Ligand Binder* web server. The free

energy calculations proceeded in general with two systems: the bound state, with the solvated protein-ligand complex, and the unbound state, with the ligand in bulk solvent. A conformational restraint potential, calculated using the average ligand structure from the bound state, was applied to keep the reference conformation.

Calculation of the conformational free energy was estimated by calculating the PMF as a function of ligand RMSD wherein the ligand conformational sampling is explicitly taken into account by umbrella sampling (US) of the ligand RMSD from the bound state in the protein-ligand complex. An offset value is applied to the ligand RMSD to create several intermediate states that define the reaction coordinate between the initial and final state of the system. The US examines how the system's energy changes as a function of a reaction coordinate parameter. Within each specific window or state of the system, a harmonic restraint is applied using an umbrella biasing potential. The restraining potentials help to reduce the degrees of freedom of the protein-ligand system and improve the sampling of the configurational space within the specific window or state of the system. Then a weighted histogram analysis method (WHAM) is used to reconstruct the potential of mean force (PMF) from the sorted trajectories of the umbrella sampling.¹¹⁸ The convergence of the simulations is examined by taking into account the statistical error measured in block-averaging and determining if there is an overlap of the free energy profiles in neighboring windows.

The translational and rotational free energy contributions were calculated as follows: 3 translational (1 distance, 1 angle, 1 dihedral) and 3 rotational (1 angle, 2 dihedral). The translational and rotational restraints were gradually turned on via the

linear coupling parameters, λ , with restraints applied to values from the reference structure.

The final absolute binding free energy (ΔG_{abs}^o) is given by,

$$\Delta G_{abs}^o = \Delta\Delta G_{int} + \Delta\Delta G_{conf} + \Delta\Delta G_{t,r} \quad (1.13)$$

where $\Delta\Delta G_{int}$ represents the free energy change due to nonbonded interactions between the ligand and its environment at the binding site (ΔG_{int}^{site}) and in the bulk solvent (ΔG_{int}^{hydr}) and $\Delta\Delta G_{t,r}$ represents free energy change due to the loss of translational/rotational freedom, and ($\Delta\Delta G_{conf}$) represents the free energy change due to the loss of conformational freedom.

Statistical errors within individual calculations performed by Jo *et al.* were approximately 1 kcal/mol and the calculated binding free energies were within an approximate 2 kcal/mol agreement of the experimental measurements and previous computational studies.¹⁰⁵ An additional benefit of this calculation approach is the ability to calculate the binding free energy of charged ligands.¹⁰⁵

1.4 Conclusions

Relative binding free energy (RBF) calculation for qualitative comparison provides an accurate estimate of the relative change in binding free energy ($\Delta\Delta G$) between two different ligands, without the intensive prep work needed to set up the calculations. However, the accuracy of RBF calculations is limited by the size of the molecule that is being modified.^{55, 101} Larger modifications require longer simulations in order to properly sample the free energy of the system. Another limitation of RBF

calculations is the inability to directly translate to an experimental measurement of affinity (K_i).

Absolute binding free energy (ABFE) calculations provide an estimate of the ligand affinity through the decoupling of a ligand binding to a protein. The accuracy of sampling can be improved by including intermediate (λ) states during the process of coupling or decoupling. The end-points of the simulation can also be divided into smaller windows to reduce the change in free energy between λ -values. The statistical data accrued in the coupling and decoupling simulations can be combined using the Bennett acceptance ratio (BAR)¹³⁷ and offer insight into the state of convergence for each λ -window.

During ABFE calculations, choosing the appropriate geometric restraints is key to sample the binding free energy accurately. Decomposition of free energy calculations provides an accurate depiction of free energy contributions. The setup of these calculations is very time-consuming however the CHARMM-GUI *Ligand Binder* offers a user-friendly web interface that makes it convenient to set up these calculations. The use of this tool with a well-defined, properly equilibrated reference structure of the protein-ligand system can result in an accurate ABFE calculation of a ligand to a protein. The next chapter discusses in detail the parameters used for performing the RBE and ABFE calculations on SERT inhibitors.

1.5 References

1. Penmatsa, A., and Gouaux, E. (2014) How LeuT shapes our understanding of the mechanisms of sodium-coupled neurotransmitter transporters. *J Physiol* 592, 863-869.
2. Yamashita, A., Singh, S. K., Kawate, T., Jin, Y., and Gouaux, E. (2005) Crystal structure of a bacterial homologue of Na⁺/Cl⁻-dependent neurotransmitter transporters. *Nature* 437, 215-223.

3. Kristensen, A. S., Andersen, J., Jorgensen, T. N., Sorensen, L., Eriksen, J., Loland, C. J., Stromgaard, K., and Gether, U. (2011) SLC6 neurotransmitter transporters: structure, function, and regulation. *Pharmacol Rev* 63, 585-640.
4. Pramod, A. B., Foster, J., Carvelli, L., and Henry, L. K. (2013) SLC6 transporters: structure, function, regulation, disease association and therapeutics. *Mol Aspects Med* 34, 197-219.
5. Colas, C., Ung, P. M., and Schlessinger, A. (2016) SLC Transporters: Structure, Function, and Drug Discovery. *MedChemComm* 7, 1069-1081.
6. Schlessinger, A., Matsson, P., Shima, J. E., Pieper, U., Yee, S. W., Kelly, L., Apeltsin, L., Stroud, R. M., Ferrin, T. E., Giacomini, K. M., and Sali, A. (2010) Comparison of human solute carriers. *Protein Sci* 19, 412-428.
7. Rudnick, G., Kramer, R., Blakely, R. D., Murphy, D. L., and Verrey, F. (2014) The SLC6 transporters: perspectives on structure, functions, regulation, and models for transporter dysfunction. *Pflugers Arch* 466, 25-42.
8. Forrest, L. R., Tavoulari, S., Zhang, Y. W., Rudnick, G., and Honig, B. (2007) Identification of a chloride ion binding site in Na⁺/Cl⁻-dependent transporters. *Proc Natl Acad Sci U S A* 104, 12761-12766.
9. Torres, G. E., Gainetdinov, R. R., and Caron, M. G. (2003) Plasma membrane monoamine transporters: structure, regulation and function. *Nat Rev Neurosci* 4, 13-25.
10. Lieberman, J. A., Kane, J. M., and Alvir, J. (1987) Provocative tests with psychostimulant drugs in schizophrenia. *Psychopharmacology* 91, 415-433.
11. Anderson, I. M. (2000) Selective serotonin reuptake inhibitors versus tricyclic antidepressants: a meta-analysis of efficacy and tolerability. *J Affect Disord* 58, 19-36.
12. Best, J., Nijhout, H. F., and Reed, M. (2011) Bursts and the Efficacy of Selective Serotonin Reuptake Inhibitors. *Pharmacopsychiatry* 44, S76-S83.
13. Amara, S. G., and Sonders, M. S. (1998) Neurotransmitter transporters as molecular targets for addictive drugs. *Drug Alcohol Depend* 51, 87-96.
14. Cheng, M. H., Block, E., Hu, F., Cobanoglu, M. C., Sorkin, A., and Bahar, I. (2015) Insights into the Modulation of Dopamine Transporter Function by Amphetamine, Orphenadrine, and Cocaine Binding. *Front Neurol* 6, 134.
15. Rothman, R. B., and Baumann, M. H. (2003) Monoamine transporters and psychostimulant drugs. *Eur J Pharmacol* 479, 23-40.

16. Krishnamurthy, H., Piscitelli, C. L., and Gouaux, E. (2009) Unlocking the molecular secrets of sodium-coupled transporters. *Nature* 459, 347-355.
17. Torrado, A., Lamas, C., Agejas, J., Jimenez, A., Diaz, N., Gilmore, J., Boot, J., Findlay, J., Hayhurst, L., Wallace, L., Broadmore, R., and Tomlinson, R. (2004) Novel selective and potent 5-HT reuptake inhibitors with 5-HT1D antagonist activity: chemistry and pharmacological evaluation of a series of thienopyran derivatives. *Bioorg Med Chem* 12, 5277-5295.
18. Herold, F., Chodkowski, A., Izbicki, L., Turlo, J., Dawidowski, M., Kleps, J., Nowak, G., Stachowicz, K., Dybala, M., Siwek, A., Mazurek, A. P., Mazurek, A., and Plucinski, F. (2011) Novel 4-aryl-pyrido[1,2-c]pyrimidines with dual SSRI and 5-HT(1A) activity. part 3. *Eur J Med Chem* 46, 142-149.
19. Zhu, X. Y., Etukala, J. R., Eyunni, S. V. K., Setola, V., Roth, B. L., and Ablordeppey, S. Y. (2012) Benzothiazoles as probes for the 5HT1A receptor and the serotonin transporter (SERT): a search for new dual-acting agents as potential antidepressants. *Eur J Med Chem* 53, 124-132.
20. Artigas, F. (2013) Serotonin receptors involved in antidepressant effects. *Pharmacol Ther* 137, 119-131.
21. Lin, H., Sassano, M. F., Roth, B. L., and Shoichet, B. K. (2013) A pharmacological organization of G protein-coupled receptors. *Nature methods* 10, 140-146.
22. Darras, F. H., Pockes, S., Huang, G., Wehle, S., Strasser, A., Wittmann, H. J., Nimczick, M., Sotriffer, C. A., and Decker, M. (2014) Synthesis, biological evaluation, and computational studies of Tri- and tetracyclic nitrogen-bridgehead compounds as potent dual-acting AChE inhibitors and hH3 receptor antagonists. *ACS Chem Neurosci* 5, 225-242.
23. Larsen, M. B., Elfving, B., and Wiborg, O. (2004) The chicken serotonin transporter discriminates between serotonin-selective reuptake inhibitors. A species-scanning mutagenesis study. *J Biol Chem* 279, 42147-42156.
24. Richelson, E. (1996) Synaptic effects of antidepressants. *J Clin Psychopharmacol* 16, 1S-7S; discussion 7S-9S.
25. Ferguson, J. M. (2001) SSRI Antidepressant Medications: Adverse Effects and Tolerability. *Prim Care Companion J Clin Psychiatry* 3, 22-27.
26. Aan Het Rot, M., Zarate, C. A., Jr., Charney, D. S., and Mathew, S. J. (2012) Ketamine for depression: where do we go from here? *Biol Psychiatry* 72, 537-547.
27. Vu, A. T., Cohn, S. T., Zhang, P., Kim, C. Y., Mahaney, P. E., Bray, J. A., Johnston, G. H., Koury, E. J., Cosmi, S. A., Deecher, D. C., Smith, V. A., Harrison, J. E.,

Leventhal, L., Whiteside, G. T., Kennedy, J. D., and Trybulski, E. J. (2010) 1-(Indolin-1-yl)-1-phenyl-3-propan-2-olamines as Potent and Selective Norepinephrine Reuptake Inhibitors. *J Med Chem* 53, 2051-2062.

28. Eildal, J. N. N., Andersen, J., Kristensen, A. S., Jørgensen, A. M., Bang-Andersen, B., Jørgensen, M., and Strømgaard, K. (2008) From the selective serotonin transporter inhibitor citalopram to the selective norepinephrine transporter inhibitor talopram: synthesis and structure-activity relationship studies. *J Med Chem* 51, 3045-3048.

29. Surratt, C. K., Ukairo, O. T., and Ramanujapuram, S. (2005) Recognition of psychostimulants, antidepressants, and other inhibitors of synaptic neurotransmitter uptake by the plasma membrane monoamine transporters. *AAPS J* 7, E739-751.

30. Levinstein, M. R., and Samuels, B. A. (2014) Mechanisms underlying the antidepressant response and treatment resistance. *Front Behav Neurosci* 8, 208.

31. Larsen, M. B., Sonders, M. S., Mortensen, O. V., Larson, G. a., Zahniser, N. R., and Amara, S. G. (2011) Dopamine transport by the serotonin transporter: a mechanistically distinct mode of substrate translocation. *J Neurosci* 31, 6605-6615.

32. Daws, L. C. (2009) Unfaithful neurotransmitter transporters: focus on serotonin uptake and implications for antidepressant efficacy. *Pharmacol Ther* 121, 89-99.

33. Astrup, A., Madsbad, S., Breum, L., Jensen, T. J., Kroustrup, J. P., and Larsen, T. M. Effect of tesofensine on bodyweight loss, body composition, and quality of life in obese patients: a randomised, double-blind, placebo-controlled trial. *The Lancet* 372, 1906-1913.

34. Hanson, N. D., Owens, M. J., and Nemeroff, C. B. (2011) Depression, antidepressants, and neurogenesis: a critical reappraisal. *Neuropsychopharmacology* 36, 2589-2602.

35. Crisafulli, C., Fabbri, C., Porcelli, S., Drago, A., Spina, E., De Ronchi, D., and Serretti, A. (2011) Pharmacogenetics of antidepressants. *Front Pharmacol* 2, 6.

36. Cryan, J. F., Valentino, R. J., and Lucki, I. (2005) Assessing substrates underlying the behavioral effects of antidepressants using the modified rat forced swimming test. *Neurosci Biobehav Rev* 29, 547-569.

37. Cryan, J. F., and Holmes, A. (2005) The ascent of mouse: advances in modeling human depression and anxiety. *Nat Rev Drug Discov* 4.

38. Cryan, J. F., Mombereau, C., and Vassout, A. (2005) The tail suspension test as a model for assessing antidepressant activity: review of pharmacological and genetic studies in mice. *Neurosci Biobehav Rev* 29, 571-625.

39. Cryan, J. F., Page, M. E., and Lucki, I. (2005) Differential behavioral effects of the antidepressants reboxetine, fluoxetine, and moclobemide in a modified forced swim test following chronic treatment. *Psychopharmacology* 182, 335-344.
40. Piscitelli, C. L., Krishnamurthy, H., and Gouaux, E. (2010) Neurotransmitter/sodium symporter orthologue LeuT has a single high-affinity substrate site. *Nature* 468, 1129-1132.
41. Krishnamurthy, H., and Gouaux, E. (2012) X-ray structures of LeuT in substrate-free outward-open and apo inward-open states. *Nature* 481, 469-474.
42. Penmatsa, A., Wang, K. H., and Gouaux, E. (2013) X-ray structure of dopamine transporter elucidates antidepressant mechanism. *Nature* 503, 85-90.
43. Wang, H., Goehring, A., Wang, K. H., Penmatsa, A., Ressler, R., and Gouaux, E. (2013) Structural basis for action by diverse antidepressants on biogenic amine transporters. *Nature* 503, 141-145.
44. Wang, K. H., Penmatsa, A., and Gouaux, E. (2015) Neurotransmitter and psychostimulant recognition by the dopamine transporter. *Nature* 521, 322-327.
45. Penmatsa, A., Wang, K. H., and Gouaux, E. (2015) X-ray structures of Drosophila dopamine transporter in complex with nisoxetine and reboxetine. *Nat Struct Mol Biol* 22, 506-508.
46. Forrest, L. R., Zhang, Y. W., Jacobs, M. T., Gesmonde, J., Xie, L., Honig, B. H., and Rudnick, G. (2008) Mechanism for alternating access in neurotransmitter transporters. *Proc Natl Acad Sci U S A* 105, 10338-10343.
47. Kazmier, K., Sharma, S., Quick, M., Islam, S. M., Roux, B., Weinstein, H., Javitch, J. A., and McHaourab, H. S. (2014) Conformational dynamics of ligand-dependent alternating access in LeuT. *Nat Struct Mol Biol* 21, 472-479.
48. Singh, S. K., Yamashita, A., and Gouaux, E. (2007) Antidepressant binding site in a bacterial homologue of neurotransmitter transporters. *Nature* 448, 952-956.
49. Singh, S. K., Piscitelli, C. L., Yamashita, A., and Gouaux, E. (2008) A competitive inhibitor traps LeuT in an open-to-out conformation. *Science* 322, 1655-1661.
50. Coleman, J. A., Green, E. M., and Gouaux, E. (2016) X-ray structures and mechanism of the human serotonin transporter. *Nature* 532, 334-339.
51. Indarte, M., Liu, Y., Madura, J. D., and Surratt, C. K. (2010) Receptor-Based Discovery of a Plasmalemmal Monoamine Transporter Inhibitor via High-Throughput Docking and Pharmacophore Modeling. *ACS Chem Neurosci* 1, 223-233.

52. Thomas, J. R., Gedeon, P. C., and Madura, J. D. (2014) Structural dynamics of the monoamine transporter homologue LeuT from accelerated conformational sampling and channel analysis. *Proteins* 82, 2289-2302.
53. Hong, W. C., Kopajtic, T. A., Xu, L., Lomenzo, S. A., Jean, B., Madura, J. D., Surratt, C. K., Trudell, M. L., and Katz, J. L. (2016) 2-Substituted 3 β -Aryltropane Cocaine Analogs Produce Atypical DAT Inhibitor Effects Without Inducing Inward-Facing DAT Conformations. *J Pharmacol Exp Ther*, 624-634.
54. Gedeon, P. C., et al. (2010) Molecular dynamics of leucine and dopamine transporter proteins in a model cell membrane lipid layer. *Proteins* 78, 797-811.
55. Zhao, C., Caplan, D. A., and Noskov, S. Y. (2010) Evaluations of the Absolute and Relative Free Energies for Antidepressant Binding to the Amino Acid Membrane Transporter LeuT with Free Energy Simulations. *J Chem Theory Comput* 6, 1900-1914.
56. Zhao, Y., Terry, D., Shi, L., Weinstein, H., Blanchard, S. C., and Javitch, J. A. (2010) Single-molecule dynamics of gating in a neurotransmitter transporter homologue. *Nature* 465, 188-193.
57. Chang, Y.-W., Chen, S., Tocheva, E. I., Treuner-Lange, A., Löbach, S., Søgaard-Andersen, L., and Jensen, G. J. (2014) Correlated cryogenic photoactivated localization microscopy and cryo-electron tomography. *Nature methods* 11, 737-739.
58. Fujiyoshi, Y., and Unwin, N. (2008) Electron crystallography of proteins in membranes. *Curr Opin Struct Biol* 18, 587-592.
59. Raman, P., Cherezov, V., and Caffrey, M. (2006) The Membrane Protein Data Bank. *Cell Mol Life Sci* 63, 36-51.
60. Zomot, E., Bendahan, A., Quick, M., Zhao, Y., Javitch, J. A., and Kanner, B. I. (2007) Mechanism of chloride interaction with neurotransmitter:sodium symporters. *Nature* 449, 726-730.
61. Beuming, T., Kniazeff, J., Bergmann, M. L., Shi, L., Gracia, L., Raniszewska, K., Newman, A. H., Javitch, J. A., Weinstein, H., Gether, U., and Loland, C. J. (2008) The binding sites for cocaine and dopamine in the dopamine transporter overlap. *Nat Neurosci* 11, 780-789.
62. Malinauskaite, L., Quick, M., Reinhard, L., Lyons, J. A., Yano, H., Javitch, J. A., and Nissen, P. (2014) A mechanism for intracellular release of Na⁺ by neurotransmitter/sodium symporters. *Nat Struct Mol Biol* 21, 1006-1012.
63. Bisgaard, H., Larsen, M. A., Mazier, S., Beuming, T., Newman, A. H., Weinstein, H., Shi, L., Loland, C. J., and Gether, U. (2011) The binding sites for benzotropines and dopamine in the dopamine transporter overlap. *Neuropharmacology* 60, 182-190.

64. Kantcheva, A. K., Quick, M., Shi, L., Winther, A. M., Stolzenberg, S., Weinstein, H., Javitch, J. A., and Nissen, P. (2013) Chloride binding site of neurotransmitter sodium symporters. *Proc Natl Acad Sci U S A* 110, 8489-8494.
65. Kniazeff, J., Shi, L., Loland, C. J., Javitch, J. A., Weinstein, H., and Gether, U. (2008) An intracellular interaction network regulates conformational transitions in the dopamine transporter. *J Biol Chem* 283, 17691-17701.
66. Stolzenberg, S., Quick, M., Zhao, C., Gotfryd, K., Khelashvili, G., Gether, U., Loland, C. J., Javitch, J. A., Noskov, S., Weinstein, H., and Shi, L. (2015) Mechanism of the Association between Na⁺ Binding and Conformations at the Intracellular Gate in Neurotransmitter:Sodium Symporters. *J Biol Chem* 290, 13992-14003.
67. Larsen, M. A., Plenge, P., Andersen, J., Eildal, J. N., Kristensen, A. S., Bogeso, K. P., Gether, U., Stromgaard, K., Bang-Andersen, B., and Loland, C. J. (2016) Structure-activity relationship studies of citalopram derivatives: examining substituents conferring selectivity for the allosteric site in the 5-HT transporter. *Br J Pharmacol* 173, 925-936.
68. Zhen, J., and Reith, M. E. (2016) Impact of disruption of secondary binding site S2 on dopamine transporter function. *J Neurochem* 138, 694-699.
69. LeVine, M. V., Cuendet, M. A., Khelashvili, G., and Weinstein, H. (2016) Allosteric Mechanisms of Molecular Machines at the Membrane: Transport by Sodium-Coupled Symporters. *Chem Rev* 116, 6552-6587.
70. Gur, M., Cheng, M. H., Zomot, E., and Bahar, I. (2017) Effect of Dimerization on the Dynamics of Neurotransmitter:Sodium Symporters. *J Phys Chem B*.
71. Razavi, A. M., Khelashvili, G., and Weinstein, H. (2017) A Markov State-based Quantitative Kinetic Model of Sodium Release from the Dopamine Transporter. *Scientific reports* 7, 40076.
72. Chavent, M., Duncan, A. L., and Sansom, M. S. (2016) Molecular dynamics simulations of membrane proteins and their interactions: from nanoscale to mesoscale. *Curr Opin Struct Biol* 40, 8-16.
73. Bahar, I., Cheng, M. H., Lee, J. Y., Kaya, C., and Zhang, S. (2015) Structure-Encoded Global Motions and Their Role in Mediating Protein-Substrate Interactions. *Biophys J* 109, 1101-1109.
74. Andersen, J., Ladefoged, L. K., Wang, D., Kristensen, T. N., Bang-Andersen, B., Kristensen, A. S., Schiott, B., and Stromgaard, K. (2015) Binding of the multimodal antidepressant drug vortioxetine to the human serotonin transporter. *ACS Chem Neurosci* 6, 1892-1900.

75. Cheng, M. H., and Bahar, I. (2015) Molecular Mechanism of Dopamine Transport by Human Dopamine Transporter. *Structure* 23, 2171-2181.
76. Bisha, I., and Magistrato, A. (2016) The molecular mechanism of secondary sodium symporters elucidated through the lens of the computational microscope. *RSC Adv* 6, 9522-9540.
77. Grouleff, J., Koldso, H., Miao, Y., and Schiott, B. (2017) Ligand Binding in the Extracellular Vestibule of the Neurotransmitter Transporter Homologue LeuT. *ACS Chem Neurosci* 8, 619-628.
78. Manepalli, S., Geffert, L. M., Surratt, C. K., and Madura, J. D. (2011) Discovery of novel selective serotonin reuptake inhibitors through development of a protein-based pharmacophore. *J Chem Inf Model* 51, 2417-2426.
79. Schlessinger, A., Geier, E., Fan, H., Irwin, J. J., Shoichet, B. K., Giacomini, K. M., and Sali, A. (2011) Structure-based discovery of prescription drugs that interact with the norepinephrine transporter, NET. *Proc Natl Acad Sci U S A* 108, 15810-15815.
80. Nolan, T. L., Lapinsky, D. J., Talbot, J. N., Indarte, M., Liu, Y., Manepalli, S., Geffert, L. M., Amos, M. E., Taylor, P. N., Madura, J. D., and Surratt, C. K. (2011) Identification of a novel selective serotonin reuptake inhibitor by coupling monoamine transporter-based virtual screening and rational molecular hybridization. *ACS Chem Neurosci* 2, 544-552.
81. Nolan, T. L., Geffert, L. M., Kolber, B. J., Madura, J. D., and Surratt, C. K. (2014) Discovery of novel-scaffold monoamine transporter ligands via in silico screening with the S1 pocket of the serotonin transporter. *ACS Chem Neurosci* 5, 784-792.
82. Gabrielsen, M., Ravna, A. W., Kristiansen, K., and Sylte, I. (2012) Substrate binding and translocation of the serotonin transporter studied by docking and molecular dynamics simulations. *J Mol Model* 18, 1073-1085.
83. Gabrielsen, M., Kurczab, R., Ravna, A. W., Kufareva, I., Abagyan, R., Chilmonczyk, Z., Bojarski, A. J., and Sylte, I. (2012) Molecular mechanism of serotonin transporter inhibition elucidated by a new flexible docking protocol. *Eur J Med Chem* 47, 24-37.
84. Gabrielsen, M., Kurczab, R., Siwek, A., Wolak, M., Ravna, A. W., Kristiansen, K., Kufareva, I., Abagyan, R., Nowak, G., Chilmonczyk, Z., Sylte, I., and Bojarski, A. J. (2014) Identification of novel serotonin transporter compounds by virtual screening. *J Chem Inf Model* 54, 933-943.
85. Zhou, Z., Zhen, J., Karpowich, N. K., Goetz, R. M., Law, C. J., Reith, M. E. A., and Wang, D.-N. N. (2007) LeuT-desipramine structure reveals how antidepressants block neurotransmitter reuptake. *Science* 317, 1390-1393.

86. Sinning, S., Musgaard, M., Jensen, M., Severinsen, K., Celik, L., Koldsø, H., Meyer, T., Bols, M., Jensen, H. H., Schiøtt, B., and Wiborg, O. (2010) Binding and orientation of tricyclic antidepressants within the central substrate site of the human serotonin transporter. *J Biol Chem* 285, 8363-8374.
87. Zhou, Z., Zhen, J., Karpowich, N. K., Law, C. J., Reith, M. E. a., and Wang, D.-n. N. (2009) Antidepressant specificity of serotonin transporter suggested by three LeuT-SSRI structures. *Nat Struct Mol Biol* 16, 652-657.
88. Topiol, S., Bang-Andersen, B., Sanchez, C., Plenge, P., Loland, C. J., Juhl, K., Larsen, K., Bregnedal, P., and Bogeso, K. P. (2017) X-ray structure based evaluation of analogs of citalopram: Compounds with increased affinity and selectivity compared with R-citalopram for the allosteric site (S2) on hSERT. *Bioorg Med Chem Lett* 27, 470-478.
89. Kortagere, S., Fontana, A. C. K., Renée Rose, D., and Mortensen, O. V. (2013) Identification of an allosteric modulator of the serotonin transporter with novel mechanism of action. *Neuropharmacology* 72, 282-290.
90. Mortensen, O. V., and Kortagere, S. (2015) Designing modulators of monoamine transporters using virtual screening techniques. *Front Pharmacol* 6, 223.
91. Schmitt, K. C., and Reith, M. E. (2010) Regulation of the dopamine transporter: aspects relevant to psychostimulant drugs of abuse. *Ann N Y Acad Sci* 1187, 316-340.
92. Liang, Y. J., Zhen, J., Chen, N., and Reith, M. E. (2009) Interaction of catechol and non-catechol substrates with externally or internally facing dopamine transporters. *J Neurochem* 109, 981-994.
93. Schmitt, K. C., Zhen, J., Kharkar, P., Mishra, M., Chen, N., Dutta, A. K., and Reith, M. E. A. (2008) Interaction of cocaine-, benztropine-, and GBR12909-like compounds with wild-type and mutant human dopamine transporters: molecular features that differentially determine antagonist-binding properties. *J Neurochem* 107, 928-940.
94. Loland, C. J., Desai, R. I., Zou, M. F., Cao, J., Grundt, P., Gerstbrein, K., Sitte, H. H., Newman, A. H., Katz, J. L., and Gether, U. (2008) Relationship between conformational changes in the dopamine transporter and cocaine-like subjective effects of uptake inhibitors. *Mol Pharmacol* 73, 813-823.
95. Schneider, G., and Bohm, H. J. (2002) Virtual screening and fast automated docking methods. *Drug Discov Today* 7, 64-70.
96. Seifert, M. H., and Lang, M. (2008) Essential factors for successful virtual screening. *Mini Rev Med Chem* 8, 63-72.
97. Seifert, M. H. (2009) Targeted scoring functions for virtual screening. *Drug Discov Today* 14, 562-569.

98. Chen, Z., Li, H.-l., Zhang, Q.-j., Bao, X.-g., Yu, K.-q., Luo, X.-m., Zhu, W.-l., and Jiang, H.-l. (2009) Pharmacophore-based virtual screening versus docking-based virtual screening: a benchmark comparison against eight targets. *Acta Pharmacol Sin* 30, 1694-1708.
99. Wei, B. Q., Weaver, L. H., Ferrari, A. M., Matthews, B. W., and Shoichet, B. K. (2004) Testing a Flexible-receptor Docking Algorithm in a Model Binding Site. *J Mol Biol* 337, 1161-1182.
100. Eldridge, M. D., Murray, C. W., Auton, T. R., Paolini, G. V., and Mee, R. P. (1997) Empirical scoring functions: I. The development of a fast empirical scoring function to estimate the binding affinity of ligands in receptor complexes. *J Comput Aided Mol Des* 11, 425-445.
101. Wang, J., Deng, Y., and Roux, B. (2006) Absolute binding free energy calculations using molecular dynamics simulations with restraining potentials. *Biophys J* 91, 2798-2814.
102. Singh, N., and Warshel, A. (2010) Absolute binding free energy calculations: on the accuracy of computational scoring of protein-ligand interactions. *Proteins* 78, 1705-1723.
103. Mobley, D. L., and Klimovich, P. V. (2012) Perspective: Alchemical free energy calculations for drug discovery. *J Chem Phys* 137, 230901.
104. Gapsys, V., Seeliger, D., and de Groot, B. L. (2012) New Soft-Core Potential Function for Molecular Dynamics Based Alchemical Free Energy Calculations. *J Chem Theory Comput* 8, 2373-2382.
105. Jo, S., Jiang, W., Lee, H. S., Roux, B., and Im, W. (2013) CHARMM-GUI Ligand Binder for Absolute Binding Free Energy Calculations and Its Application. *J Chem Inf Model* 53, 267-277.
106. Shaw, D. E., Chao, J. C., Eastwood, M. P., Gagliardo, J., Grossman, J. P., Ho, C. R., Lerardi, D. J., Kolossváry, I., Klepeis, J. L., Layman, T., McLeavey, C., Deneroff, M. M., Moraes, M. A., Mueller, R., Priest, E. C., Shan, Y., Spengler, J., Theobald, M., Towles, B., Wang, S. C., Dror, R. O., Kuskin, J. S., Larson, R. H., Salmon, J. K., Young, C., Batson, B., and Bowers, K. J. (2008) Anton, a special-purpose machine for molecular dynamics simulation. *Communications of the ACM* 51, 91-97.
107. Towns, J., Cockerill, T., Dahan, M., Foster, I., Gaither, K., Grimshaw, A., Hazlewood, V., Lathrop, S., Lifka, D., Peterson, G. D., Roskies, R., Scott, J. R., and Wilkens-Diehr, N. (2014) XSEDE: Accelerating Scientific Discovery. *Comput Sci Eng* 16, 62-74.

108. Gilson, M. K., Given, J. a., Bush, B. L., and McCammon, J. a. (1997) The statistical-thermodynamic basis for computation of binding affinities: a critical review. *Biophys J* 72, 1047-1069.
109. Jorgensen, W. L. (2009) Efficient drug lead discovery and optimization. *Acc Chem Res* 42, 724-733.
110. Gumbart, J. C., Roux, B., and Chipot, C. (2013) Standard binding free energies from computer simulations: What is the best strategy? *J Chem Theory Comput* 9, 794-802.
111. Rocklin, G. J., Boyce, S. E., Fischer, M., Fish, I., Mobley, D. L., Shoichet, B. K., and Dill, K. a. (2013) Blind prediction of charged ligand binding affinities in a model binding site. *J Mol Biol* 425, 4569-4583.
112. Zhou, H. X., and Gilson, M. K. (2009) Theory of free energy and entropy in noncovalent binding. *Chem Rev* 109, 4092-4107.
113. Woo, H. J., and Roux, B. (2005) Calculation of absolute protein-ligand binding free energy from computer simulations. *Proc Natl Acad Sci U S A* 102, 6825-6830.
114. Mobley, D. L., Chodera, J. D., and Dill, K. a. (2006) On the use of orientational restraints and symmetry corrections in alchemical free energy calculations. *J Chem Phys* 125, 084902.
115. General, I. J., Dragomirova, R., and Meirovitch, H. (2011) Calculation of the Absolute Free Energy of Binding and Related Entropies with the HSMD-TI Method: The FKBP12-L8 Complex. *J Chem Theory Comput* 7, 4196-4207.
116. Wang, L., Berne, B. J., and Friesner, R. A. (2012) On achieving high accuracy and reliability in the calculation of relative protein-ligand binding affinities. *Proc Natl Acad Sci U S A* 109, 1937-1942.
117. Kumar, S., Rosenberg, J. M., Bouzida, D., Swendsen, R. H., and Kollman, P. A. (1992) The weighted histogram analysis method for free-energy calculations on biomolecules. I. The method. *J Comput Chem* 13, 1011-1021.
118. Souaille, M., and Roux, B. t. (2001) Extension to the weighted histogram analysis method: combining umbrella sampling with free energy calculations. *Comput Phys Comm* 135, 40-57.
119. Chipot, C., Pohorille, A. (2007) *Free Energy Calculations: Theory and Applications in Chemistry and Biology*, Springer Berlin Heidelberg New York.
120. Pohorille, A., Jarzynski, C., and Chipot, C. (2010) Good practices in free-energy calculations. *J Phys Chem B* 114, 10235-10253.

121. Illingworth, C. J., Morris, G. M., Parkes, K. E., Snell, C. R., and Reynolds, C. A. (2008) Assessing the Role of Polarization in Docking. *J Phys Chem A* 112, 12157-12163.
122. Davis, J. E., and Patel, S. (2010) Revised Charge Equilibration Parameters for More Accurate Hydration Free Energies of Alkanes. *Chem Phys Lett* 484, 173.
123. Miyamoto, S., and Kollman, P. A. (1993) Absolute and relative binding free energy calculations of the interaction of biotin and its analogs with streptavidin using molecular dynamics/free energy perturbation approaches. *Proteins* 16, 226-245.
124. Page, M. I., and Jencks, W. P. (1971) Entropic contributions to rate accelerations in enzymic and intramolecular reactions and the chelate effect. *Proc Natl Acad Sci U S A* 68, 1678-1683.
125. Liu, P., Dehez, F., Cai, W., and Chipot, C. (2012) A Toolkit for the Analysis of Free-Energy Perturbation Calculations. *J Chem Theory Comput* 8, 2606-2616.
126. Gumbart, J. C., Roux, B., and Chipot, C. (2013) Efficient determination of protein-protein standard binding free energies from first principles. *J Chem Theory Comput* 9, 3789-3798.
127. Jorgensen, W. L. (1989) Free energy calculations: a breakthrough for modeling organic chemistry in solution. *Acc Chem Res* 22, 184-189.
128. Kollman, P. (1993) Free energy calculations: Applications to chemical and biochemical phenomena. *Chem Rev* 93, 2395-2417.
129. Jorgensen, W. L., Chandrasekhar, J., Madura, J. D., Impey, R. W., and Klein, M. L. (1983) Comparison of simple potential functions for simulating liquid water. *J Chem Phys* 79, 926-935.
130. Maréchal, Y. (2007) The Hydrogen Bond: Formation, Thermodynamic Properties, Classification. In *The Hydrogen Bond and the Water Molecule*, pp 3-24, Elsevier, Amsterdam.
131. Maréchal, Y. (2007) The Water Molecule in (Bio)Macromolecules. In *The Hydrogen Bond and the Water Molecule*, pp 249-275, Elsevier, Amsterdam.
132. Jorgensen, W. L., and Ravimohan, C. (1985) Monte Carlo simulation of differences in free energies of hydration. *J Chem Phys* 83, 3050-3054.
133. Yu, Y. B., Privalov, P. L., and Hodges, R. S. (2001) Contribution of translational and rotational motions to molecular association in aqueous solution. *Biophys J* 81, 1632-1642.

134. Deng, Y., and Roux, B. (2009) Computations of standard binding free energies with molecular dynamics simulations. *J Phys Chem B* 113, 2234-2246.
135. Swanson, J. M. J., Henchman, R. H., and McCammon, J. A. (2004) Revisiting free energy calculations: a theoretical connection to MM/PBSA and direct calculation of the association free energy. *Biophys J* 86, 67-74.
136. Im, W., Bernèche, S., and Roux, B. (2001) Generalized solvent boundary potential for computer simulations. *J Chem Phys* 114, 2924-2937.
137. Bennett, C. H. (1976) Efficient estimation of free energy differences from Monte Carlo data. *J Comp Phys* 22, 245-268.

CHAPTER 2

2 METHODS

2.1 Modeling the binding of DAT inhibitors

2.1.1 DAT homology models

The FASTA sequence of rat dopamine transporter (DAT) protein (SwissProt locus SC6A3_RAT; accession number P23977; NCBI accession number AAB21099) was used and aligned to template the homologous, bacterial, *Aquifex aeolicus* leucine transporter (LeuT_{Aa}) from Protein Data Bank (PDB) entry 2A65.^{1, 2} The best model obtained using the Robetta server (<http://robetta.bakerlab.org>), a full-chain protein structure prediction server, was chosen based on docking energies for dopamine and amphetamine in the Molecular Operating Environment (MOE) software (v2008.10).³⁻⁵ Hydrogen atoms were added and partial charges assigned using the AMBER99⁶ all-atom force field, and the model was minimized followed by 35 ns of classical MD on the model before the protein was embedded in a membrane.⁴ The final protein model represented an outward-facing conformation lacking the DAT N-terminal cytoplasmic tail (residues 1 – 59).

The newly constructed DAT model was embedded in a 1-palmitoyl-2-oleoyl-sn-glycero-3-phosphoethanolamine (POPE) bilayer created with the Membrane Builder plugin of VMD.⁷ The system was solvated with approximately 32,000 TIP3P water

molecules distributed on either side of the membrane. 0.2 M NaCl was added using the Autoionize plugin of VMD to achieve an overall neutral system. The single bilayer system was duplicated, reflected, and translated in the z-direction to be merged with the original to create a dual bilayer system. One DAT model was in a bound state (two sodium ions, one dopamine molecule) and the other represented an unbound apoprotein (APO) state. Additionally, two dopamine molecules were added to the extracellular bath. The final system size was 118 Å x 118 Å x 227 Å with 274,292 atoms.

The complete dual bilayer system was minimized for 40,000 steps with a 1 femtosecond (fs) timestep. The system was equilibrated from 100 K to 300 K in 10 K increments over a period of 50,000 steps. The equilibrated DAT system was simulated using the Nanoscale Molecular Dynamics (NAMD) (v2.10b1) to produce 600 nanoseconds (ns) of production time with a 2 fs timestep. The Langevin thermostat was utilized and set to 300 K; the Langevin piston was used for an isobaric-isothermal (NPT) ensemble with periodic boundary conditions. Particle mesh Ewald (PME)⁸ was used for electrostatics, with a grid spacing of 1.0 Å.

2.1.2 System preparation and simulation details

The trajectory of DAT was superposed with the coordinates of the inward-facing (IF) LeuT (PDB entry 3TT3)⁹ and outward-facing (OF) dDAT (PDB entry 4M48)¹⁰ crystal structures. The root-mean-square deviation (RMSD) was measured for the C α atoms of TM1- 12 with reference to the outward-facing crystal structure of dDAT¹⁰ and the inward-facing crystal structure of LeuT⁹ (**Figure 1.5**). N- and C-terminal tails, as well as the extracellular and intracellular loops, were excluded from the RMSD calculations.

Sodium and chloride ions (2 Na⁺, 1 Cl⁻) were included in the DAT homology models based on ion coordinates within the crystal structures of LeuT⁹ and dDAT.¹⁰⁻¹² Each protein system was inserted into a 110 Å x 110 Å POPE lipid membrane using the CHARMM-GUI Membrane Builder.¹³⁻¹⁸ The system was solvated with the TIP3P¹⁹ water model and ion concentration of 0.15 M NaCl. The final system size was 123 Å x 123 Å x 105 Å and with approximately 110,000 atoms.

A 50 picosecond (ps) energy minimization was performed on the APO DAT models to eliminate steric clashes. A 10 ns equilibration was carried out with harmonic restraints placed on the protein backbone atoms (C α , N) with a force constant of 1.0 kcal/mol/Å. MD was performed without the harmonic restraints for an additional 10 ns. The MD was conducted with the NPT ensemble in NAMD (v2.10b1) with PBC. Langevin dynamics and the damping Langevin piston were utilized to maintain 310 K temperature and 1 atm pressure, respectively, with a damping coefficient of 10.0 ps⁻¹. The Langevin piston was assigned a target pressure of 1 atm, an oscillation period of 100 fs, and a damping timescale of 50 fs. A cutoff distance of 12.0 Å was applied for short-range electrostatic, and a switch distance of 8.0 Å was used for van der Waals (vdW) interactions. The PME algorithm was used to estimate the long-range electrostatic interactions with, a grid spacing of 1.0 Å.⁸ A time step of 2 fs was utilized for the integration of motion for short- and long-range interactions.

The OF and IF DAT systems were used for modeling the binding of the DAT inhibitors (cocaine, benzotropine (BZT), LX10, and LX11). MOE (v2013.0802)³ was used to generate docked poses of cocaine, BZT, LX10 or LX11 within the primary binding site (S1) of the OF and IF DAT models. The docking site was defined with the placement of

dummy atoms using the Site Finder tool of MOE. The induced fit docking protocol was implemented using the Triangle Matcher placement method and refined with the Amber10: EHT force field. The docked poses for each molecule were London dG-scored (MOE)³ and the top scoring poses were evaluated for intermolecular interactions with DAT residues similar to those seen in the 4M48 crystal structure with dDAT bound to nortriptyline.¹⁰

To generate the DAT-inhibitor systems, first cocaine was docked into S1 of APO OF DAT and BZT docked into S1 of APO IF DAT and the systems were simulated for 5 ns with MD. In the OF DAT, cocaine was replaced by BZT, LX10, and LX11 for each subsequent DAT-inhibitor complex in the outward-facing conformation. In the IF DAT, BZT was replaced by cocaine, LX10, and LX11 to create DAT-inhibitor complexes in the IF DAT conformation.

The CHARMM36 force field was used for parameterizing the protein, lipid, and water molecules in all MD simulations.^{16, 18, 20, 21} Force field parameters previously developed for cocaine were used, and force field parameters for BZT, LX10 and LX11 were obtained from the ParamChem web server (v0.9.7.1) with the v2b8 CHARMM General Force Field (CGenFF), which is compatible with the CHARMM36 force field.^{20, 22} The 8 DAT-inhibitor systems and two APO DAT systems were subjected to 100 ns of MD.

2.1.3 Solvent accessibility surface area analysis

Solvent accessibility surface area (SASA) for DAT residues was measured using VMD.⁷ Residues for the external cavity were defined by DAT residues lining the

extracellular pathway above the externally-accessible gating residue pairs in the trans-membrane domains surrounding the binding site: Y88 (TM1), W84 (TM1), R85 (TM1), F155 (TM3), I311 (TM6), D312 (TM6), T315 (TM6), D475 (TM10), T481 (TM10). Residues for the internally open cavity were defined by selected residues that line the cytoplasmic pathway: F69 (TM1), G75 (TM1), G257 (TM5), S261 (TM5), V265 (TM5), T268 (TM5), F331 (TM6), G424 (TM8), E427 (TM8) and T431 (TM8). Heavy atoms of selected residues were determined to be solvent-accessible with a 1.4 Å probe radius.

2.2 Lead optimization of a SERT inhibitor

2.2.1 Relative free energy calculations of ethane to methanol

Free energy of hydration for ethane to methanol in a solvent water box was calculated using free energy perturbation (FEP)/ MD simulations. The alchemical transformation was carried out bi-directionally in separate free energy calculations for the coupling and decoupling of the atoms with the solvent.^{23, 24} At the beginning of the simulation ($\lambda = 0$), only the atoms of ethane are interacting with the solvent (**Figure 2.1**). Then the vdW and electrostatic interactions of the atoms belonging to ethane are scaled down to zero while the vdW and electrostatic interactions of the atoms belonging to methanol are introduced. At the end of the simulation ($\lambda = 1$), only the atoms of methanol are interacting with the solvent. The reverse alchemical transformation was also performed ($\lambda = 1$ to 0), where the atoms of methanol vanish and ethane appears in its position.

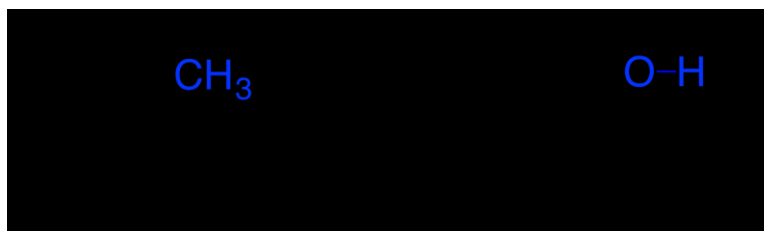


Figure 2.1: Alchemical transformation of ethane to methanol. Charges for the atoms are listed under each atom group. Atom charges are assigned from Jorgensen *et al.*^{21, 25} For ethane: each methyl group is given a charge of 0.000; for methanol: the methyl group has a charge of 0.265, the oxygen atom is given a charge of -0.700, and the hydrogen atom is given a charge of 0.435. At $\lambda = 0$ only the atoms of ethane are interacting with its environment. The vdW and electrostatic interactions of the methyl group belonging to ethane are scaled down to zero while the vdW and electrostatic interactions of the hydroxyl group belonging to methanol are introduced. At $\lambda = 1$ only the atoms of methanol are interacting with its environment. 25 λ -windows of even distribution ($\Delta\lambda = 0.04$) were used for the transformation.

A dual topology was used to generate the coordinate file with atoms of ethane and methanol represented. Charges used by Jorgensen *et al.*²⁵ were assigned to the atoms of ethane and methanol (**Figure 2.1**). The molecule was solvated with 340 TIP3P water molecules using VMD.^{7, 19} A series of free energy perturbation (FEP)/ MD simulations were carried out to perform the alchemical transformation. The bi-directional FEP simulation was performed over a reaction pathway stratified in 25 λ -windows of even distribution ($\Delta\lambda = 0.04$). The system was energy minimized for 25 ps followed by 800 ps FEP simulation in NAMD v2.9 in the NPT ensemble with periodic boundary conditions at 300 K and 1 atm.²⁶ The statistical data accrued in the coupling and decoupling simulations were combined using the Bennett acceptance ratio (BAR).²⁷ The BAR was used as part of the ParseFEP plugin in VMD to provide a maximum-likelihood estimator of the free energy change.^{26, 28, 29}

2.2.2 Free energy calculation of T4 lysozyme to FK5

The protocol outlined by Jo *et al.* for performing the ABFE calculation of T4 lysozyme bound to FK5 (PDB entry 1FKJ) was followed, and results were reproduced (**Figure 2.2**).³⁰ The structure of T4 lysozyme bound to FK5 was obtained from the RCSB protein databank and uploaded to the CHARMM-GUI *Ligand Binder* Web interface. The force field parameters defined in the CHARMM standard force field were used for defining the protein atoms. The CGenFF force field parameters for FK5 was automatically generated with the ligand structure file obtained from the unmodified PDB entry. The generated force field for the ligand had a charge penalty of about 100 and a parameter penalty of about 141. Optimization was not performed by Jo *et al.* therefore an optimization was not attempted in this work.

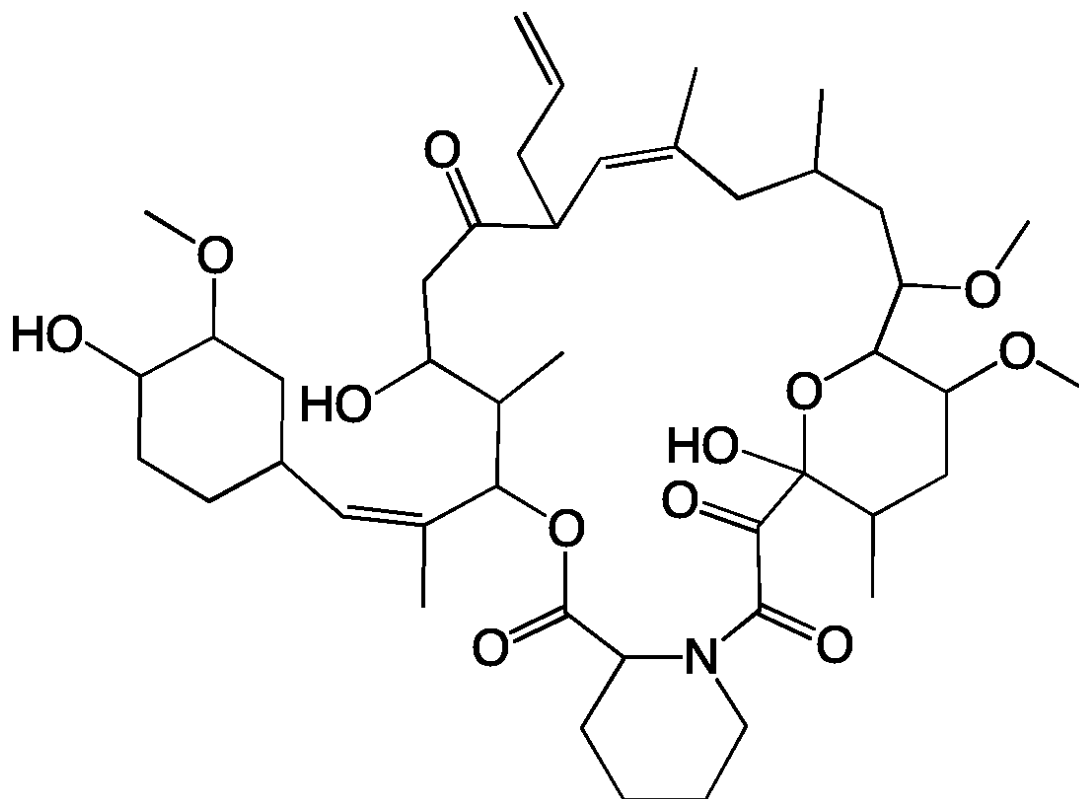


Figure 2.2: Structure of K506 (FK5) ligand.³⁰ The force field for FK5 was automatically generated by CGenFF v2b8 with the ligand structure files obtained from the PDB entry 1FKJ.

The protein-ligand complex was solvated in a spherical water box for a reduced system. The extent of the ligand was determined by the interface, and the size of the spherical water box was created for the bound and unbound states with an additional 10 Å and 5 Å from the extent of the ligand. The inner region was then extended by 3 Å to define a smooth spherical dielectric cavity. Water molecules within the outer region were treated implicitly with a dielectric constant of 1 inside the protein as well as the inner and extended regions, and 80 otherwise.³¹ The grand canonical Monte Carlo (GCMC) method was used to hydrate and equilibrate the inner regions. During the hydration 20 cycles of MC and MD simulation were used where each cycle consisted of 10,000 MC moves followed by 10,000 MD steps with a 2 fs time step. A harmonic restraint potential with a

force constant of $5.0 \text{ kcal/ (mol}\cdot\text{\AA}^2)$ was applied to the protein and the ligand molecule throughout the MD simulations. The simulations were carried out using Langevin dynamics at 300 K with a friction coefficient of 5 ps^{-1} assigned to all non-hydrogen atoms. After 20 cycles of GCMC/MD simulations, the protein–ligand complex was equilibrated for 200 ps at 300 K using Langevin dynamics without the positional harmonic restraint. The anchoring atoms for defining the protein-ligand translational and rotational restraints were chosen automatically by the Web server. The procedure for assigning the anchoring atoms are detailed by Jo *et al.*³⁰ The last 190 ps of equilibration was used to calculate the average reference distances, angles, and dihedrals for the translational/rotational restraints. The averaged and minimized ligand structure was used as the reference configuration for the conformational restraint. In the bulk solvent, the ligand molecule was equilibrated for 200 ps at 300 K using the SSBP (spherical solvent boundary potential) and Langevin dynamics.

The free energies associated with restriction of ligand conformation to the reference conformation (ΔG_{conf}), restriction of ligand orientation and translation ($\Delta G_{t,r}$), and interactions with surrounding environments (ΔG_{int}) were calculated with FEP/MD simulations. The FEP/MD simulations were divided into 137 independent windows. During the simulations, the perturbation energies for each state were collected.

The conformational free energies (ΔG_{conf}^{site} and ΔG_{conf}^{hydr}) associated with restricting the ligand conformation in the bound state were estimated by calculating the potential of mean force (PMF) as a function of ligand RMSD using umbrella sampling simulations.³⁰ Twenty-one biasing windows were used with the RMSD offset value from 0.0 to 5.0 Å in

steps of 0.25 Å. Each window was simulated using a force constant of 10 kcal/(mol·Å²) for 110 ps.

The CHARMM input files for the simulation generated by the CHARMM-GUI *Ligand Binder* tool were unchanged.^{14, 17, 18, 30} The reproduced calculations were compared to the results reported by Jo *et al.* and to the experimental binding free energy of T4 lysozyme bound to FK5.³⁰

2.2.3 Free energy calculation of LeuT substrates

The protocol outlined by Gumbart *et al.* was followed to perform the ABFE calculation of leucine in LeuT.³² The crystal structure of LeuT with leucine (PDB entry 3F3A)³³ was solvated using the TIP3P¹⁹ water model (71,000 and 8,000 for bound and unbound, respectively). The CHARMM36 force field was used to define all the atoms in the system.^{16, 20, 22, 34} The bound and unbound systems underwent an isobaric-isothermal (NPT) MD for 100 ps of minimization and thermalization followed by 300 ps of equilibration.

The coupling and decoupling of leucine binding in LeuT was performed in a bi-directional (forward/backward) alchemical transformation. A harmonic potential was placed on the orientation, position, and conformation of the ligand binding to bias the ligand-protein complex toward the bound state from the crystal structure (**Figure 2.3**). Harmonic restraints were applied to the translation (r, θ, ϕ) and the rotation (Θ, Φ, Ψ) of the ligand with respect to the protein (**Figure 1.13**). The introduced restraining potentials were used to maintain the position and orientation of the ligand around the adopted pose in the bound complex. The restraining potentials are intended to help enhance

configurational sampling and correctly handle the decoupled ligand states. Groups of atoms are defined to form the reference frame of the ligand (L_1, L_2, L_3), and the protein (P_1, P_2, P_3) and harmonic restraints are applied to the root-mean-square deviation (RMSD) with respect to the native conformation of the protein-ligand complex (**Figure 2.3**). The distance (r) between P_1 and L_1 was set to 5.5 Å. The angle (θ) formed by $P_2 - P_1 - L_1$ was set to 60.0°. The dihedral angle (ϕ) formed by $P_3 - P_2 - P_1 - L_1$ was set to -65.0°. The angle (Θ) formed by $P_1 - L_1 - L_2$ was set to 75.0°. The dihedral angle (Φ) formed by $P_2 - P_1 - L_1 - L_2$ was set to 50.0°. The dihedral angle (Ψ) formed by $P_1 - L_1 - L_2 - L_3$ was set to 103.0°. A force constant of 10.0 kcal/mol/Å² was applied to the distance and RMSD, and a force constant of 0.1 kcal/mol/Å² was applied to all the angles.

The simulations used NAMD2.9 with Langevin dynamics and an isobaric-isothermal (NPT) ensemble, where the temperature and pressure were kept constant at 300 K and 1 atm. Free energy perturbation was used for the reversible coupling of the ligand to its environment. In the bulk aqueous medium, 50- λ windows of even width were used. Each window consisted of 25,000 equilibration steps, followed by 75,000 data-collection steps at 2 fs time steps for a total simulation time of 10 ns. In the bound state, the ligand was reversibly coupled to the protein. 50- λ windows of even width were used with 50,000 steps of equilibration and 150,000 steps of data-collection at 1 fs time steps for a total simulation time of 10 ns. The forward and backward transformation for each state was combined using the BAR to calculate the maximum-likelihood estimator of the free energy change.^{27, 35, 36}

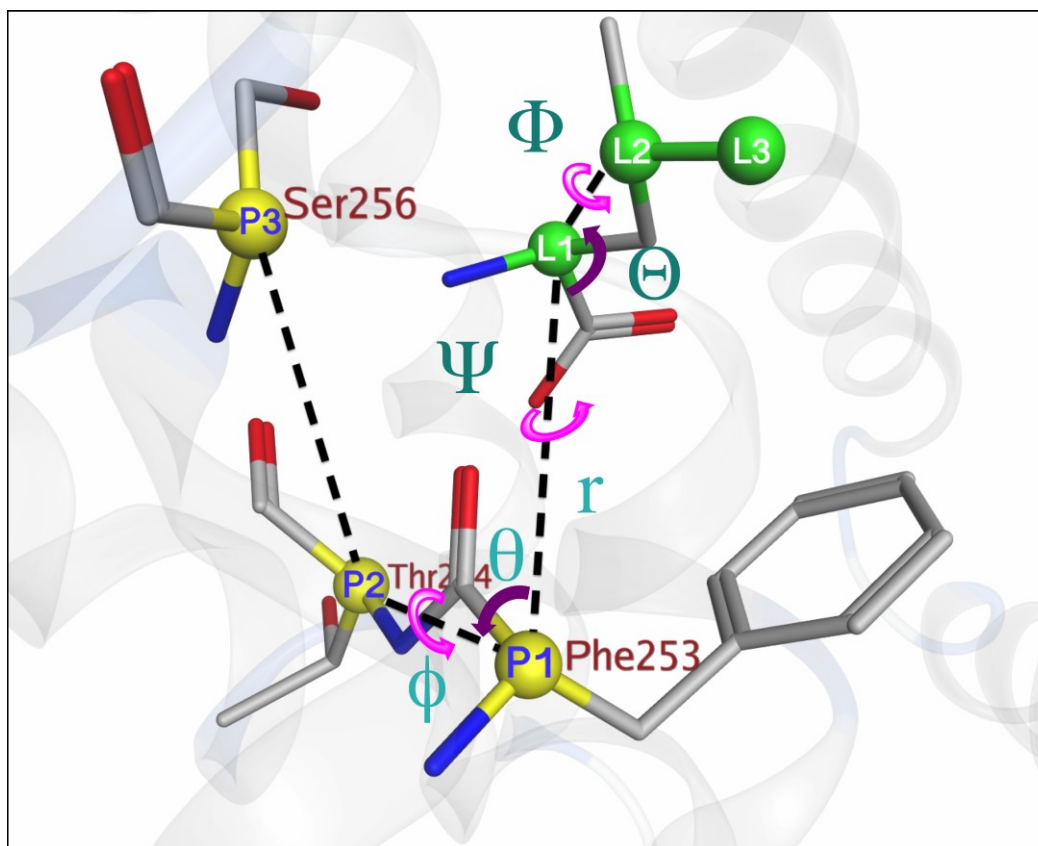


Figure 2.3: Reference frame defining the binding of leucine in LeuT (PDB entry 3F3A). Groups of atoms are defined to form the reference frame of the ligand (L_1 , L_2 , L_3) and the protein (P_1 , P_2 , P_3). Restraints are placed on the position (r , P_1 - L_1 distance; θ , P_1 - P_2 - L_1 angle; ϕ , P_3 - P_2 - P_1 - L_1 dihedral angle) and the translation (Θ , P_1 - L_1 - L_2 angle; Φ , P_1 - L_1 - L_2 - L_3 dihedral angle; Ψ , P_2 - P_1 - L_1 - L_2 dihedral angle) of leucine (green) with respect to LeuT (yellow), as well as restraints on its RMSD with respect to its binding conformation.

Calculation of the free energy contributions was carried out in the framework of thermodynamic integration (TI), within the collective variables (colvars) module of NAMD, where the free energy change is determined with numerical integration methods. The free energy contribution from the restraint potential acting on a collective variable was determined alchemically, by decreasing the force constant in a stepwise fashion from its nominal value to zero (similarly in the opposite direction using the coupling parameter). The nominal value of the force constant (k) represents the value of the force

constant at $\lambda = 1$, i.e., k_1 . At $\lambda = 0$, the force constant, k_0 , is equal to 0 kcal/mol/Å². The restraint potentials were scaled over 6 ns using 14 $-\lambda$ windows. For each value of λ and for each defined collective variable, $dG/d\lambda$ was computed. The free energy contribution due to the respective harmonic restraint is obtained by integrating the gradient profile. This allowed for calculations of the individual contributions from the restraint potentials.

2.2.4 Free energy calculation of fluoxetine in SERT

The SERT homology model previously developed by Manepalli *et al.* was used for all docking and free energy calculations performed in SERT.³⁷ R-fluoxetine was docked into the S2 binding site of SERT using the induced fit protocol in MOE (**Figure 2.4**). Triangle Matcher was the docking placement method, London dG was the initial scoring method, and the Amber10: EHT force field was used to refine the interactions. GBVI/WSA dG was used as the final scoring method. A maximum of 30 poses was retained during the docking simulations (with duplicates removed). The top-scoring pose was selected for free energy calculations. The protein-ligand complex was used for ABFE calculations following the protocol outlined by Jo *et al.* The CHARMM-GUI *Ligand Binder* web server was used to generate the CHARMM input files used to calculate the ABFE of R-fluoxetine in SERT (**Figure 2.4**). The force field for R-fluoxetine and SERT were defined using CHARMM CGenFF v2b8.^{20, 22} Optimization was not performed on force field parameters. The input files from *Ligand Binder* were unmodified.

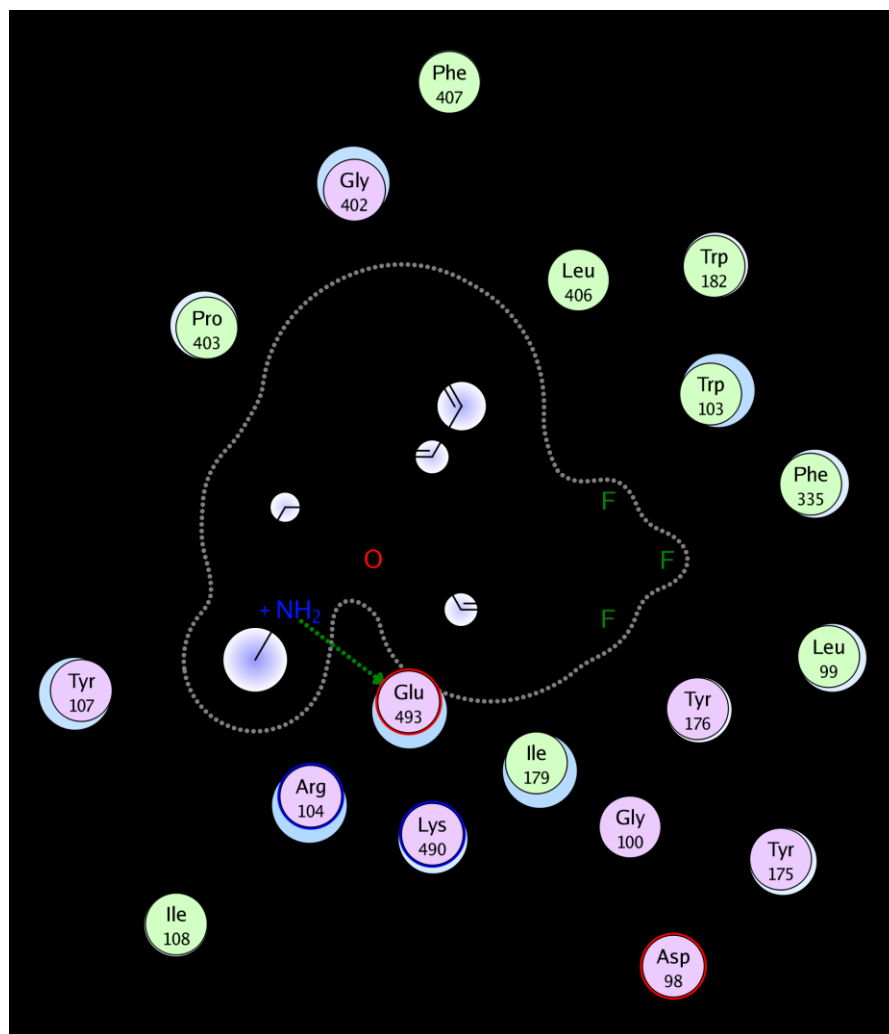


Figure 2.4: Binding interactions of the docked pose of R-fluoxetine within the S2 binding site of SERT. R-fluoxetine was docked into SERT using the induced fit protocol in MOE. Docked poses were scored and ranked using the London dG scoring function. The top-scoring pose was subjected to visual inspection for optimal intermolecular interactions with SERT residues. The dashed green arrow represents a potential hydrogen bond interaction between the amine of R-fluoxetine and the side-chain of Glu493.

The protein-ligand complex was solvated in a spherical water box for a reduced system. The extent of the ligand was determined by the interface and the size of the spherical water box was determined for the bound and unbound states with an additional 10 Å and 5 Å from the extent of the ligand. Twenty cycles of MC and MD simulation were used and each cycle consisted of 10,000 MC moves followed by 10,000 MD steps

with a 2 fs time step to hydrate and equilibrate the inner regions. A harmonic restraint potential with a force constant of 5.0 kcal/ (mol·Å²) was applied to the protein and the ligand molecule throughout the MD simulations. The simulations were carried out using Langevin dynamics at 300 K with a friction coefficient of 5 ps⁻¹ assigned to all non-hydrogen atoms. Then the protein–ligand complex was equilibrated for 200 ps at 300 K using Langevin dynamics without the positional harmonic restraint. The anchoring atoms for defining the protein-ligand translational and orientational restraints were chosen automatically by the *Ligand Binder* Web server. The procedure for assigning the anchoring atoms are detailed by Jo *et al.*³⁰ The last 190 ps of equilibration was used to calculate the average reference distances, angles, and dihedrals for the translational/orientational restraints. The averaged and minimized ligand structure was used as the reference configuration for the conformational restraint. In the bulk solvent, the ligand molecule was equilibrated for 200 ps at 300 K using the SSBP and Langevin dynamics.

The free energies associated with restriction of the ligand conformation to the reference conformation (ΔG_{conf}), restriction of the ligand orientation and translation ($\Delta G_{t,r}$), and interactions with surrounding environments (ΔG_{int}) were calculated with FEP/MD simulations. The FEP/MD simulations were divided into 137 independent windows. The conformational free energies (ΔG_{conf}^{site} and ΔG_{conf}^{hydr}) associated with restricting the ligand conformation in the bound state was estimated by calculating the potential of mean force (PMF) as a function of ligand RMSD using umbrella sampling simulations.³⁰ Twenty-one biasing windows were used with the RMSD offset value from 0.0 to 5.0 Å in steps of 0.25 Å. Each window was simulated using a force constant of 10

kcal/(mol·Å²) for 110 ps. Then the perturbation energies associated with the bound and unbound was calculated.

2.2.5 Free energy calculation of SM11 in SERT

SM11 was docked into the S1 and S2 pockets of SERT using an induced fit docking protocol with the MOE software (v2013.0802) (**Figure 2.5, Figure 2.6**).³ Triangle Matcher was the docking placement method, London dG was the initial scoring method, and the Amber10: EHT force field was used to refine the interactions. GBVI/WSA dG was used as the final scoring method. A maximum of 30 poses was retained during the docking simulations (with duplicates removed). The top-scoring pose was subjected to visual inspection for optimal intermolecular interactions with SERT residues. One pose in S1 was found to bind with similar orientation to the pharmacophore developed based on the proposed binding in MAT crystal structures (**Figure 2.6**).³⁸ The final docked binding pose of SM11 in SERT overlapped with the binding of the S-citalopram molecule in the S2 site of the crystal structure of SERT (**Figure 2.5**).³⁹

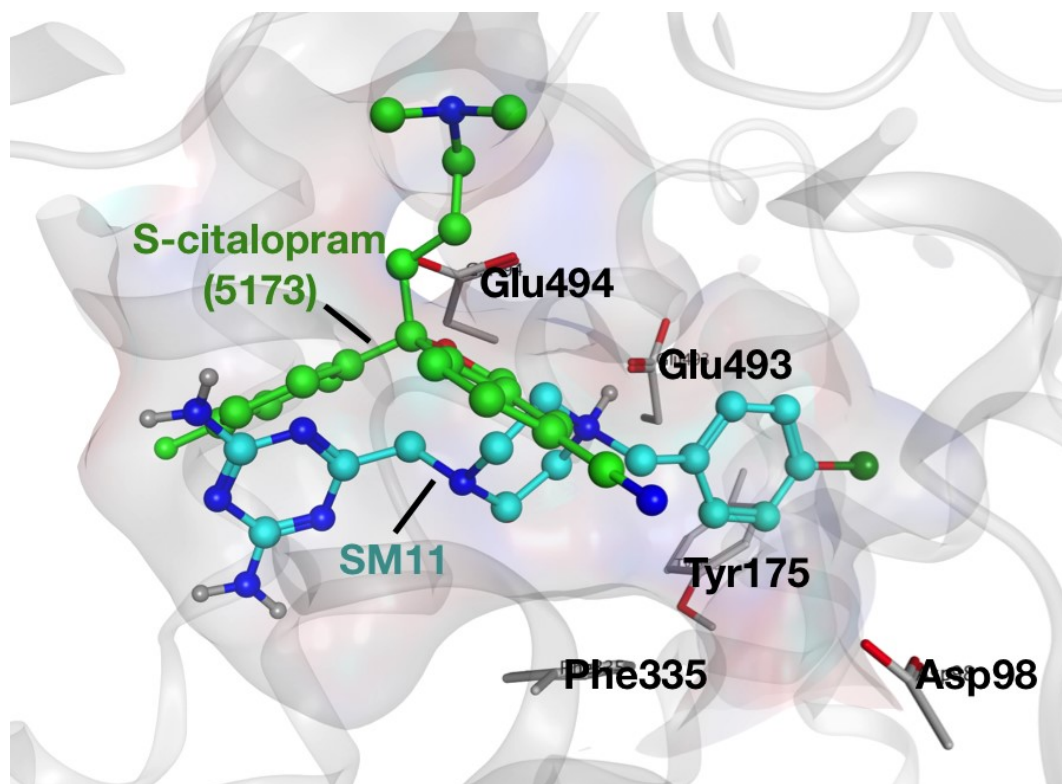


Figure 2.5: SM11 (cyan ball-and-stick) in S2 of SERT overlapped with S-citalopram (green ball-and-stick) in SERT co-crystal 5I73.³⁹ SERT homology model coordinates were superposed with SERT crystal structure coordinates. Residues from SERT crystal structure are shown for the S2 binding site.

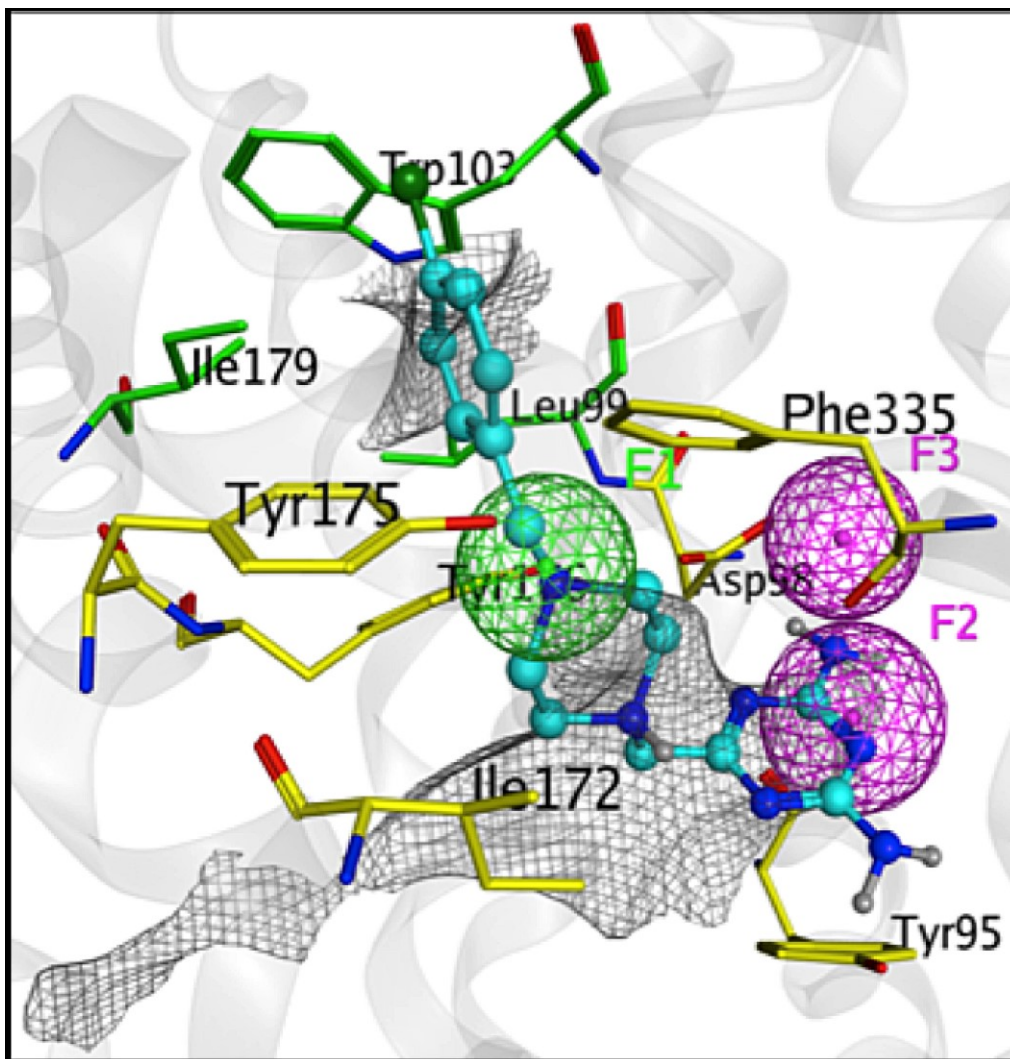


Figure 2.6: SM11 (cyan ball-and-stick) in S1 of SERT. S1 residues are colored in yellow sticks and S2 residues are colored in green sticks. Color spheres represent pharmacophore features used to dock SM11 in S1 with MOE.³ F1: Donor (green), F2: Acceptor (magenta), and F3: Acceptor (magenta) each with a radius of 1 Å.

The Nanoscale Molecular Dynamics (NAMD) program (v2.9b1) was used for performing the free energy calculations.²⁶ The Langevin dynamics was used with an isobaric-isothermal ensemble (NPT), where the temperature and pressure were kept constant at 300 K and 1 atm. Free energy perturbation (FEP) was used for the reversible coupling of the ligand with its environment in the bound and unbound state. During the

alchemical transformation in the bound state, several harmonic restraints were placed on the ligand to prevent deviation from the binding pocket once the electrostatic and vdW interactions were turned off.^{6, 32, 40, 41} Groups of heavy atoms were defined to form the reference frame of the ligand (L_1, L_2, L_3) and the protein (P_1, P_2, P_3). For the ligand, the methylene bridge connecting the 4-chlorobenzyl to the 6-4-piperazine, and the 6-4-piperazine to the 1,3,5-triazine-2,4-diamine were used to define L_1 , and L_2 . L_3 was defined by the cyclic amine at the 1-position of the 1,3,5-triazine-2,4-diamine. For the protein, the center of mass for the backbone atoms ($C\alpha, N, O$) of residues Phe335, Tyr175, Tyr176 were used to define P_1, P_2, P_3 , respectively. Harmonic restraints were applied on the position (r, θ, ϕ), and the translation (Θ, Φ, Ψ) of the ligand with respect to the protein (**Figure 2.7**). Harmonic restraints were also applied on the ligand RMSD with respect to the native conformation in the protein-ligand complex. The distance (r) between P_1 and L_1 was set to 5.5 Å. The angle (θ) formed by $P_2 - P_1 - L_1$ was set to 42.0°. The dihedral angle (ϕ) formed by $P_3 - P_2 - P_1 - L_1$ was set to 111.0°. The angle (Θ) formed by $P_1 - L_1 - L_2$ was set to 31.0°. The dihedral angle (Φ) formed by $P_2 - P_1 - L_1 - L_2$ was set to -111.0°. The dihedral angle (Ψ) formed by $P_1 - L_1 - L_2 - L_3$ was set to -32.0°. A force constant of 10.0 kcal/mol/Å² was applied to the distance and RMSD, and a force constant of 0.1 kcal/mol/Å² was applied to all the angles. The free energies associated with the translational, rotational ($\Delta\Delta G_{t,r}$) and conformational ($\Delta\Delta G_{conf}$) restraints were calculated for contribution to the standard binding free energy of the ligand to the protein.³⁰ Calculations were applied in the bound state of ligand interacting in the protein binding pocket as well as in the unbound state of the ligand interacting in bulk aqueous solvent.

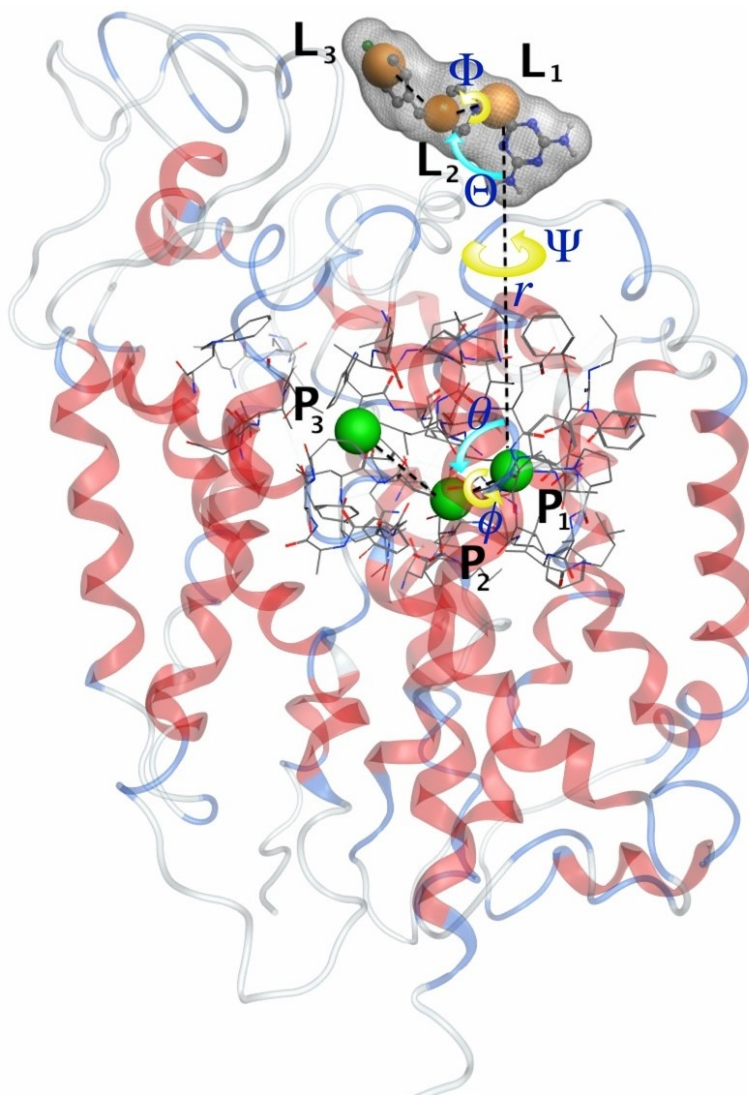


Figure 2.7: Groups of atoms to define the reference frame of SM11 (L_1 , L_2 , L_3) binding to SERT (P_1 , P_2 , P_3). These harmonic restraint potentials act to prevent SM11 from deviating from its binding site during perturbation. Restraints are placed on the position (r , P_1 - L_1 distance; θ , P_1 - P_2 - L_1 angle; ϕ , $P_3 - P_2 - P_1 - L_1$ dihedral angle) and the translation (Θ , $P_1 - L_1 - L_2$ angle; Φ , $P_1 - L_1 - L_2 - L_3$ dihedral angle; Ψ , $P_2 - P_1 - L_1 - L_2$ dihedral angle) of SM11 with respect to SERT, as well as restraints on the ligand RMSD with respect to its binding conformation.

In the bulk aqueous medium, 50 windows of even width were used. Each window consisted of 25,000 equilibration steps, followed by 75,000 data collection steps at 2 fs

time steps for a total simulation time of 10 ns. In the bound state, the ligand was reversibly coupled to the protein. 50 windows of even width were used with 50,000 steps of equilibration and 150,000 steps of data collection at 1 fs time steps for a total simulation time of 10 ns. The bidirectional transformation was performed for both the bound and unbound states, where the data for the coupling and decoupling of the ligand were combined using the Bennett acceptance ratio (BAR) to calculate the maximum-likelihood estimate of the free energy change.²⁷

The *Ligand Binder* web server was also used to generate CHARMM input files for calculating the absolute binding free energy of SM11 in SERT with harmonic restraints placed on the ligand.^{14, 18, 30} The CHARMM input files generated by *Ligand Binder* were not modified.

2.2.6 Measuring the affinity of SERT inhibitors

Stably-transfected human embryonic kidney (HEK)-293-hSERT cells were previously prepared in collaboration with Dr. Mads Larsen and Dr. Susan Amara (University of Pittsburgh, Pittsburgh, PA).³⁷ The HEK293-hSERT were incubated at 37 °C in a 5% CO₂ environment. Once the cells reached approximately 90% confluence, the culture was washed with 10 mL cold phosphate-buffered saline (DPBS) before being scraped from the culture plates and transferred to 15 mL culture tubes. The solution was centrifuged at low speed (700 g) for 10 min. The supernatant was removed and 500 µL cold TE buffer (50 mM Tris, pH 7.5, 1mM EDTA) was added to the cell pellet for resuspension. Homogenate was transferred to cold 1.5 mL microcentrifuge tubes and centrifuged at 100 000g at 4 °C for 30 min (Sorvall Discovery M150 centrifuge). The

supernatant was discarded, and the pellet was resuspended in cold binding buffer (50 mM Tris, pH 7.5, 100 mM NaCl) for competitive membrane binding.

The competitive membrane binding assay was used to measure the affinity of citalopram, SM11 and SM11 analogs (BJ11, BJ12, BJ13, and BJ14) for SERT. SM11 and BJ11 were purchased from Enamine.³⁷ BJ12, BJ13, and BJ14 were synthesized by Dr. Robert B. Lettan II (Chatham University). The affinity for SERT was determined by the ligand's ability to displace [¹²⁵I]-RTI-55, a radiolabeled cocaine analog with high-affinity for SERT, from binding to SERT as a function of increasing concentrations of the non-radioactive drug. Increasing concentrations of citalopram (10 μM to 1 nM), SM11 and SM11 analogs (1 nM to 1 mM) were used for the binding assays, which were performed in triplicate (n=3). [¹²⁵I]-RTI-55 inhibition was measured using a gamma-radiation counter to measure how much of [¹²⁵I]-RTI-55 was present at different concentrations of the non-radioactive drugs. [¹²⁵I]-RTI-55 was purchased from PerkinElmer (Foster City, CA).⁴²

The membranes were placed in solution with 0.1 nM concentration of [¹²⁵I]-RTI-55. A serial dilution of non-radioactive drugs was added to the membrane solution. Paroxetine at 10 μM concentration was used to measure nonspecific binding. The solutions were incubated at room temperature for one hour with gentle shaking followed by filtration through GF/B filters (presoaked in 0.5% polyethyleneimine solution (v/v)). A Beckman gamma counter was used to measure the presence of [¹²⁵I]-RTI-55 to determine how much citalopram was able to compete with radioligand binding. The measured affinity (K_i) was analyzed using GraphPad Prism 5.0. The K_i of the inhibitor was determined using the Cheng-Prusoff equation,

$$K_i = \frac{IC_{50}}{1 + \frac{[[^{125}\text{I}]-\text{RTI}-55]}{K_d}} \quad (2.1)$$

where IC_{50} is the inhibitor concentration required to displace 50% of the radioligand, $[[^{125}\text{I}]-\text{RTI}-55]$ is the radioligand concentration, and K_d is the dissociation constant of the radioligand.

2.3 References

1. Yamashita, A., Singh, S. K., Kawate, T., Jin, Y., and Gouaux, E. (2005) Crystal structure of a bacterial homologue of Na⁺/Cl⁻-dependent neurotransmitter transporters. *Nature* 437, 215-223.
2. Berman, H. M., Battistuz, T., Bhat, T. N., Bluhm, W. F., Bourne, P. E., Burkhardt, K., Feng, Z., Gilliland, G. L., Iype, L., Jain, S., Fagan, P., Marvin, J., Padilla, D., Ravichandran, V., Schneider, B., Thanki, N., Weissig, H., Westbrook, J. D., and Zardecki, C. (2002) The Protein Data Bank. *Acta Crystallogr D Biol Crystallogr* 58, 899-907.
3. MOE (The Molecular Operating Environment). (2017) 2015.08 ed., Chemical Computing Group Inc., 1010 Sherbrooke St. W, Suite 910 Montreal, Quebec, Canada H3A 2R7.
4. Gedeon, P. C., et al. (2010) Molecular dynamics of leucine and dopamine transporter proteins in a model cell membrane lipid layer. *Proteins* 78, 797-811.
5. Indarte, M., Madura, J. D., and Surratt, C. K. (2008) Dopamine transporter comparative molecular modeling and binding site prediction using the LeuT(Aa) leucine transporter as a template. *Proteins* 70, 1033-1046.
6. Wang, J., Cieplak, P., and Kollman, P. A. (2000) How well does a restrained electrostatic potential (RESP) model perform in calculating conformational energies of organic and biological molecules? *J Comput Chem* 21, 1049-1074.
7. W Dalke, A., and Schulten, K. (1996) VMD: Visual Molecular Dynamics. *J Mol Graph* 14, 33-38, 27-38.
8. Essmann, U., Perera, L., Berkowitz, M. L., Darden, T., Lee, H., and Pedersen, L. G. (1995) A smooth particle mesh Ewald method. *J Chem Phys* 103, 8577-8593.

9. Krishnamurthy, H., and Gouaux, E. (2012) X-ray structures of LeuT in substrate-free outward-open and apo inward-open states. *Nature* 481, 469-474.
10. Penmatsa, A., Wang, K. H., and Gouaux, E. (2013) X-ray structure of dopamine transporter elucidates antidepressant mechanism. *Nature* 503, 85-90.
11. Pramod, A. B., Foster, J., Carvelli, L., and Henry, L. K. (2013) SLC6 transporters: structure, function, regulation, disease association and therapeutics. *Mol Aspects Med* 34, 197-219.
12. Forrest, L. R., Tavoulari, S., Zhang, Y. W., Rudnick, G., and Honig, B. (2007) Identification of a chloride ion binding site in Na⁺/Cl⁻-dependent transporters. *Proc Natl Acad Sci U S A* 104, 12761-12766.
13. Jo, S., Kim, T., and Im, W. (2007) Automated builder and database of protein/membrane complexes for molecular dynamics simulations. *PLoS One* 2, e880.
14. Jo, S., Kim, T., Iyer, V. G., and Im, W. (2008) CHARMM-GUI: a web-based graphical user interface for CHARMM. *J Comput Chem* 29, 1859-1865.
15. Jo, S., Lim, J. B., Klauda, J. B., and Im, W. (2009) CHARMM-GUI Membrane Builder for mixed bilayers and its application to yeast membranes. *Biophys J* 97, 50-58.
16. Klauda, J. B., Venable, R. M., Freites, J. A., O'Connor, J. W., Tobias, D. J., Mondragon-Ramirez, C., Vorobyov, I., MacKerell, A. D., Jr., and Pastor, R. W. (2010) Update of the CHARMM all-atom additive force field for lipids: validation on six lipid types. *J Phys Chem B* 114, 7830-7843.
17. Wu, E. L., Cheng, X., Jo, S., Rui, H., Song, K. C., Davila-Contreras, E. M., Qi, Y., Lee, J., Monje-Galvan, V., Venable, R. M., Klauda, J. B., and Im, W. (2014) CHARMM-GUI Membrane Builder toward realistic biological membrane simulations. *J Comput Chem* 35, 1997-2004.
18. Lee, J., Cheng, X., Swails, J. M., Yeom, M. S., Eastman, P. K., Lemkul, J. A., Wei, S., Buckner, J., Jeong, J. C., Qi, Y., Jo, S., Pande, V. S., Case, D. A., Brooks, C. L., 3rd, MacKerell, A. D., Jr., Klauda, J. B., and Im, W. (2016) CHARMM-GUI Input Generator for NAMD, GROMACS, AMBER, OpenMM, and CHARMM/OpenMM Simulations Using the CHARMM36 Additive Force Field. *J Chem Theory Comput* 12, 405-413.
19. Jorgensen, W. L., Chandrasekhar, J., Madura, J. D., Impey, R. W., and Klein, M. L. (1983) Comparison of simple potential functions for simulating liquid water. *J Chem Phys* 79, 926-935.
20. Vanommeslaeghe, K., Hatcher, E., Acharya, C., Kundu, S., Zhong, S., Shim, J., Darian, E., Guvench, O., Lopes, P., Vorobyov, I., and Mackerell, A. D., Jr. (2010)

CHARMM general force field: A force field for drug-like molecules compatible with the CHARMM all-atom additive biological force fields. *J Comput Chem* 31, 671-690.

21. Best, R. B., Zhu, X., Shim, J., Lopes, P. E., Mittal, J., Feig, M., and Mackerell, A. D., Jr. (2012) Optimization of the additive CHARMM all-atom protein force field targeting improved sampling of the backbone phi, psi and side-chain chi(1) and chi(2) dihedral angles. *J Chem Theory Comput* 8, 3257-3273.

22. Yu, W., He, X., Vanommeslaeghe, K., and MacKerell, A. D., Jr. (2012) Extension of the CHARMM General Force Field to sulfonyl-containing compounds and its utility in biomolecular simulations. *J Comput Chem* 33, 2451-2468.

23. Kollman, P. (1993) Free energy calculations: Applications to chemical and biochemical phenomena. *Chem Rev* 93, 2395-2417.

24. Miyamoto, S., and Kollman, P. A. (1993) Absolute and relative binding free energy calculations of the interaction of biotin and its analogs with streptavidin using molecular dynamics/free energy perturbation approaches. *Proteins* 16, 226-245.

25. Jorgensen, W. L., and Ravimohan, C. (1985) Monte Carlo simulation of differences in free energies of hydration. *J Chem Phys* 83, 3050-3054.

26. Phillips, J. C., Braun, R., Wang, W., Gumbart, J., Tajkhorshid, E., Villa, E., Chipot, C., Skeel, R. D., Kale, L., and Schulten, K. (2005) Scalable molecular dynamics with NAMD. *J Comput Chem* 26, 1781-1802.

27. Bennett, C. H. (1976) Efficient estimation of free energy differences from Monte Carlo data. *J Comp Phys* 22, 245-268.

28. Liu, P., Dehez, F., Cai, W., and Chipot, C. (2012) A Toolkit for the Analysis of Free-Energy Perturbation Calculations. *J Chem Theory Comput* 8, 2606-2616.

29. Hémin, J., Harrison, C., and Chipot, C. (2012) *In Silico* alchemy: A tutorial for alchemical free-energy perturbation calculations with NAMD.

30. Jo, S., Jiang, W., Lee, H. S., Roux, B., and Im, W. (2013) CHARMM-GUI Ligand Binder for Absolute Binding Free Energy Calculations and Its Application. *J Chem Inf Model* 53, 267-277.

31. Im, W., Beglov, D., and Roux, B. (1998) Continuum Solvation Model: computation of electrostatic forces from numerical solutions to the Poisson-Boltzmann equation. *Computer Physics Communications* 111, 59-75.

32. Gumbart, J. C., Roux, B., and Chipot, C. (2013) Standard binding free energies from computer simulations: What is the best strategy? *J Chem Theory Comput* 9, 794-802.

33. Singh, S. K., Piscitelli, C. L., Yamashita, A., and Gouaux, E. (2008) A competitive inhibitor traps LeuT in an open-to-out conformation. *Science* 322, 1655-1661.
34. Mackerell, A. D., Jr., Feig, M., and Brooks, C. L., 3rd. (2004) Extending the treatment of backbone energetics in protein force fields: limitations of gas-phase quantum mechanics in reproducing protein conformational distributions in molecular dynamics simulations. *J Comput Chem* 25, 1400-1415.
35. Shirts, M. R., and Chodera, J. D. (2008) Statistically optimal analysis of samples from multiple equilibrium states. *J Chem Phys* 129, 124105.
36. Mobley, D. L., and Klimovich, P. V. (2012) Perspective: Alchemical free energy calculations for drug discovery. *J Chem Phys* 137, 230901.
37. Manepalli, S., Geffert, L. M., Surratt, C. K., and Madura, J. D. (2011) Discovery of novel selective serotonin reuptake inhibitors through development of a protein-based pharmacophore. *J Chem Inf Model* 51, 2417-2426.
38. Zhou, Z., Zhen, J., Karpowich, N. K., Goetz, R. M., Law, C. J., Reith, M. E. A., and Wang, D.-N. N. (2007) LeuT-desipramine structure reveals how antidepressants block neurotransmitter reuptake. *Science* 317, 1390-1393.
39. Coleman, J. A., Green, E. M., and Gouaux, E. (2016) X-ray structures and mechanism of the human serotonin transporter. *Nature* 532, 334-339.
40. Gumbart, J. C., Roux, B., and Chipot, C. (2013) Efficient determination of protein-protein standard binding free energies from first principles. *J Chem Theory Comput* 9, 3789-3798.
41. Wang, J., Deng, Y., and Roux, B. (2006) Absolute binding free energy calculations using molecular dynamics simulations with restraining potentials. *Biophys J* 91, 2798-2814.
42. Manepalli, S., Surratt, C. K., Madura, J. D., and Nolan, T. L. (2012) Monoamine transporter structure, function, dynamics, and drug discovery: a computational perspective. *AAPS J* 14, 820-831.

CHAPTER 3

3 MODELING THE BINDING OF DAT INHIBITORS IN DISCRETE DAT CONFORMATIONS

3.1 Introduction

The recreational psychostimulant cocaine inhibits dopamine reuptake from the synapse, resulting in excessive stimulation of postsynaptic dopamine receptors in brain areas associated with reward and addiction.¹ Cocaine binds to and stabilizes the outward- (extracellular-) facing conformation of the dopamine transporter (DAT) protein, while the low abuse potential DAT inhibitor benztropine prefers the inward- (cytoplasmic-) facing conformation (**Figure 3.1**). A correlation has been previously postulated between psychostimulant abuse potential and preference for the outward-facing DAT conformation.²

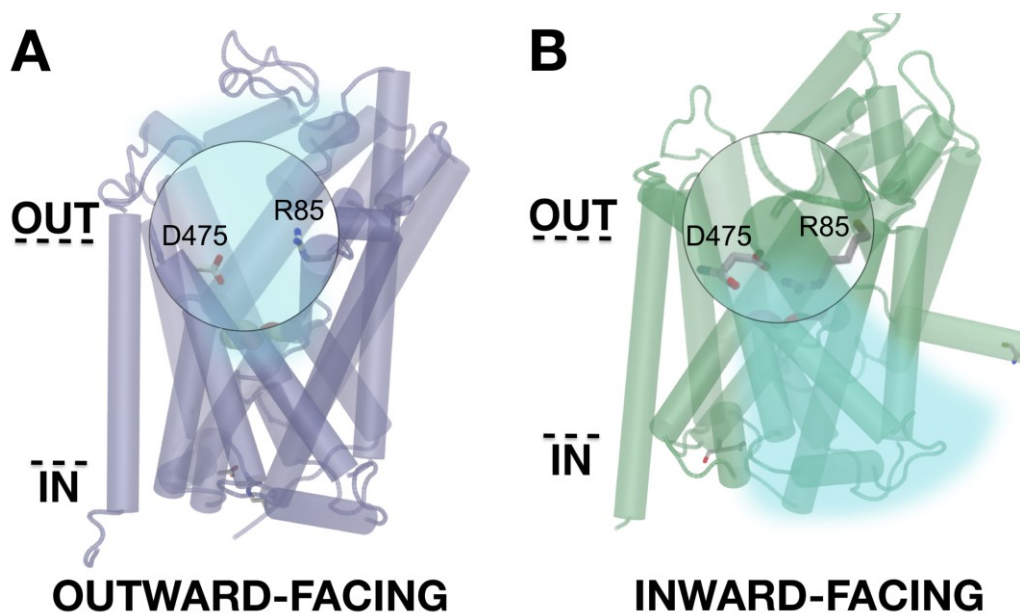


Figure 3.1: A) The outward- (extracellular-) facing (OF) conformation of the dopamine transporter (DAT) protein and B) the inward- (cytoplasmic-) facing (IF) conformation. OF DAT and IF DAT structures are expected to have different intramolecular interactions. For example, the salt bridge interaction between D475 and R85 is destabilized in the OF conformation and stabilized in the IF conformation. Regions highlighted in blue represent the pathway allowing access to the central binding site from either the extracellular pathway or the internally open intracellular pathway for the outward-facing or inward-facing conformation.

The phenylpiperazine groups have been related to the reward effects of DAT inhibitors such as cocaine,³ while a diphenylether moiety is a feature of the less abusable DAT inhibitor bupropion and its analogs (**Figure 1.4**).⁴ However, the 3 β -aryltropane cocaine analogs LX10 and LX11 (**Figure 1.6**), differing only in stereochemistry and sharing a preference for the outward-facing DAT, are reported to vary widely in abuse potential in an animal model.⁵ Furthermore, LX10 has 10-fold greater affinity than LX11 (**Table 3.1**). In search of the molecular basis for DAT conformation preference, complexes of cocaine, bupropion, LX10 or LX11 bound to each DAT conformation were subjected to 100 ns of all-atom molecular dynamics simulation. Computational methods were employed to detect subtle differences in binding of LX10 and LX11 to the

OF DAT. Results were consistent with previous findings from cysteine accessibility assays used to assess an inhibitor's DAT conformation preference.⁵

The binding interactions between the inhibitors and DAT were examined and structural analysis of the protein-ligand system revealed distinct differences in the binding of the LX10 and LX11 in the outward-facing conformation. The respective 2 β - and 2 α -substituted phenyltropanes of LX10 and LX11 interacted with hydrophobic regions of the DAT S1 binding site that were inaccessible to cocaine. Solvent accessibility measurements also revealed subtle differences in inhibitor positioning within a given DAT conformation. This work serves to advance our understanding of the conformational selectivity of DAT inhibitors and suggests that MD may be useful in antipsychostimulant therapeutic design.

Table 3.1: DAT affinity K_i values (mean \pm s.e.m.) for cocaine and two 3 β -aryltropane analogs.⁵ Affinity measured for DAT obtained by displacement of the cocaine analog radioligand [³H]-WIN 35,428.

Compound	DAT K_i (nM)
Cocaine	98 \pm 6.6
LX10	19 \pm 0.2
LX11	352 \pm 44

3.2 Results and Discussion

All-atom MD simulations were performed to evaluate the binding of four DAT inhibitors that have been shown through cysteine accessibility assays to stabilize particular DAT conformations.⁵ Previous studies of DAT conformations after 35 ns MD suggested that cocaine, LX10 and LX11 prefer the OF DAT conformation and BZT prefers the IF DAT conformation.⁵ The present study examines differences in the OF DAT conformations of the four inhibitors after 100 ns MD.

This work began prior to the availability of the cocaine-*Drosophila* DAT (dDAT) co-crystal 4XP4;⁶ thus, the cocaine-bound OF rat DAT (rDAT) homology model was superposed with the 4XP4 coordinates (**Figure 3.2**) to ensure that the present system was experimentally relevant.⁶ Furthermore, the rDAT homology model was used instead of the hDAT because the pharmacological assays performed by Hong *et al.* were conducted in the rat.⁵ The rat and human amino acids sequences are 92% conserved,⁷ and identical with respect to the S1 binding site.

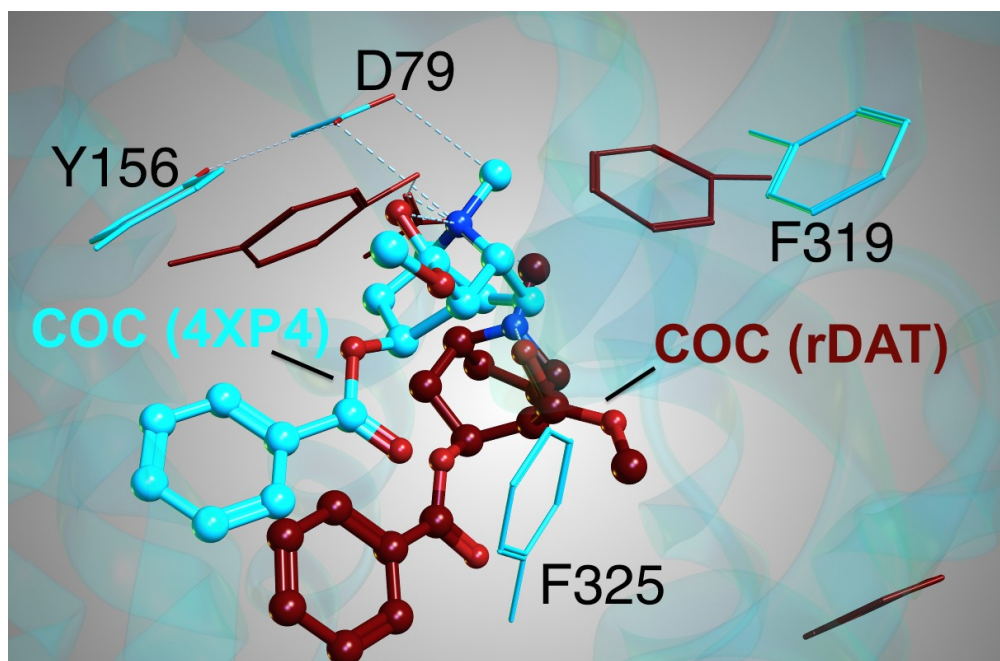


Figure 3.2: PDB coordinates of the *Drosophila* DAT co-crystalized with cocaine (cyan),⁶ superposed with the rat DAT homology model bound to cocaine (red). Essential S1 pocket side chains are annotated and color-coordinated with the ligand for a given model.

The RMSD (**Figure 3.3**) and RMSF (**Figure 3.4**) were measured for the backbone atoms of DAT after 100 ns of MD to assess the stability of the system. Additionally, the key residues that are in the binding site were inspected for comparison. For the cocaine-bound OF DAT, a cocaine-D79 (TM1) residue ion pair was observed, as was a shift in

the TM3 – TM8 extracellular gate residue pair Y156-F319 characteristic of the outward-occluded conformation.⁸ Although the D79-Y156 distance is reported to be too large for a hydrogen bond interaction,⁹ 100 ns of MD indicated a stable H-bond (**Figure 3.5**). In the dDAT co-crystal, cocaine was found to have a face-to-edge interaction with F325 (TM6); however, after 100 ns of MD the F325 side chain had disengaged from cocaine (**Figure 3.2**). Overall, the rDAT homology model was sufficient to reproduce the experimentally determined binding orientation of cocaine in OF dDAT.⁶

RMSD was measured after minimization for 100 ns of MD for each DAT-inhibitor system (**Figure 3.3**). The initial structure of cocaine bound to OF DAT was used as a reference structure for measurements in the OF conformation. The RMSD measured in IF DAT was made with reference to the initial structure of BZT bound to DAT. The movement of the inhibitors in the binding site was evaluated in OF and IF DAT after each system was aligned to DAT TM1-12.

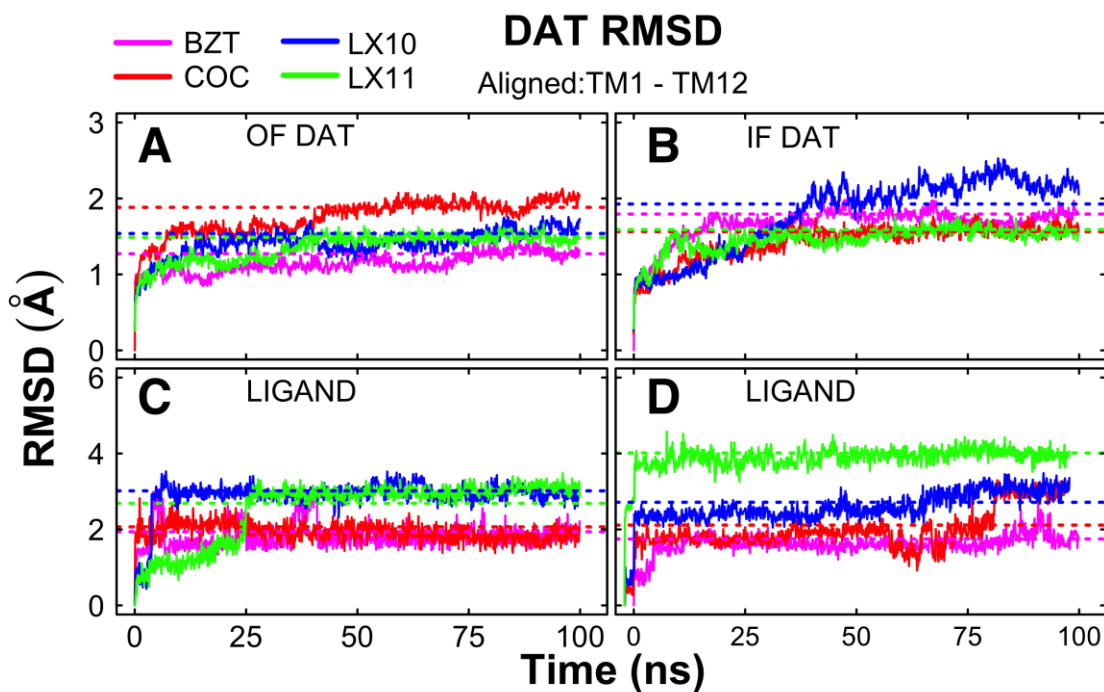


Figure 3.3: RMSD measured for each DAT-inhibitor system after 100 ns MD. A) RMSD measured in OF DAT with initial structure of cocaine bound to DAT was used as a reference structure for measurements. B) RMSD measured in IF DAT with initial structure of BZT bound to DAT was used as a reference structure for measurements. C-D) Ligand RMSD in OF and IF DAT binding site.

The RMSF of the protein residues in OF and IF DAT were measured for each inhibitor-bound complex (**Figure 3.4**). The extracellular and intracellular loops are expected to experience greater fluctuation than the transmembrane (TM) helices. Cocaine, benztropine, and LX10 share similar fluctuation in the respective OF and IF conformations. The binding of LX11 indicates there is greater stability of TM2, TM4, TM6, TM8 and TM10.

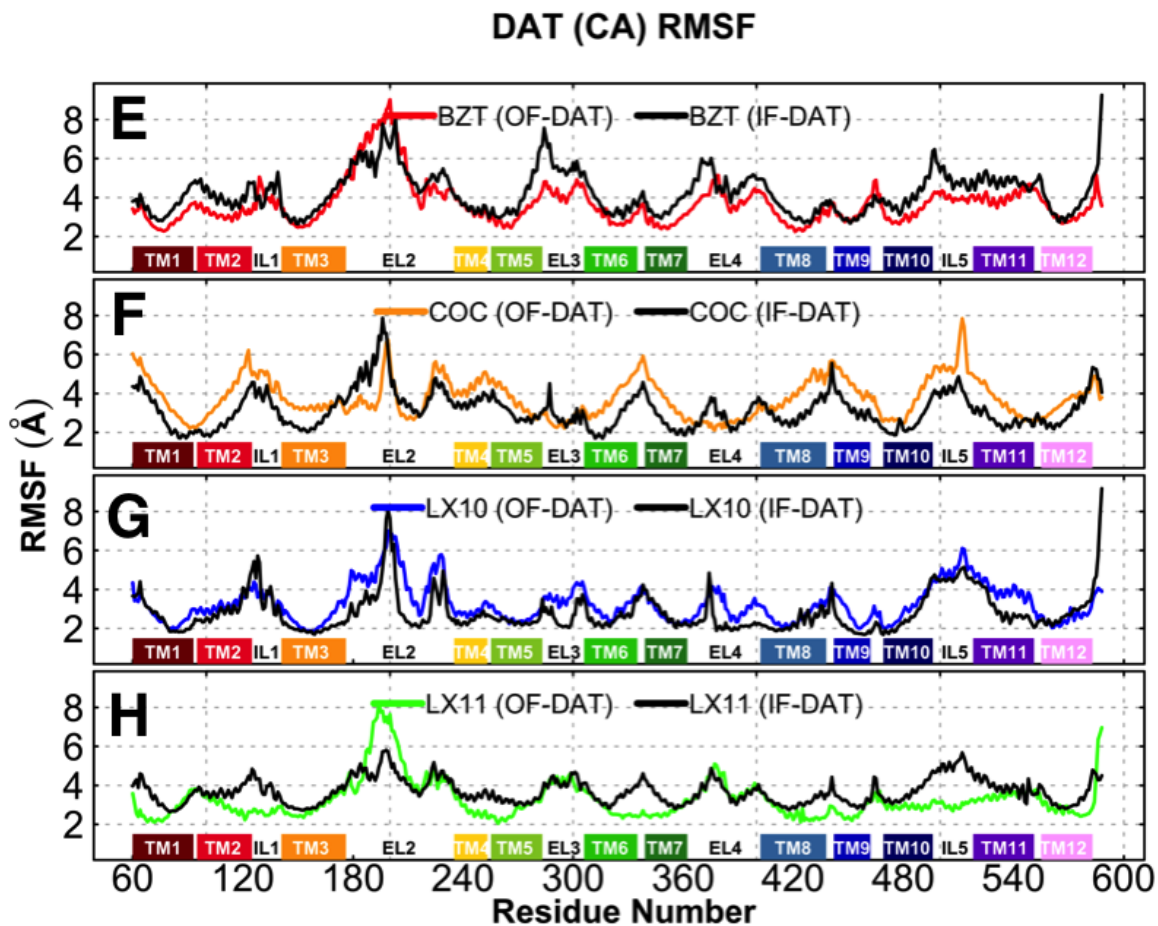


Figure 3.4: RMSF measured for $C\alpha$ of DAT inhibitor-bound OF and IF conformations. E) BZT; F) COC; G) LX10; H) LX11. Black lines represent inhibitors bound in IF DAT superposed with the respective inhibitors bound systems in OF DAT.

For OF DAT, D79 - Y156 separation was greater than 4 Å, indicating a loss of interaction. At $t=85$ ns, however, the interaction formed intermittently. For IF DAT, D79 - Y156 separation was less than 3.5 Å, suggesting an interaction. At $t=50$ ns, fluctuations appeared in this distance, and at $t=80$ ns, an interaction was no longer observed. For cocaine and BZT OF and IF DAT complexes, the D79-Y156 interaction was stable throughout the 100 ns simulation. A slight fluctuation was seen in the LX11-bound IF DAT. In the IF DAT-LX10 complex, the interaction was lost at $t=30$ ns.

D79-Y156

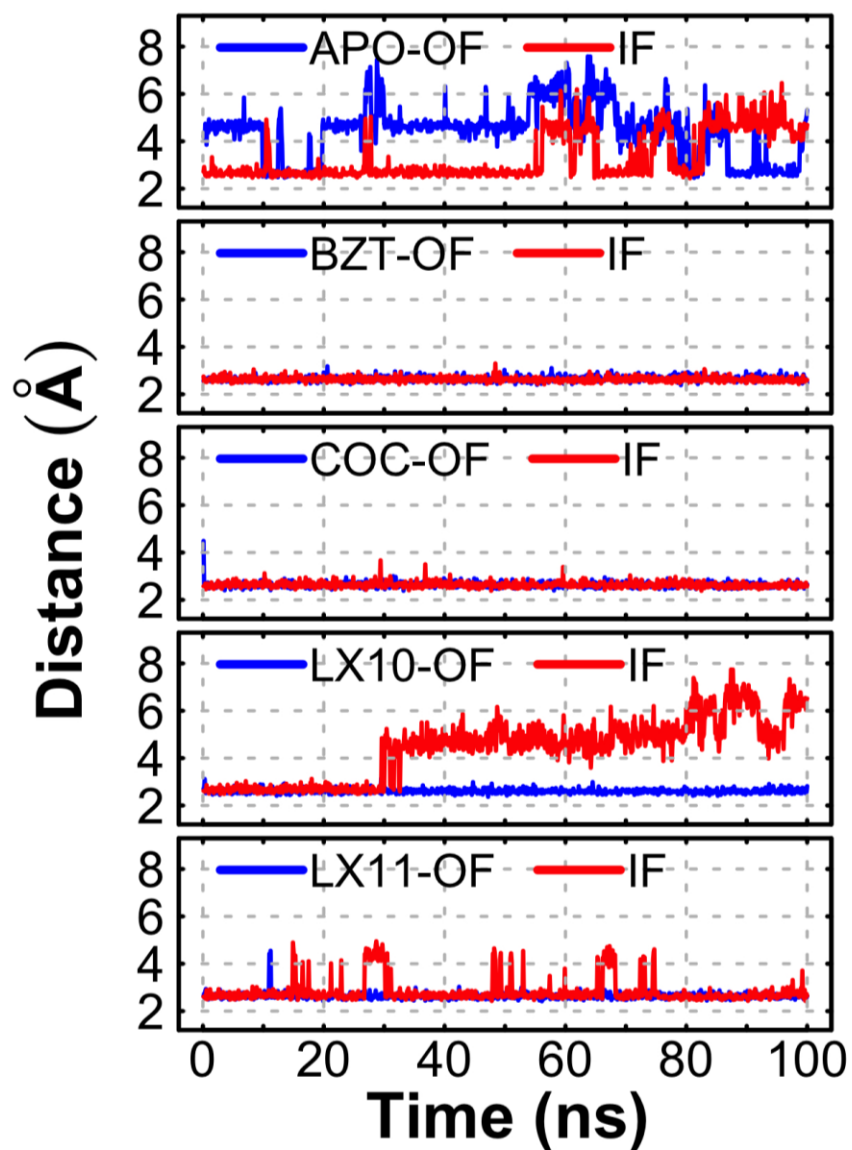


Figure 3.5: Distances measured between the closest oxygen atoms of D79 and Y156 for the OF (blue) and IF (red) DAT. Distances were measured for DAT apoprotein (APO) systems in the inward-facing and outward-facing conformations for comparison to inhibitor-bound systems.

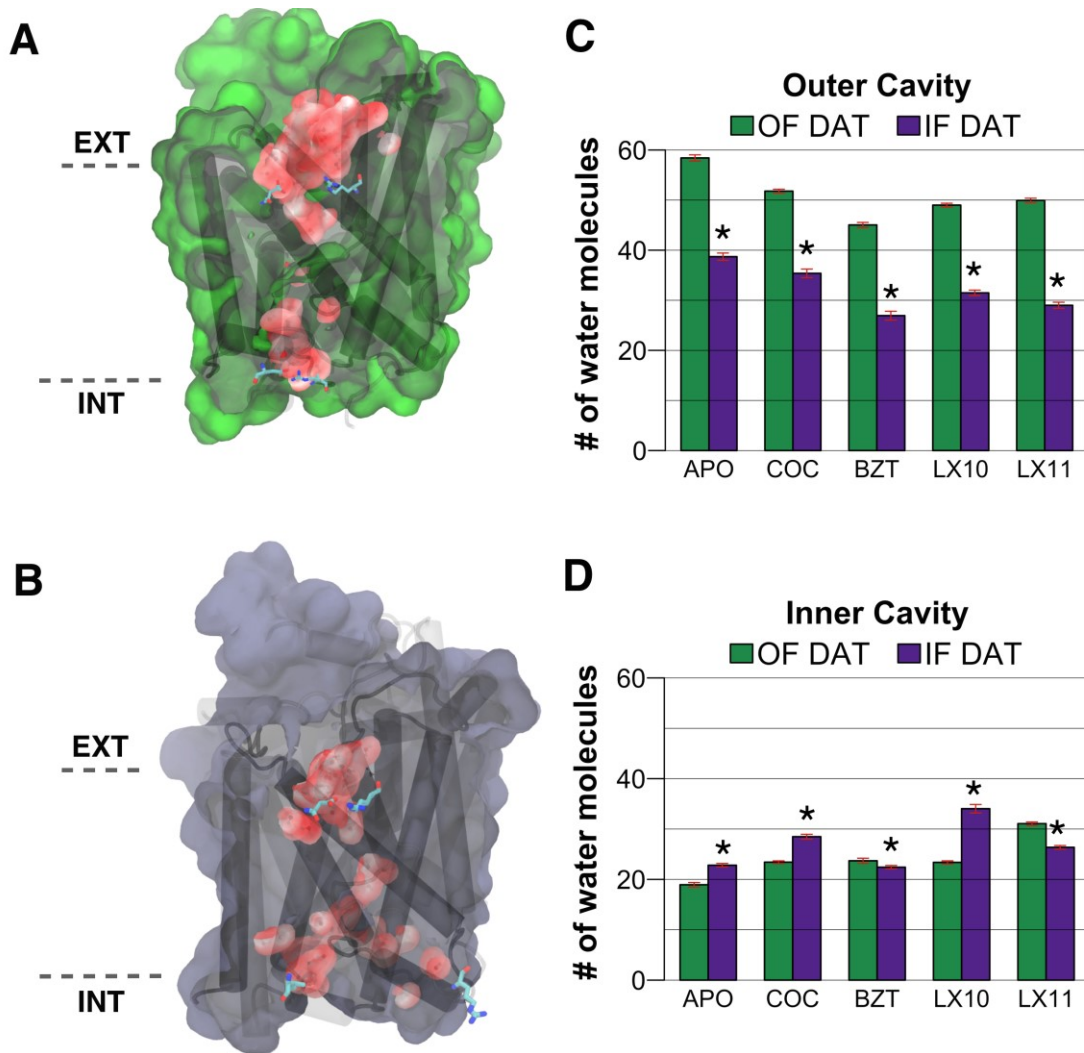


Figure 3.6: Representation of the water molecules (red spheres) within the outer and inner cavities in the A) OF and B) IF DAT. C, D) Number of water molecules within 5 Å of the residues in the outer (residues D79 (TM1), W84 (TM1), R85 (TM1), Y88 (TM 1), F155 (TM3), Y156 (TM3), I311 (TM6), D312 (TM6), T315 (TM6), F319 (TM6), D475 (TM10), T481 (TM10)) and inner (residues F69 (TM1), G75 (TM1), F76 (TM1), G257 (TM5), S261 (TM5), V265 (TM5), T268 (TM5), F325 (TM6), F331 (TM6), G424 (TM8), E427 (TM8) and T431 (TM8)) cavities. The average number of water molecules was analyzed between each pair of OF (green) and IF (violet) systems by two-tailed t-test. * $P < 0.05$; error bars (red) represent the standard error of the mean.

Access to the S1 binding site is dependent on the ability of the ligand to travel from the extracellular space and reach the site.¹⁰⁻¹³ In the OF DAT conformation, the “outer cavity” includes the extracellular vestibule and S1 pocket, and is larger than the

“inner cavity” delineated by the internal gate residues. The two external gate residue pairs R85-D475 and Y156-F319, when disrupted, allow accessibility to the S1 pocket from the extracellular space. In contrast, the IF DAT intact external gate interactions and disruption of the internal gate residue pair R60-D435 yield an internally open cavity that reaches into S1.¹⁰⁻¹³ Thus, the hydration of the outer and inner cavities differs for the outward- and inward-facing conformations (**Figure 3.6**).

The hydration of the two cavities was evaluated for the final 50 ns of MD. Outer cavity hydration was greater for all OF DAT simulations than for IF DAT (**Figure 3.6C**). The number of water molecules in the inner cavity was less for OF DAT than IF DAT in the APO, cocaine and LX10 systems. Interestingly, the accumulation of water molecules in the inner cavity for the BZT- and LX11-bound systems was greater in OF DAT than in IF DAT (**Figure 3.6D**), which would suggest the binding of these ligands stabilizes a DAT conformation that allows for increased solvation of the inner cavity.

Salt bridge side chain interactions for the external and internal gates were evaluated to determine the accessibility of the binding site from the extracellular and intracellular spaces (**Figure 3.7A**, **Figure 3.7B**). The distance was measured between the residues comprising the extracellular (R85-D475) gate salt bridge (**Figure 3.7A**) as well as the intracellular (R60-D435) gate salt bridge (**Figure 3.7B**). Interactions were evaluated using the shortest distance measured between an arginine nitrogen atom and an aspartic acid carboxylate oxygen. Distances greater than 3.5 Å indicated loss of interaction between the gating residues. Thus, for the IF DAT, one would expect to see distances that are ≤ 3.5 Å.

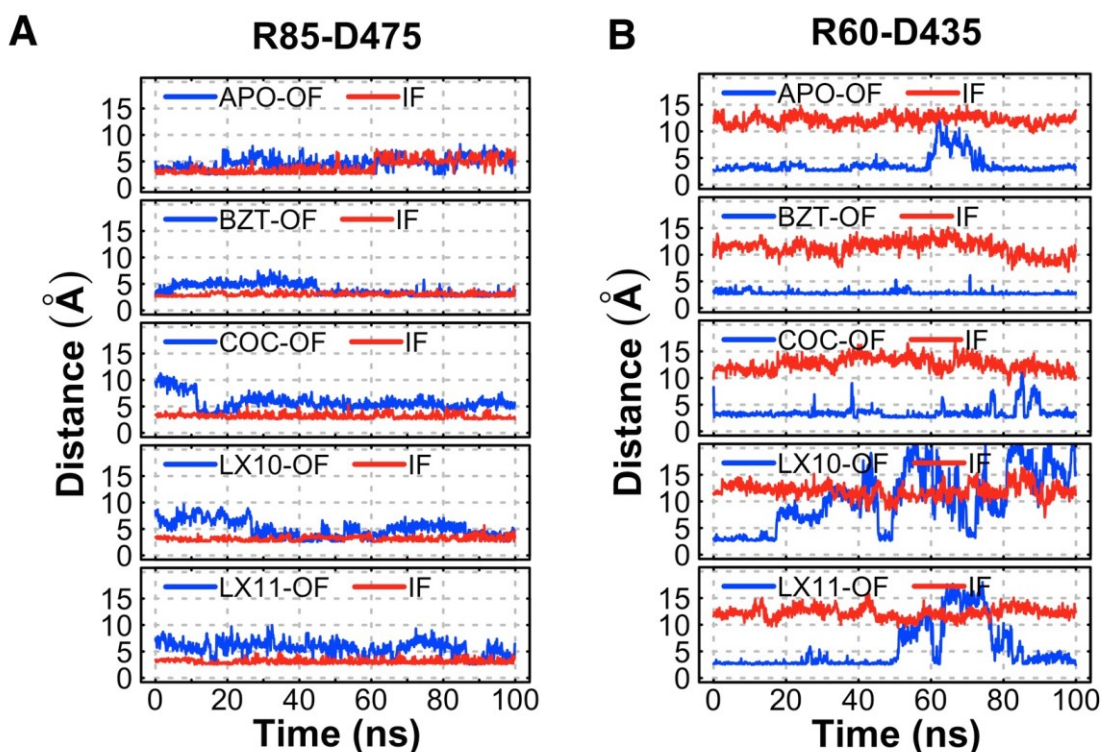


Figure 3.7: Distances measured between amino acid side chains for A) the external gate residue pair R85-D475 and B) the internal gate residue pair R60-D435 in inhibitor-bound OF (blue) and IF (red) DAT after 100 ns MD.

The distance measured between the R85 and D475 side chains in the OF DAT-cocaine complex indicated no direct bridging during the final 75 ns of the MD simulation. In contrast, the R85-D475 separation in the OF DAT-BZT complex after 45 ns indicated a stable salt bridge (**Figure 3.7A**). The distance measurements between the extracellular gate residues R85 and D475 further support the preference of BZT for IF DAT, reducing extracellular accessibility to the S1 binding site, whereas the binding of cocaine to outward-facing DAT allows for access to the binding site from the extracellular side of the protein, consistent with cysteine accessibility assays.⁵

The solvent accessible surface area (SASA) was monitored for the residues in the outer and inner cavities. The SASA values measured from the trajectories for OF and IF

DAT conformations differed substantially and revealed details of which conformation was being sampled with inhibitors bound (**Figure 3.8C**, **Figure 3.8D**).^{14, 15} SASA measured in the defined outer cavity in the OF DAT conformation (**Figure 3.8C**, blue lines) should offer a larger outer cavity, allowing for greater water penetration compared to that of the IF DAT (**Figure 3.8C**, red lines). The SASAs of the inner cavity of OF and IF DAT were measured to determine the extent of IF DAT and the intracellular accessibility. The inner cavity is defined here by accessibility to the cytoplasm-proximate residues previously determined to line the cytoplasmic half of the substrate permeation pathway, plus the S1 pocket in the case of IF DAT (**Figure 3.8D**). A larger inner cavity is expected for the IF DAT conformation (**Figure 3.8D**, red lines) relative to that of the OF DAT conformation (**Figure 3.8D**, blue lines).

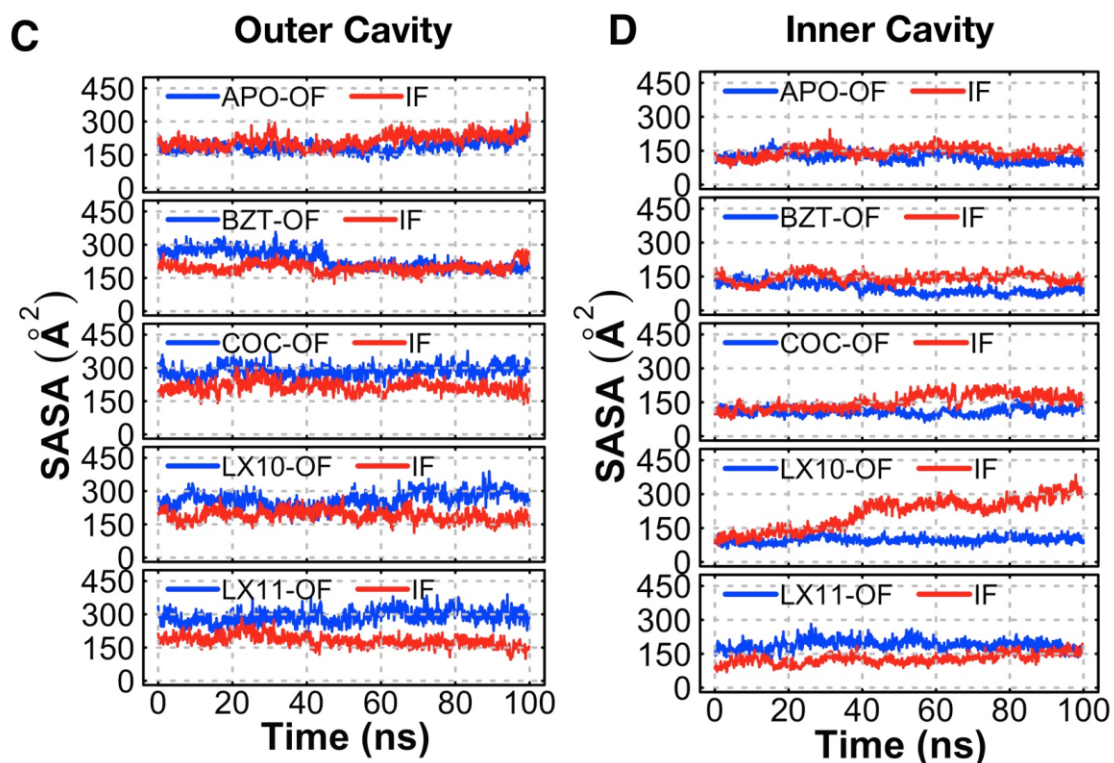


Figure 3.8: SASA measurements for OF DAT (blue) or IF DAT (red) after 100 ns simulation for C) the outer cavity and D) the inner cavity.

In the BZT-bound system, the distance between R85 and D475 in OF DAT decreased from approximately 5 Å to 3.1 Å during the last 50 ns of the simulation (Figure 3.7A, blue line). There was also a decrease in SASA to an average value of 195 Å² at t=45 ns (Figure 3.8C, blue line). A similar SASA value was found for IF DAT. This is an indication of reduced accessibility from the extracellular space and is characteristic of the inward-facing conformation. The measured values in both OF and IF DAT further support the expected binding of BZT to reduce external accessibility. The distance measured between internal gate residues R60 and D435 in IF DAT was greater than 10 Å, indicating no salt bridge; however, in OF DAT the salt bridge remains intact throughout the entire 100 ns.

Conversely, cocaine, LX10 and LX11 are expected to stabilize the outward-facing conformation.⁵ In the OF DAT cocaine-bound system, there was a significant decrease from 10 Å to 3 Å in the first 10 ns of the simulation, followed by an increase in the distance between the residues during the last 50 ns. The distance averaged 5.3 Å, suggesting breakage of the external gate R85-D475 bridge (**Figure 3.7A**), whereas the internal R60-D435 bridge was intact for OF DAT (**Figure 3.7B**).

The measured distance between R85-D475 in the LX10- and LX11-bound OF DAT fluctuated mildly but fairly constantly. Notably, the LX10-DAT complex appeared to allow the salt bridge to form starting at $t=25$ ns, which correlates with the loss of the intracellular gate bridge R60-D435 (**Figure 3.7A**, **Figure 3.7B**, blue lines). The inter-residue distance then fluctuates wildly for LX10 starting at approximately 18 ns, forming intermittent interactions for the remainder of the simulation, whereas the distance measured in IF DAT between R60 and D435 had stabilized. There are also measured fluctuations for LX11-DAT; however, the interaction is eventually stabilized. Fluctuations measured for this internal gate in OF DAT are likely due to the size of the LX ligands within the S1 binding site, and in increased interaction with TM8, causing a displacement of D435 (**Figure 3.9A**, **Figure 3.10**).

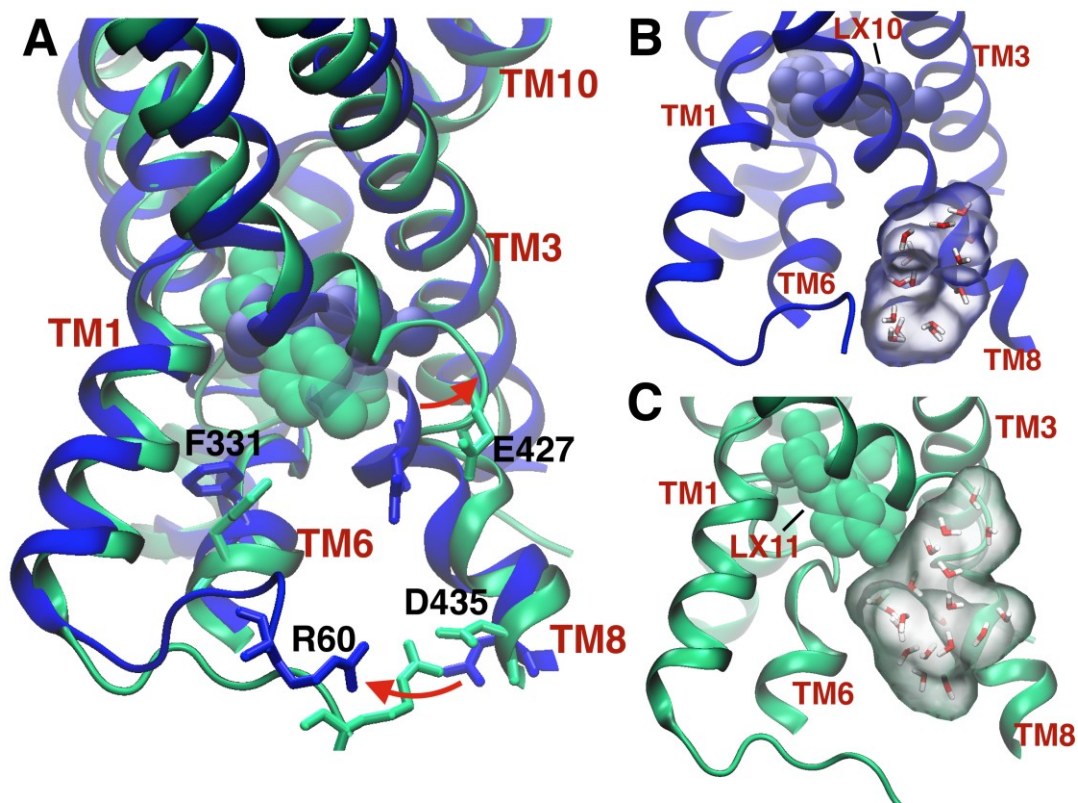


Figure 3.9: A) LX10 (blue) and LX11 (green) in OF DAT are superposed for comparison of the inhibitors in the S1 binding pocket. The ligands (vdW spheres) and DAT residues (sticks) are color-coded. The tropane C3 chlorophenyl ring and a ring portion of the C2 diphenyl ether moiety of LX11 are oriented toward the intracellular space after 100 ns of MD. The red arrows indicate regions of structural differences seen after 100 ns. B) LX10 and C) LX11 bound in IF DAT, with water molecules solvating the inner cavity. Surfaces (gray) surrounding the water molecules show regions of solvation. The snapshots represent the last frame of the simulation. Average values are given in Figure 2D.

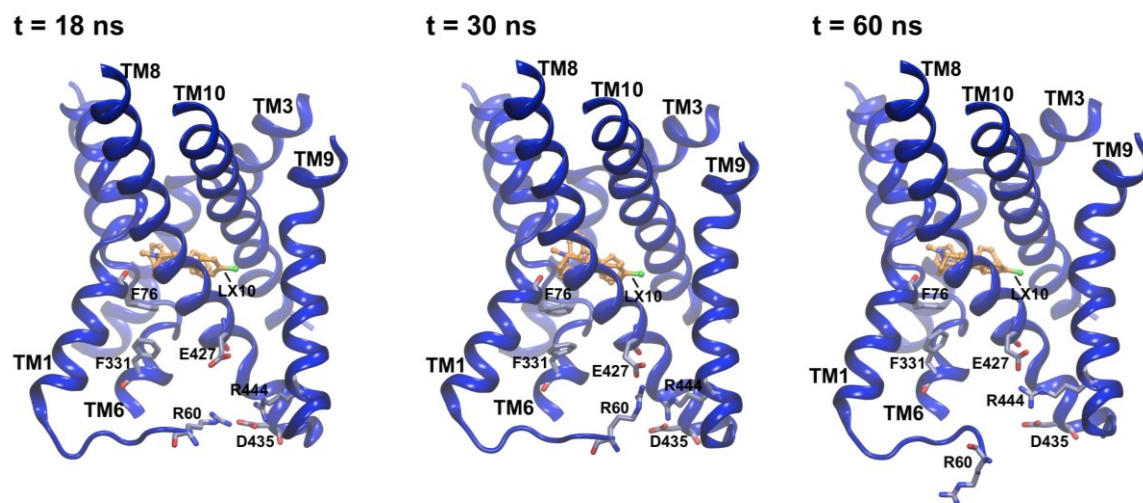


Figure 3.10: Snapshots of inner gate R60-D435 disposition (Fig. 5B) in the OF DAT-LX10 bound system at $t = 18, 30,$ and 60 ns. LX10 (gray, ball-and-stick) is bound in S1; DAT residues are represented as teal ball-and-sticks. At $t = 18$ ns, the R60-D435 salt bridge is intact. There is a loss of interaction at approximately $t = 35$ ns. At $t = 60$ ns, R444 moves within proximity of D435; however, the interaction between R60-D435 remains disrupted.

SASAs measured for the inner and outer cavities for cocaine- and BZT-DAT complexes were as expected for OF DAT and IF DAT, respectively (**Figure 3.8C**, **Figure 3.8D**). Moreover, the number of water molecules measured in the outer DAT cavity for the DAT-cocaine and DAT-benztrapine complexes supported the reduced accessibility of the outer cavity by solvent molecules when benztrapine is bound (**Figure 3.11A**). LX10 binding to IF DAT enlarged the inner cavity from 75 \AA^2 to approximately 270 \AA^2 . Unexpectedly, the binding of LX11 to the OF DAT resulted in a larger inner cavity than for IF DAT. Comparison with the values seen for the outer cavity suggests that the binding of LX11 to OF DAT results in an opening of both the outer and inner cavities (**Figure 3.8C**, **Figure 3.8D**). Though the increase in the measured SASA of the outer cavity supports findings from cysteine accessibility assays,⁵ the values measured for the inner cavity with LX11 bound suggest that the inhibitor could stabilize a conformation of

the transporter that is simultaneously open to some extent to the external and internal spaces.

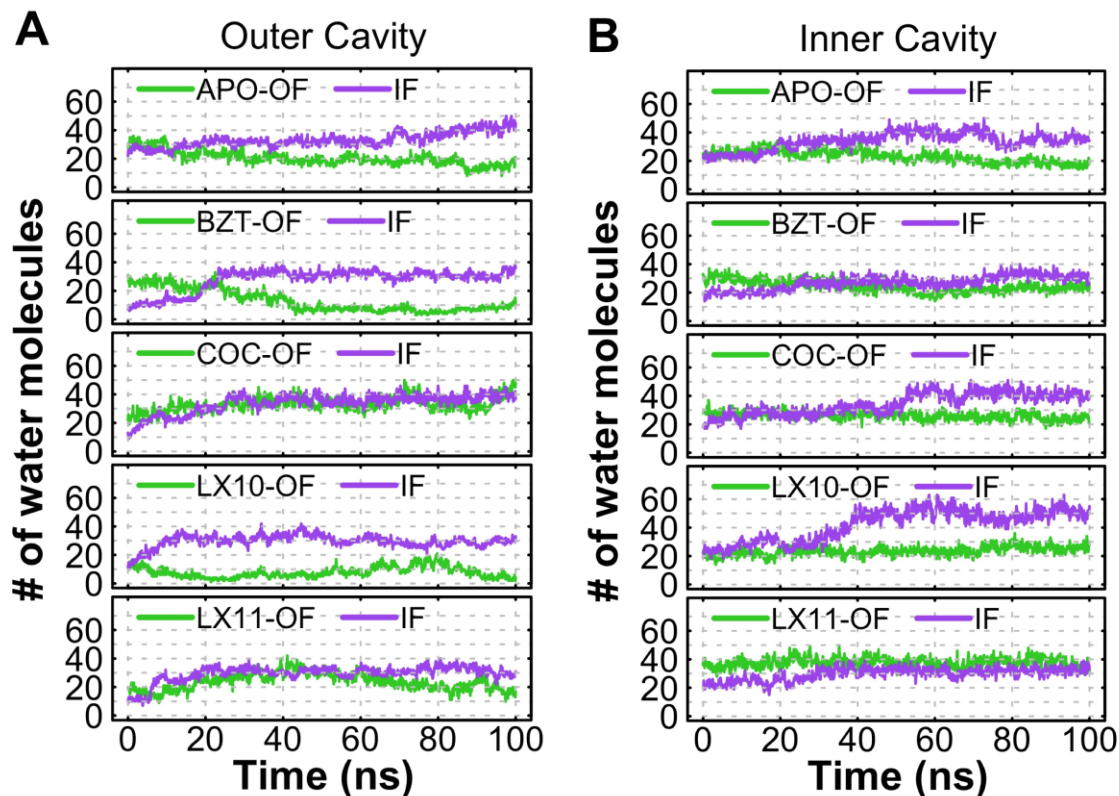


Figure 3.11: The number of water molecules analyzed between each pair of OF (green) and IF (violet) systems for the 100 ns trajectory. The plots represent the number of water molecules within 5 Å of the residues in the A) outer (residues D79 (TM1), W84 (TM1), R85 (TM1), Y88 (TM 1), F155 (TM3), Y156 (TM3), I311 (TM6), D312 (TM6), T315 (TM6), F319 (TM6), D475 (TM10), T481 (TM10)) and B) inner (residues F69 (TM1), G75 (TM1), F76 (TM1), G257 (TM5), S261 (TM5), V265 (TM5), T268 (TM5), F325 (TM6), F331 (TM6), G424 (TM8), E427 (TM8) and T431 (TM8)) cavities.

Differences in inner cavity hydration were observed for OF DAT bound to LX10 and LX11 (**Figure 3.9**). The LX10 interaction with TM1 and TM6 resulted in breakage of the internal R60-D435 gate (**Figure 3.9A**, blue), in agreement with the distance measured for this gate pair (**Figure 3.8B**). Unlike LX10, DAT binding of LX11 caused a TM8 shift that increased inner cavity space, enhancing hydration of the inner cavity

(**Figure 3.9B**, **Figure 3.9C**). The binding of LX11 in OF DAT sustained a shift within the binding site (**Figure 3.3C**.) Relative to LX10-DAT, there are approximately 15 more water molecules in the LX11- DAT inner cavity that approach the cytoplasmic interface (**Figure 3.6D**).

A network of ionic interactions at the cytoplasmic interface maintains a DAT conformation closed to the cytoplasm.¹⁶ The distances between the charged residues in the inner cavity were measured to provide quantitative differences between LX10 and LX11 DAT complexes (**Figure 3.12**). Residue pairs included R60 (TM1) – E427 (TM8), D435 (TM8) – R444 (TM9), E61 (TM1) – R444 (TM9), and D435 (TM8) – K133 (IL2, connecting TM2 and TM3). The interactions were measured at the shortest distance possible between the arginine/lysine side chain nitrogen atoms and the aspartate/glutamate carboxylate oxygen atoms.^{16, 17}

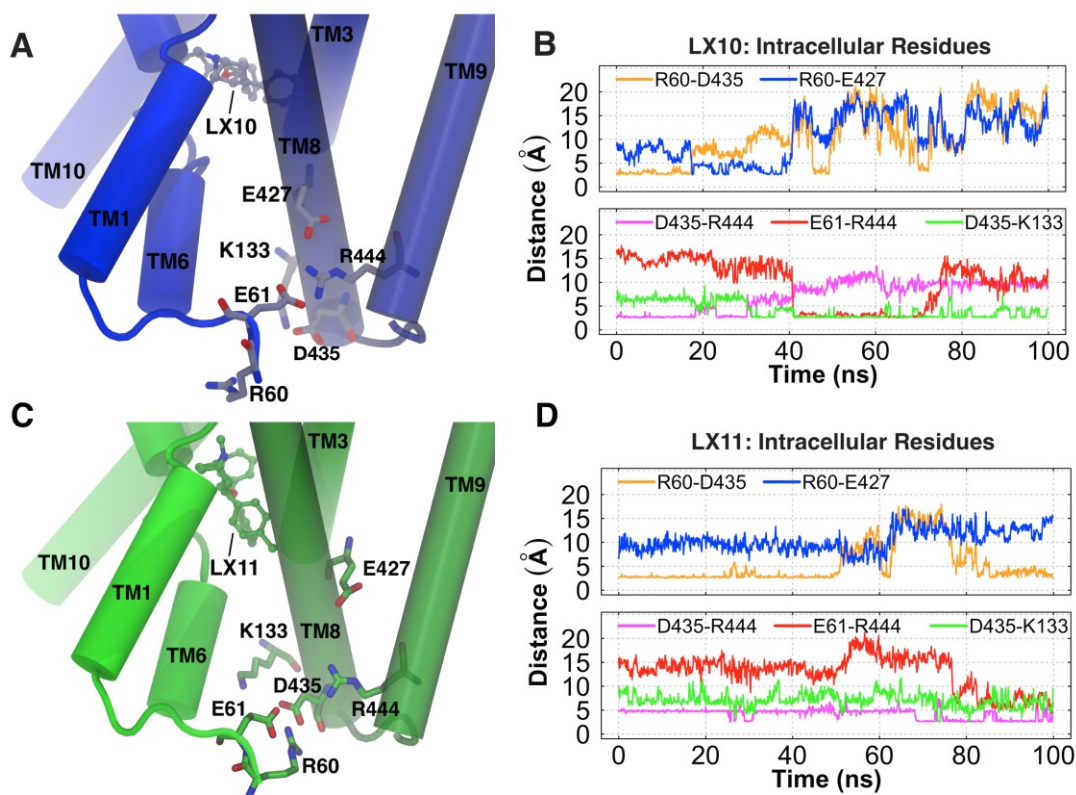


Figure 3.12: For the A, B) LX10 or C, D) LX11 complex with OF DAT, distances between amino acid residue side chains at the TM-cytoplasm interface: R60-D435 (orange), R60- E427 (blue), D435-R444 (pink), E61-R444 (red) and D435-K133 (green). Values represent the shortest possible distance between the nitrogen of arginine/lysine side chains and carboxylate oxygen atoms of aspartate/glutamate side chains.

For LX10-bound DAT (**Figure 3.12A**), D435 is interacting with both R60 (orange) and R444 (pink) until 18 ns into the simulation. R60 – D435 is disrupted at that point, followed by breakage of the D435 – R444 interaction at 30 ns and alignment of D435 with K133 (green). R60 trades its D435 interaction for a brief interaction with E427 (blue), lasting about 20 ns, before this bond distance fluctuates. Upon loss of the D435 interaction (pink), R444 forms a bridge with E61 (red) at approximately 40 ns, lasting until the 75 ns mark. During this time frame D435 makes brief contact with R60, but never regains a stable interaction with either R60 or R444. For LX11-bound DAT

(**Figure 3.12B**), the distance between R60 and D435 (orange) remains fairly constant until the 50 ns mark. The bond breaks for 30 ns before reforming at $t = 80$ ns. At that time, E61 is within proximity of R444 (red), but unlike LX10-DAT, the E61 – R444 interaction is never formed.

Comparison of the two DAT complexes indicates the interaction between R60 and D435 is more stable in the LX11-bound DAT. The distance between D435 and R444 (**Figure 3.12B**, red) was stable at 5 Å for LX11-DAT before decreasing to allow bond formation, which may have stabilized the R60 – D435 bond at 80 ns. It should be noted that the DAT model lacks the N-terminal cytoplasmic tail (residues 1 – 59). Omitting this is fairly standard for integral membrane proteins considering that such regions have too many degrees of freedom to be represented accurately; nevertheless, the DAT N-tail could interact with regions at the cytoplasmic interface including R60 and D435. For LX10-DAT, the distance between R60 and D435 increases and continues to fluctuate, and the distance between D435 and R444 remains constant at 10 Å. Unlike LX11-DAT (**Figure 3.12B**, blue), an interaction forms between R60 and E437 in LX10-DAT (**Figure 3.12A**, blue). Despite the fluctuation measured in the distance between R60 and D435 in the LX10-bound systems in OF DAT (**Figure 3.7**, blue lines), the SASA of the inner cavity and the number of water molecules remained constant (**Figure 3.6**). In the LX10-bound IF DAT system, the distance between R60 and D435 remained constant (**Figure 3.7**, red lines), but there was increased hydration of the inner cavity (**Figure 3.6**).

The stability of the DAT backbone atoms was evaluated using root-mean-square fluctuation (RMSF; **Figure 3.13A**). RMSF of all DAT $C\alpha$ atoms was measured over 100 ns to track the movement and stability of DAT residues upon the binding of inhibitors.

RMSF comparison of cocaine-DAT with LX10- and LX11-DAT showed that LX10 (blue) is similar to cocaine (orange) in measured fluctuations, with a variation seen in EL4. In contrast, LX11-DAT (green) displayed a greater RMSF difference relative to cocaine- DAT in the extracellular and intracellular loops. RMSF traces for LX10- and LX11-OF DAT complexes were superposed for comparison. The fluctuations were very similar for these two systems except in TM6, TM7, EL1, EL4, and IL5.

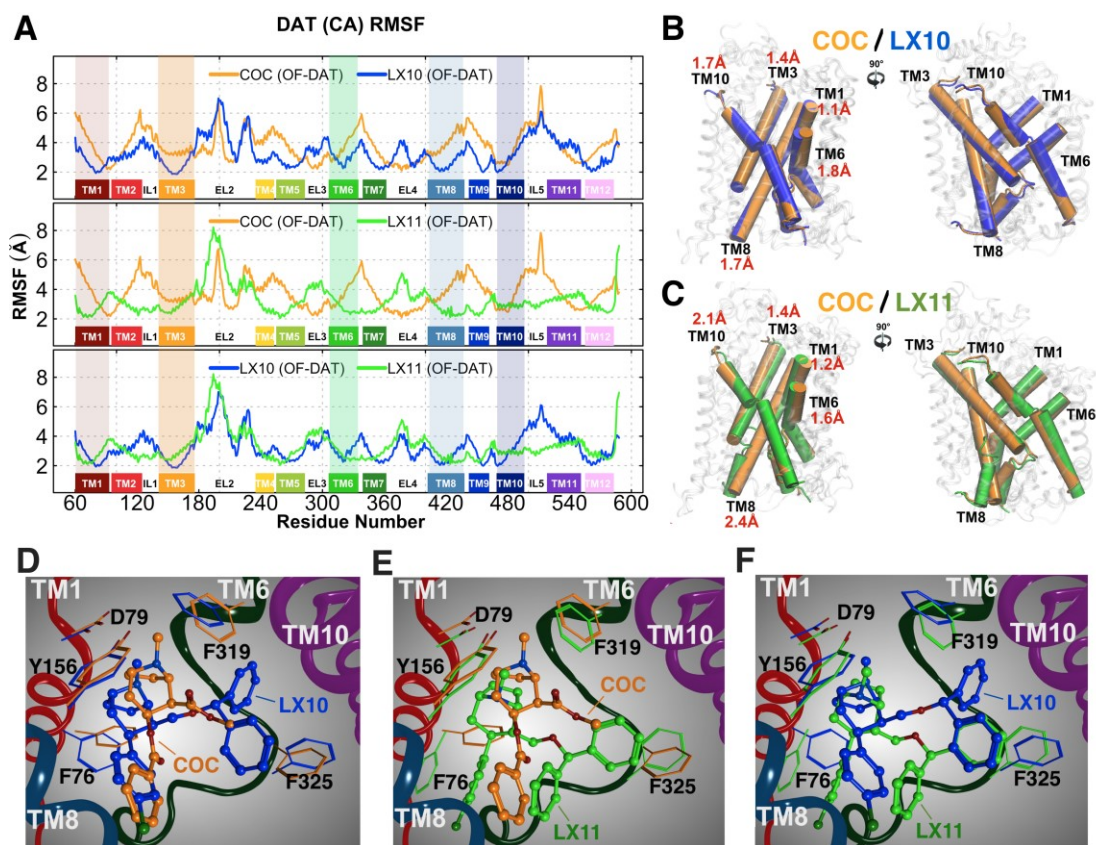


Figure 3.13: A) RMSF calculations for the C α atoms of OF DAT residues. RMSF values are plotted against residue number. RMSF traces are superposed to better compare the inhibitor-bound systems: Cocaine (orange) and LX10 (blue), cocaine (orange) and LX11 (green), and LX10 (blue) and LX11 (green). B, C) The final snapshot of the 100 ns simulation is represented and the OF DAT bound to cocaine (orange) was superposed with the OF DAT bound to LX10 (blue) or LX11 (green). The final structure of OF DAT bound to cocaine (orange) after 100 ns MD was used as the reference structure in RMSD measurements for the C α atoms of residues in TM1, TM3, TM6, TM8, and TM10 for the 100 ns trajectory of LX10 and LX11 bound in OF DAT. D-F) Binding site interactions in OF DAT superposed after 100 ns simulation. Ligands are represented as ball-and-stick; colored side chains corresponding to the inhibitor-bound systems are represented as lines. D) COC (orange) and LX10 (blue); E) COC (orange) and LX11 (green); F) LX10 (blue) and LX11 (green).

The RMSD was measured for the backbone atoms in TM1, TM3, TM6, TM8 and TM10 to assess the effect of inhibitor binding on the transmembrane helices surrounding the binding site (**Figure 3.13B**, **Figure 3.13C**). OF DAT bound to cocaine (orange) was used as the reference structure to compare the outward-facing DAT complexes with

LX10 (blue) and LX11 (green). Comparison of the RMSD values indicates LX10 interaction with atoms in TM1, TM3, TM6, TM8 and TM10 is similar to cocaine, with a measured deviation less than 2 Å. However, comparison of LX11 to cocaine showed deviation in TM8 and TM10, with values greater than 2 Å (**Figure 3.13B**). Specifically, the binding of LX11 resulted in RMSDs of 2.4 Å and 2.1 Å in TM8 and TM10, respectively, whereas with LX10 there was an RMSD of 1.7 Å for both TM8 and TM10 (**Figure 3.13B**). The OF DAT apoprotein was also compared to cocaine, LX10 and LX11 (**Figure 3.14**). Comparison of the RMSD with reference to OF DAT apoprotein (purple) indicates that binding of cocaine (orange), LX10 (blue) or LX11 (green) resulted in a RMSD greater than 2 Å in TM10; binding of LX11 also created a RMSD greater than 2 Å in TM8. It should be noted that the RMSD measured between cocaine and LX11 in TM8 (**Figure 3.13B**) represents the deviation measured for the entire 100 ns, whereas **Figure 3.13B** represents a snapshot of the final coordinates of the systems after 100 ns of MD.

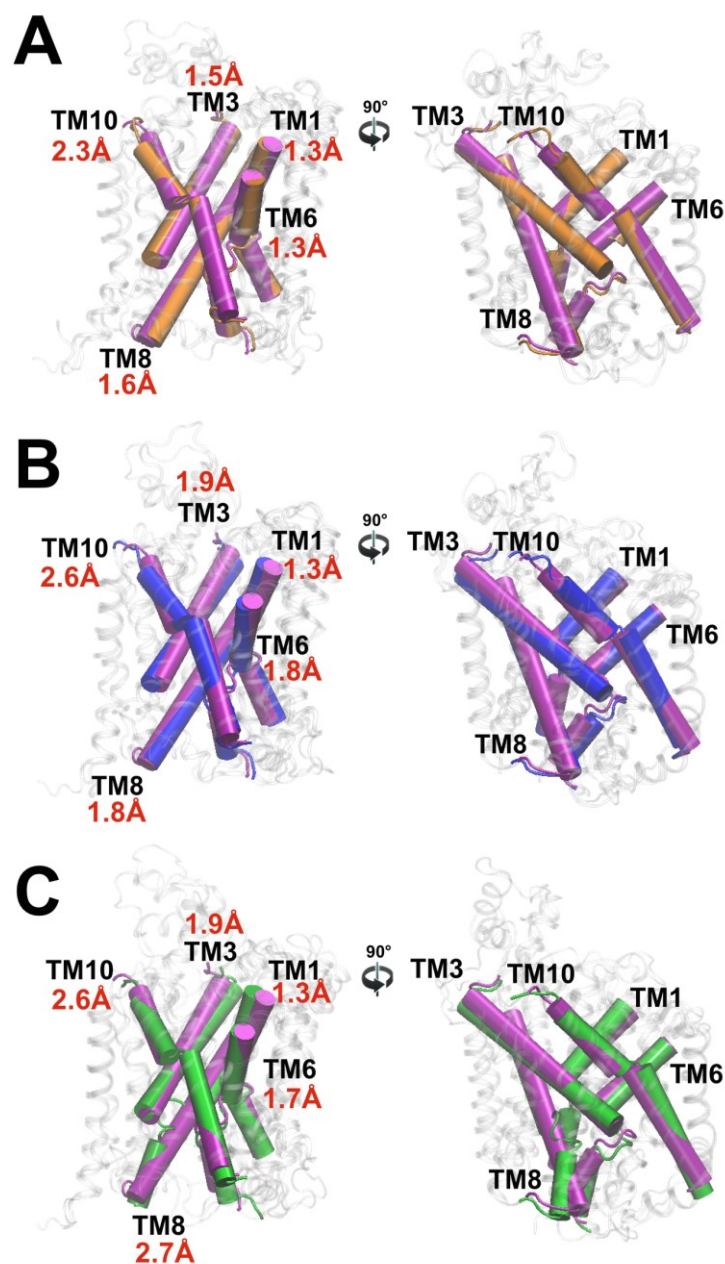


Figure 3.14: The OF structure of APO DAT (purple) superposed with OF DAT bound to A) cocaine (orange), B) LX10 (blue) or C) LX11 (green). RMSD (Å) was measured for the backbone atoms in TM1, TM3, TM6, TM8, and TM10 after 100 ns. APO OF DAT (purple) was used as the reference structure for all RMSD measurements.

Inspection of the binding revealed that in all cases, the inhibitors were found to interact favorably with the charged aspartate D79 residue of the S1 pocket (**Figure 3.15**).

In the OF DAT systems, all inhibitors were similarly wedged between TM6a and TM6b (**Figure 3.13D-F**), and the respective 2β - and 2α -substituted phenyltropanes of LX10 and LX11 interacted with hydrophobic regions of the binding site that were inaccessible to cocaine (**Figure 3.13D**, **Figure 3.13E**).

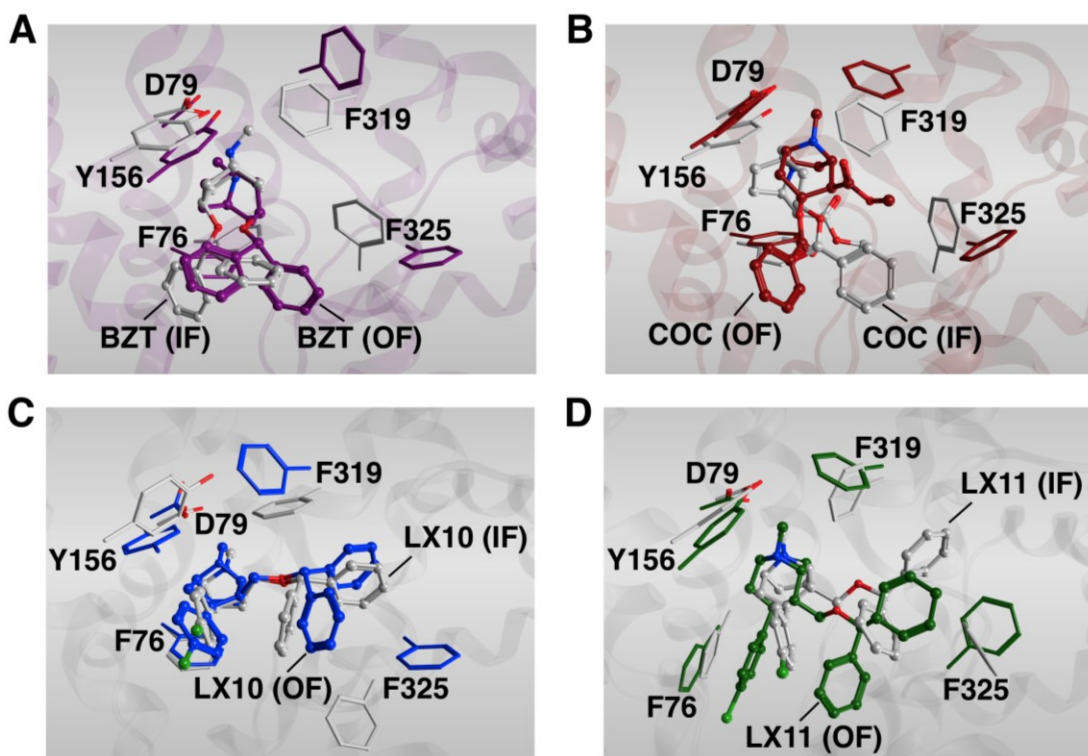


Figure 3.15: Binding site interactions in OF DAT superposed with IF DAT after 100 ns simulation. Ligands are represented as ball-and-stick; colored side chains corresponding to the inhibitor-bound systems are represented as lines. A) BZT; B) COC; C) LX10; D) LX11.

The chlorophenyl groups of LX10 and LX11 interacted with TM8. For LX10, these substituents share the same DAT region as the benzene ring of cocaine, although the chlorophenyl group penetrated deeper into the S1 pocket, situated between Phe319 (TM6a) and Phe325 (TM6b) (**Figure 3.13D**). However, the interaction of LX11 with TM8 occurred on the other side of the helix (**Figure 3.13F**), with the chlorophenyl ring

penetrating farther toward the intracellular side of the protein and causing a displacement of E427 (TM8) (**Figure 3.9A**). This results in increased solvation of the inner cavity compared to LX10 (**Figure 3.9B**, **Figure 3.9C**). The LX11 diphenyl moiety also reaches deeper into the pocket with another portion of the substituent, between Phe319 (TM6a) and Phe325 (TM6b), similar to LX10 (**Figure 3.13F**). A portion of the diphenyl moiety of LX10 interacted more so with TM6. The difference in TM6 interaction between LX10 and LX11 is supported by the RMSF measured for the OF DAT C α residues (**Figure 3.13A**), where the TM6 residues are more stable in LX11-DAT than in LX10-DAT or COC-DAT.

3.3 Conclusions

In the present study, the intermolecular interactions between the DAT and inhibitors of nonidentical DAT conformation preference were evaluated using MD. The MD differences observed for DAT-inhibitor complexes were consistent with reported preferences for the outward- or inward-facing (OF or IF) conformation as determined with accessible cysteine alkylation assays. A concern in interpreting such cysteine accessibility findings is that the assay requires several minutes and non-physiologic temperatures, and the cysteine alkylation itself may stabilize the DAT conformation. In contrast, MD analysis of binding of cocaine, benztropine or their analogs to the DAT allows for a true equilibrium between conformational states of the protein, and minute differences in inhibitor positioning can be detected. The distinctions in DAT interactions with LX10 and LX11 are supported by RMSF values measured for the DAT residues and changes measured in distances between salt bridge residues within OF DAT. These

results further reinforce the hypothesized similarity in DAT binding interactions for cocaine and LX10,⁵ and provide molecular insight into possible differences in LX10 and LX11 positioning in the OF DAT conformation.

While the need for an inhibitor to stabilize the OF DAT conformation in order to be an abusable drug appears unlikely, it is possible that certain DAT-inhibitor complexes adopt a 3D structure that is conducive to eliciting (or blocking) euphoria. This might be somewhat analogous to the phenomenon of “biased agonism”, in which the signal transduction pathway employed by G protein-coupled receptors is dictated by the agonist.¹⁸ For example, subtle 3-D differences between mu opioid receptor complexes with morphine versus TRV130 afford the latter drug powerful analgesic properties without sharing morphine’s abuse potential and other adverse effects.¹⁹ Similarly, changes in DAT conformation may promote interactions with selected intracellular macromolecules that provoke discrete signaling mechanisms, manifested as behavioral differences such as seen with cocaine and benztropine. A better understanding of the intricacies of DAT-inhibitor interactions may provide the next lead compounds in the elusive search for an effective therapeutic for psychostimulant abuse.

The future work of this research should involve the use of multiple computational models to simulate the binding of the inhibitors, including a system where the starting coordinates for the ligand is outside of the primary binding site.¹⁵ Furthermore, the DAT N-terminal cytoplasmic tail (residues 1 – 59) should be modeled for both potential intramolecular interactions with other DAT residues and impact on protein-protein interaction upon inhibitor binding.²⁰ Certainly, using an enhanced sampling method such as an accelerated MD approach would offer the ability to run longer timescale

simulations that will allow for more sampling of the system's degrees of freedom,²¹ thus capturing distinct changes in DAT conformation that are stabilized by inhibitor binding.

3.4 References

1. Lieberman, J. A., Kane, J. M., and Alvir, J. (1987) Provocative tests with psychostimulant drugs in schizophrenia. *Psychopharmacology* 91, 415-433.
2. Loland, C. J., Desai, R. I., Zou, M. F., Cao, J., Grundt, P., Gerstbrein, K., Sitte, H. H., Newman, A. H., Katz, J. L., and Gether, U. (2008) Relationship between conformational changes in the dopamine transporter and cocaine-like subjective effects of uptake inhibitors. *Mol Pharmacol* 73, 813-823.
3. Arbo, M. D., Bastos, M. L., and Carmo, H. F. (2012) Piperazine compounds as drugs of abuse. *Drug Alcohol Depend* 122, 174-185.
4. Ukairo, O. T., Bondi, C. D., Newman, A. H., Kulkarni, S. S., Kozikowski, A. P., Pan, S., and Surratt, C. K. (2005) Recognition of benztropine by the dopamine transporter (DAT) differs from that of the classical dopamine uptake inhibitors cocaine, methylphenidate, and mazindol as a function of a DAT transmembrane 1 aspartic acid residue. *J Pharmacol Exp Ther* 314, 575-583.
5. Hong, W. C., Kopajtic, T. A., Xu, L., Lomenzo, S. A., Jean, B., Madura, J. D., Surratt, C. K., Trudell, M. L., and Katz, J. L. (2016) 2-Substituted 3 β -Aryltropane Cocaine Analogs Produce Atypical DAT Inhibitor Effects Without Inducing Inward-Facing DAT Conformations. *J Pharmacol Exp Ther*, 624-634.
6. Wang, K. H., Penmatsa, A., and Gouaux, E. (2015) Neurotransmitter and psychostimulant recognition by the dopamine transporter. *Nature* 521, 322-327.
7. Giros, B., el Mestikawy, S., Godinot, N., Zheng, K., Han, H., Yang-Feng, T., and Caron, M. G. (1992) Cloning, pharmacological characterization, and chromosome assignment of the human dopamine transporter. *Mol Pharmacol* 42, 383-390.
8. Celik, L., Schiøtt, B., Tajkhorshid, E., and Schiøtt, B. (2008) Substrate Binding and Formation of an Occluded State in the Leucine Transporter. *Biophys J* 94, 1600-1612.
9. Beuming, T., Kniazeff, J., Bergmann, M. L., Shi, L., Gracia, L., Raniszewska, K., Newman, A. H., Javitch, J. A., Weinstein, H., Gether, U., and Loland, C. J. (2008) The binding sites for cocaine and dopamine in the dopamine transporter overlap. *Nat Neurosci* 11, 780-789.

10. Gouaux, E. (2009) Review. The molecular logic of sodium-coupled neurotransmitter transporters. *Philos Trans R Soc Lond B Biol Sci* 364, 149-154.
11. Krishnamurthy, H., Piscitelli, C. L., and Gouaux, E. (2009) Unlocking the molecular secrets of sodium-coupled transporters. *Nature* 459, 347-355.
12. Penmatsa, A., and Gouaux, E. (2014) How LeuT shapes our understanding of the mechanisms of sodium-coupled neurotransmitter transporters. *J Physiol* 592, 863-869.
13. Piscitelli, C. L., and Gouaux, E. (2012) Insights into transport mechanism from LeuT engineered to transport tryptophan. *EMBO J* 31, 228-235.
14. Shaikh, S. A., and Tajkhorshid, E. (2010) Modeling and dynamics of the inward-facing state of a Na⁺/Cl⁻ dependent neurotransmitter transporter homologue. *PLoS Comput Biol* 6.
15. Koldso, H., Autzen, H. E., Grouleff, J., and Schiott, B. (2013) Ligand induced conformational changes of the human serotonin transporter revealed by molecular dynamics simulations. *PLoS One* 8, e63635.
16. Kniazeff, J., Shi, L., Loland, C. J., Javitch, J. A., Weinstein, H., and Gether, U. (2008) An intracellular interaction network regulates conformational transitions in the dopamine transporter. *J Biol Chem* 283, 17691-17701.
17. Malinauskaite, L., Quick, M., Reinhard, L., Lyons, J. A., Yano, H., Javitch, J. A., and Nissen, P. (2014) A mechanism for intracellular release of Na⁺ by neurotransmitter/sodium symporters. *Nat Struct Mol Biol* 21, 1006-1012.
18. Rankovic, Z., Brust, T. F., and Bohn, L. M. (2016) Biased agonism: An emerging paradigm in GPCR drug discovery. *Bioorg Med Chem Lett* 26, 241-250.
19. Violin, J. D., Crombie, A. L., Soergel, D. G., and Lark, M. W. (2014) Biased ligands at G-protein-coupled receptors: promise and progress. *Trends Pharmacol Sci* 35, 308-316.
20. Khelashvili, G., Stanley, N., Sahai, M. A., Medina, J., LeVine, M. V., Shi, L., De Fabritiis, G., and Weinstein, H. (2015) Spontaneous inward opening of the dopamine transporter is triggered by PIP₂-regulated dynamics of the N-terminus. *ACS Chem Neurosci* 6, 1825-1837.
21. Pang, Y. T., Miao, Y., Wang, Y., and Mccammon, J. A. (2016) Gaussian Accelerated Molecular Dynamics in NAMD. *J Chem Theory Comput* 13, 9-19.

CHAPTER 4

4 LEAD OPTIMIZATION OF A NOVEL SERT INHIBITOR

4.1 Introduction

Increasing levels of the monoamine neurotransmitter, serotonin (5-HT), have been found to alleviate depressive symptoms.¹⁻⁸ As a result, the serotonin transporter (SERT) has become a primary target for treating depression because of its role in maintaining the balance of 5-HT in the synapse.⁹⁻¹¹ Fluoxetine (Prozac™) is well known as one of the first approved selective serotonin reuptake inhibitors (SSRIs), discovered in 1986. The molecular mechanism of binding of antidepressants to monoamine transporters remains of interest to further elucidate how such drugs modulate protein function. The crystal structures of LeuT were the first to offer insight into the allosteric binding site of MATs with the binding of SSRIs and tricyclic antidepressants (TCAs) in the S2 site.^{4, 12, 13} The LeuT co-crystal structure with R-fluoxetine bound in S2 (PDB entry 3GWV) was used for modeling the binding of R-fluoxetine in the previously developed hSERT homology model (**Figure 2.4**) followed by absolute binding free energy (ABFE) calculations for comparison to experimental affinity.⁴ Modeling the binding of existing antidepressants in the S2 site of SERT can offer insight into the allosteric binding site interactions.

A novel SERT inhibitor, SM11, was discovered through virtual screening of the ZINC molecular library using the S2 binding pocket in SERT (**Figure 4.1**).¹⁴ The

proposed SM11 binding pose within S2 includes hydrophobic interactions with Trp103, Ile179 and Phe335 and hydrogen bond interactions with Tyr107, Asp328, and Lys490 (**Figure 1.7**). The objective of this work is to apply free energy perturbation (FEP) calculations to determine which SERT binding site is employed by SM11, as well as the specific ligand-protein interactions, followed by a lead optimization based on potential binding site interactions. The binding site was identified by comparing the ABFE calculations of SM11 in the SERT S1 and S2 binding sites (**Figure 4.1**) to the experimental binding free energy, which is based on the ligand's binding affinity (K_i) for SERT.¹⁵⁻¹⁹

The ABFE method was validated based on the protocols described by Gumbart *et al.*¹⁷ and Jo *et al.*¹⁸ The systems used for validating the ABFE method include the crystal structure of leucine in LeuT (PDB entry 3F3A)²⁰ and T4 lysozyme bound to FK5 (PDB entry 1FKJ).¹⁸

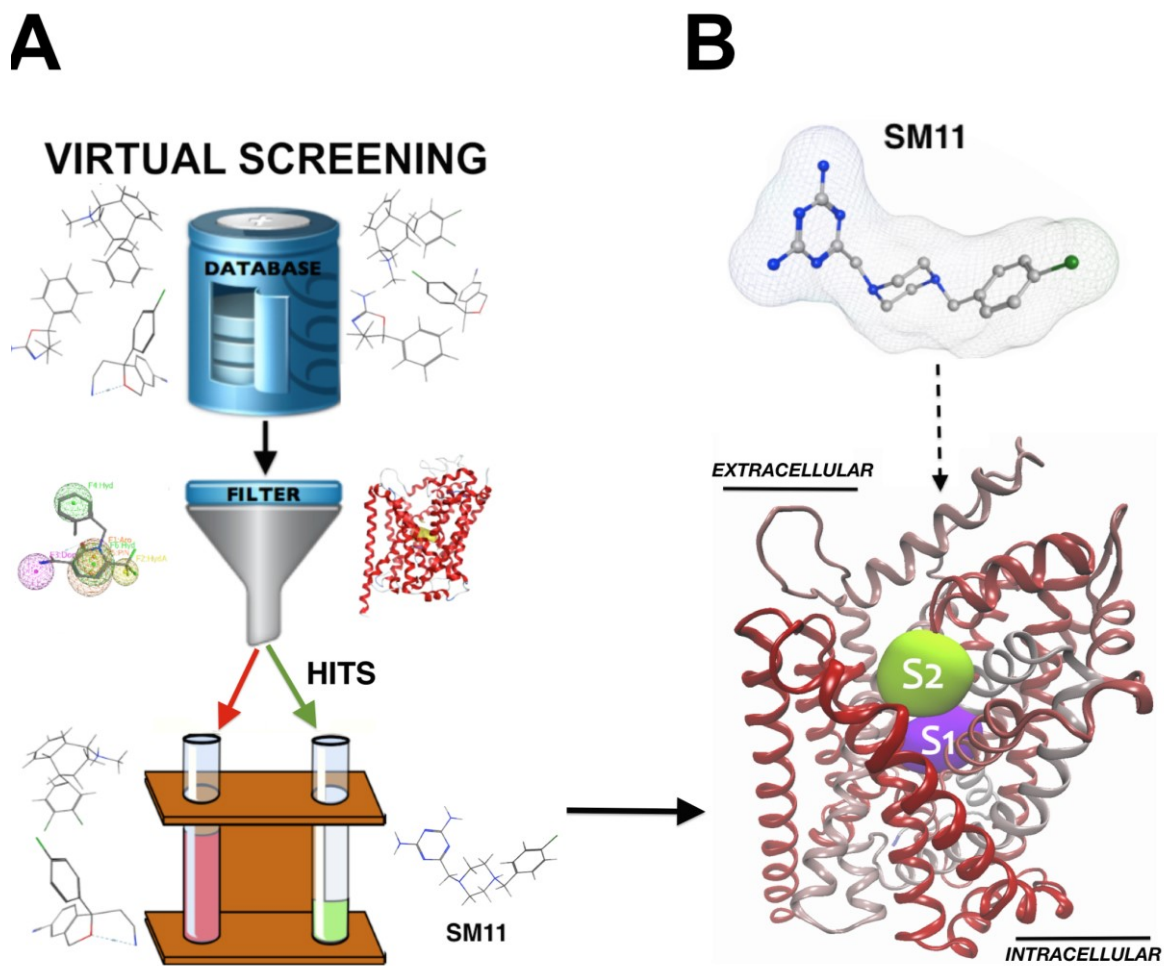


Figure 4.1: A) Schematic representation of a virtual screening that was previously performed by Manepalli *et al.* to find inhibitors capable of inhibiting SERT. The ZINC database was screened using a pharmacophore created for the S2 binding site of SERT.¹⁴ B) Schematic representation of SM11 (small molecule at top right), SERT (red ribbon rendering) and its ligand binding pockets S1 (purple) and S2 (green). SM11 was found to have binding affinity for SERT based on a previously performed competitive membrane binding assay. ABFE calculations were performed for SM11 in the S1 and S2 sites of SERT. The calculated ABFE was compared to experimental measurements of ligand affinity for SERT to determine which SERT binding site is occupied by SM11.

Experimental measurements of SM11 affinity to SERT were used to validate the calculation of the ABFE using

$$\Delta G^o = RT \ln K_i \quad (4.1)$$

where ΔG^o represents Gibbs standard binding free energy, R is the gas constant, T is the absolute temperature, and K_i is the inhibition constant measured from a competitive membrane binding assay.

The affinity of SM11 was determined by the ligand's ability to inhibit [125 I]-RTI-55, a radiolabeled ligand, from binding in SERT at increasing concentrations of SM11. Comparison of the ABFE calculation with the experimentally measured binding free energy was used to determine the binding site and binding pose of SM11 in SERT. Then several SM11 analogs were proposed, and the RBFE calculations were used to quantify the change in binding free energy associated with the modifications made to SM11.²¹⁻²³

4.2 Results and Discussion

4.2.1 Validating the free energy calculations

The relative free energy change calculated by Jorgensen *et al.* for mutating methanol to ethane in the forward ($\lambda = 0$ to $\lambda = 1$) and backward ($\lambda = 1$ to $\lambda = 0$) directions was 6.7 ± 0.2 kcal/mol and -6.8 ± 0.2 kcal/mol, respectively, comparable to the experimental hydration energy of 6.9 kcal/mol. The reproduced free energy of hydration was calculated to be -7.8 ± 0.3 kcal/mol (**Figure 4.2**). The difference between the calculated free energy of hydration and that reported by Jorgensen *et al.* can be related to a number of factors. There was a difference in the solvated systems; TIP3P water

molecules were used for the systems calculated here instead of TIP4P, which affects the number of possible intermolecular interactions between the ligand with each water molecule.^{24, 25} CHARMM27 force field with dihedral cross-term corrections (CMAP) was used and as oppose to the OPLS parameters.²⁶ Finally, specific intermolecular potential functions were assigned to the atoms in the system. In the reproduced calculations, no additional modifications were made to the system.

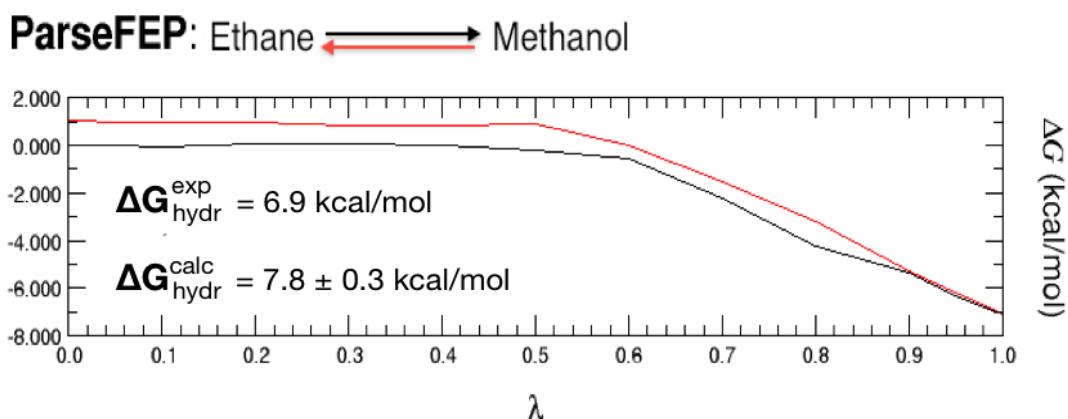


Figure 4.2: Free energy change ($\Delta G_{\text{hydr}}^{\text{calc}}$) for the forward (black) and backward (red) alchemical transformation of ethane to methanol. The ParseFEP plugin in VMD was used to generate the FEP plot,²⁷ where ΔG was calculated as a function of λ . $\Delta G_{\text{hydr}}^{\text{calc}}$ was calculated using free energy perturbation and molecular dynamics. The charge parameters assigned by Jorgensen *et al.* were used.²⁸ The experimental free energy, $\Delta G_{\text{hydr}}^{\text{exp}} = -6.9 \text{ kcal/mol}$ was comparable to the calculated free energy, $\Delta G_{\text{hydr}}^{\text{calc}} = -7.8 \pm 0.3 \text{ kcal/mol}$ (mean \pm s.d.). The statistical error was not reported for $\Delta G_{\text{hydr}}^{\text{exp}}$.

The protocol outlined by Jo *et al.* was followed to perform the alchemical transformation of T4 lysozyme bound to FK5 using the CHARMM-GUI *Ligand Binder* tool.¹⁸ **Table 4.1** summarizes the calculations performed by Jo *et al.* of T4 lysozyme bound to FK5. The same system was used to reproduce the absolute binding free energy of the T4 lysozyme to FK5 using the input files generated the *Ligand Binder* tool (**Table 4.1**). The reproduced calculations were comparable to the results reported by Jo *et al.* and to the experimental binding free energy. The differences in the calculated $\Delta G_{\text{int}}^{\text{site}}$ and

$\Delta\Delta G_{t,r}$ are likely due to the difference in the atoms chosen for the assignment of the harmonic restraints in the protein-ligand complex. The benefit of the *Ligand Binder* web server is the ability to perform these calculations without the tedious setup required in the simulation input files. The atoms that define the reference frame for the translational and rotational restraints are automatically chosen. However, if the atom sets do not properly anchor the ligand to the protein, the results may vary due to ineffective geometric restraints that are unable to maintain the appropriate orientation of the ligand to the protein. This may even lead to instabilities in the simulation and inaccurate outcome of the calculations. Therefore, these calculations still require monitoring because of the reassignments of the restraints.

Table 4.1: A) Absolute binding free energy (ABFE) calculations of T4 lysozyme bound to FK5 performed by Jo *et al.*, using the CHARMM-GUI *Ligand Binder* input files, was compared to B) the reproduced ABFE calculations of T4 lysozyme bound to FK5 using the CHARMM-GUI *Ligand Binder* input files.¹⁸ ΔG_{int}^{site} is the binding free energy associated with intermolecular interactions of the ligand in the binding site. ΔG_{int}^{hydr} is the binding free energy associated with the ligand in bulk solvent. $\Delta\Delta G_{conf}$ is the change in conformational free energy associated with the harmonic restraints applied to the ligand. $\Delta\Delta G_{t,r}$ is the free energy change associated with the translational and rotational restraints placed on the ligand. ΔG_{bind}^o is the calculated standard ABFE, which is compared to the experimental ABFE (ΔG_{exp}).

$$\Delta G_{bind}^o = \Delta G_{int}^{hydr} - \Delta G_{int}^{site} - \Delta\Delta G_{conf} - \Delta\Delta G_{t,r}$$

	ΔG_{int}^{site}	ΔG_{int}^{hydr}	$\Delta\Delta G_{conf}$	$\Delta\Delta G_{t,r}$	ΔG_{bind}^o	ΔG_{exp}
A)	-60.0 ± 1.3	-35.0 ± 1.9	2.3 ± 0.7	9.8 ± 0.0	-12.9 ± 2.4	-12.7 ± 0.2
B)	-49.0 ± 2.2	-34.2 ± 1.9	3.6 ± 1.0	-2.0 ± 0.2	-13.3 ± 2.9	-12.7 ± 0.2

All energies in kcal/mol

The protocol outlined by Gumbart *et al.*¹⁷ was followed to perform the alchemical transformation of leucine in the LeuT co-crystal structure. Table 4.3 summarizes the results from the free energy calculation of leucine in LeuT. The difference between the binding free energy within the binding site and in the bulk solvent is only 0.5 kcal/mol.

Once the conformational, rotational and positional free energy contributions are accounted for, however, the final binding free energy ΔG_{bind}^o is equal to -10.1 ± 0.4 kcal/mol, which is comparable to the experimental binding free energy equal to -10.6 ± 0.1 kcal/mol.

Table 4.2: ABFE calculations for the alchemical transformation of leucine in LeuT (PDB entry 3F3A) performed following the protocol outlined by Gumbart *et al.*¹⁷ ΔG_{int}^{site} is the binding free energy associated with intermolecular interactions of the ligand in the binding site. ΔG_{int}^{hydr} is the binding free energy associated with the ligand in bulk solvent. $\Delta\Delta G_{conf}$ is the change in conformational free energy associated with the harmonic restraints applied to the ligand in the protein binding site and in bulk solvent. $\Delta\Delta G_{t,r}$ is the free energy change associated with the translational and rotational restraints placed on the ligand in the protein binding site. ΔG_{bind}^o is the calculated standard ABFE, which is compared to the experimental ABFE (ΔG_{exp}).

$$\Delta G_{bind}^o = \Delta G_{int}^{hydr} - \Delta G_{int}^{site} - \Delta\Delta G_{conf} - \Delta\Delta G_{t,r}$$

ΔG_{int}^{site}	ΔG_{int}^{hydr}	$\Delta\Delta G_{conf}$	$\Delta\Delta G_{t,r}$	ΔG_{bind}^o	ΔG_{exp}
-59.2 ± 0.2	-59.7 ± 0.3	-0.6 ± 0.0	-9.0 ± 0.0	-10.1 ± 0.4	-10.6 ± 0.1

All energies in kcal/mol

The results of the calculations are summarized in **Table 4.3**. The resulting ΔG_{bind}^o was approximately 1.9 kcal/mol less than the experimental binding free energy. These calculations were performed prior to the availability of the hSERT co-crystal structures. The difference in the calculated results can be attributed to the use of a SERT homology model based on LeuT and modeling the ligand binding based on the LeuT interactions in the S2 site.

Table 4.3: ABFE calculations of R-fluoxetine in the S2 binding site in SERT performed using the *Ligand Binder* Web server.¹⁸ ΔG_{int}^{site} is the binding free energy associated with intermolecular interactions of the ligand in the binding site. ΔG_{int}^{hydr} is the binding free energy associated with the ligand in bulk solvent. $\Delta\Delta G_{conf}$ is the change in conformational free energy associated with the harmonic restraints applied to the ligand in the protein binding site and in bulk solvent. $\Delta\Delta G_{t,r}$ is the free energy change associated with the translational and rotational restraints placed on the ligand in the protein binding site. ΔG_{bind}^o is the calculated standard ABFE, which is compared to the experimental ABFE (ΔG_{exp}).

$$\Delta G_{bind}^o = \Delta G_{int}^{hydr} - \Delta G_{int}^{site} - \Delta\Delta G_{conf} - \Delta\Delta G_{t,r}$$

ΔG_{int}^{site}	ΔG_{int}^{hydr}	$\Delta\Delta G_{conf}$	$\Delta\Delta G_{t,r}$	ΔG_{bind}^o	ΔG_{exp}
-50.3 ± 1.0	-56.6 ± 0.5	-6.4 ± 0.5	-22.5 ± 0.2	-9.8 ± 1.0	-11.7 ± 0.3

All energies in kcal/mol

4.2.2 Determining the SERT SM11 binding site

SM11 was docked into the S1 and S2 sites of a SERT homology model based on LeuT. The protein-ligand system was embedded in a lipid bilayer and simulated for 10ns, after which the protein-ligand system was removed from the lipid bilayer and solvated in a water box before performing the free energy calculations. The binding site of SM11 was determined by applying ABFE calculations to SM11 for SERT S1 and S2 binding sites. ABFE is expressed in terms of specific intermediate steps in which the ligand-environment interactions, as well as the positional, translational, and conformational sampling of the ligand, are scaled. The calculated ΔG_{bind}^o for SM11 in S1 was -3.4 ± 1.8 kcal/mol (**Table 4.4**).

Table 4.4: ABFE calculations of SM11 in the S1 binding site in SERT performed using the *Ligand Binder* Web server.¹⁸ ΔG_{int}^{site} is the binding free energy associated with intermolecular interactions of the ligand in the binding site. ΔG_{int}^{hydr} is the binding free energy associated with the ligand in bulk solvent. $\Delta\Delta G_{conf}$ is the change in conformational free energy associated with the harmonic restraints applied to the ligand in the protein binding site and in bulk solvent. $\Delta\Delta G_{t,r}$ is the free energy change associated with the translational and rotational restraints placed on the ligand in the protein binding site. ΔG_{bind}^o is the calculated standard ABFE, which is compared to the experimental ABFE (ΔG_{exp}).

$$\Delta G_{bind}^o = \Delta G_{int}^{hydr} - \Delta G_{int}^{site} - \Delta\Delta G_{conf} - \Delta\Delta G_{t,r}$$

$\Delta\mathbf{G}_{int}^{site}$	$\Delta\mathbf{G}_{int}^{hydr}$	$\Delta\Delta\mathbf{G}_{conf}$	$\Delta\Delta\mathbf{G}_{t,r}$	$\Delta\mathbf{G}_{bind}^o$	$\Delta\mathbf{G}_{exp}$
-72.1 ± 2.0	-60.8 ± 0.8	7.4 ± 1.9	0.2 ± 0.4	-3.1 ± 1.8	-6.5 ± 0.3

All energies in kcal/mol

The calculated ΔG_{bind}^o for the S2 site was -7.8 ± 1.4 kcal/mol and is more comparable to the experimental binding free energy of -6.5 ± 0.3 kcal/mol (**Table 4.5**). Therefore the free energy calculations support SM11 binding in S2. The SERT crystal structure co-crystallized with citalopram in the S2 site was superposed with the binding of SM11 in S2 and the binding interactions within the SERT homology model were similar to those seen in the crystal structure.

Table 4.5: ABFE calculations of SM11 in the S2 binding site in SERT performed using NAMD following the protocol outlined by Gumbart *et al.*¹⁷ ΔG_{int}^{site} is the binding free energy associated with intermolecular interactions of the ligand in the binding site. ΔG_{int}^{hydr} is the binding free energy associated with the ligand in bulk solvent. $\Delta\Delta G_{conf}$ is the change in conformational free energy associated with the harmonic restraints applied to the ligand in the protein binding site and in bulk solvent. $\Delta\Delta G_{t,r}$ is the free energy change associated with the translational and rotational restraints placed on the ligand in the protein binding site. ΔG_{bind}^o is the calculated standard ABFE, which is compared to the experimental ABFE (ΔG_{exp}).

$$\Delta G_{bind}^o = \Delta G_{int}^{hydr} - \Delta G_{int}^{site} - \Delta\Delta G_{conf} - \Delta\Delta G_{t,r}$$

$\Delta\mathbf{G}_{int}^{site}$	$\Delta\mathbf{G}_{int}^{hydr}$	$\Delta\Delta\mathbf{G}_{conf}$	$\Delta\Delta\mathbf{G}_{t,r}$	$\Delta\mathbf{G}_{bind}^o$	$\Delta\mathbf{G}_{exp}$
-55.5 ± 0.6	-34.8 ± 1.2	5.7 ± 0.0	7.3 ± 0.0	-7.8 ± 1.4	-6.5 ± 0.3

All energies in kcal/mol

4.2.3 Measuring affinity of SERT inhibitors

The competitive membrane binding assay was performed to measure the affinity of SERT inhibitors. A serial dilution of citalopram in binding buffer was prepared from 10 μM to 1 nM and incubated with HEK293-hSERT membranes and [^{125}I]-RTI-55 with paroxetine (10 μM) used for non-specific binding. The affinity of citalopram was determined, in triplicate, to be $K_i = 2.4 \pm 1.2$ nM, and is comparable to the previously measured experimental affinity of 1.4 nM (Figure 4.3).²⁹

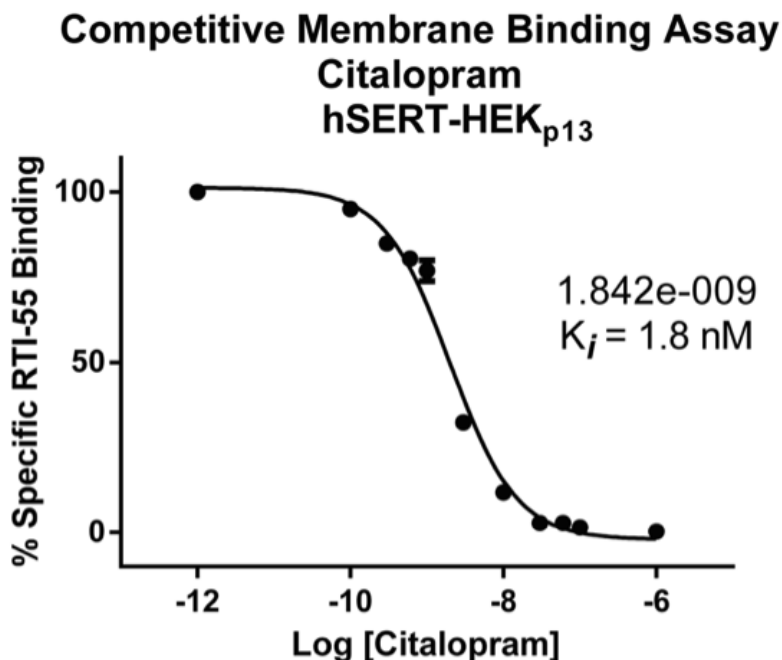


Figure 4.3: Competitive membrane binding assay used to determine the affinity (K_i) of citalopram for SERT using the HEK293-hSERT cell line. Serial dilution of citalopram was prepared from 10 μM to 1 nM and incubated with HEK293-hSERT membranes and [^{125}I]-RTI-55. Paroxetine (10 μM) was used for non-specific binding.

The affinity of SM11 for SERT was determined using the competitive membrane binding assay. The average K_i value of $17 \pm 7 \mu\text{M}^{14}$ was then converted to $\Delta G_{exp}^o = -6.5 \pm 0.3 \text{ kcal/mol}$ (Figure 4.4).

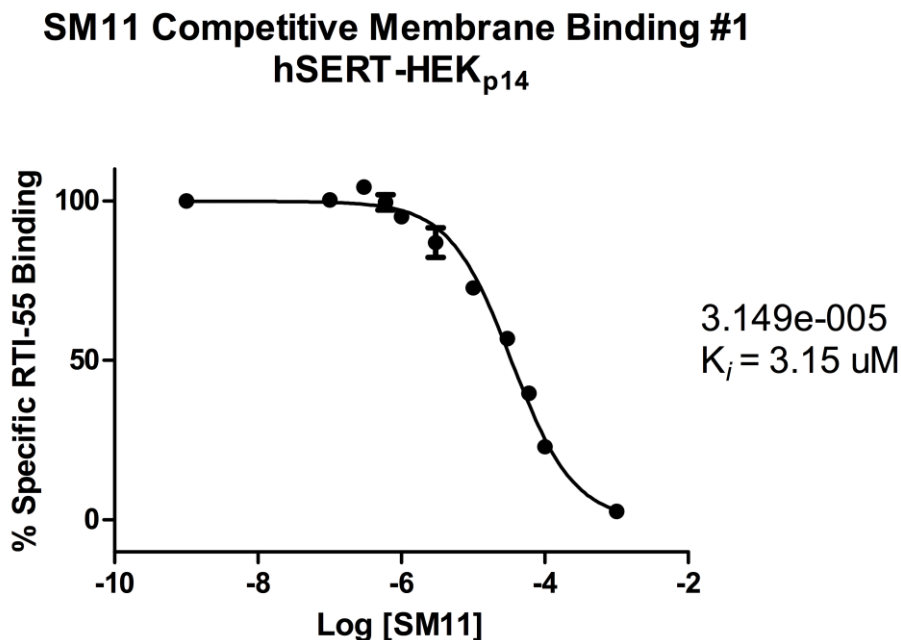


Figure 4.4: Competitive membrane binding assay of SM11 in HEK293-hSERT cell line. The affinity (K_i) was determined by SM11's ability to competitively bind with SERT against [^{125}I]-RTI-55. Experimental affinity of SM11 for SERT was $17 \pm 7 \mu\text{M}$.¹⁴

SM11 had been assumed to prefer the S2 binding site of SERT because the compound was found by S2 pocket virtual screening of a structural library of small molecules. The ABFE calculations were applied to both S1 and S2 binding sites to compare the calculated binding free energy of SM11 to experimental measurements of binding free energy. The calculations support SM11 binding in the S2 site and not in the S1 site of SERT. Evaluation of SM11 binding in the S2 site suggests an opportunity to improve interactions with SERT residues, such as a potential hydrogen bond with Glu493 (Figure 4.5). Several analogs have been proposed as modifications to SM11 that would

result in greater affinity for SERT. Relative binding free energy calculations were executed to determine if the modifications would be energetically favorable.

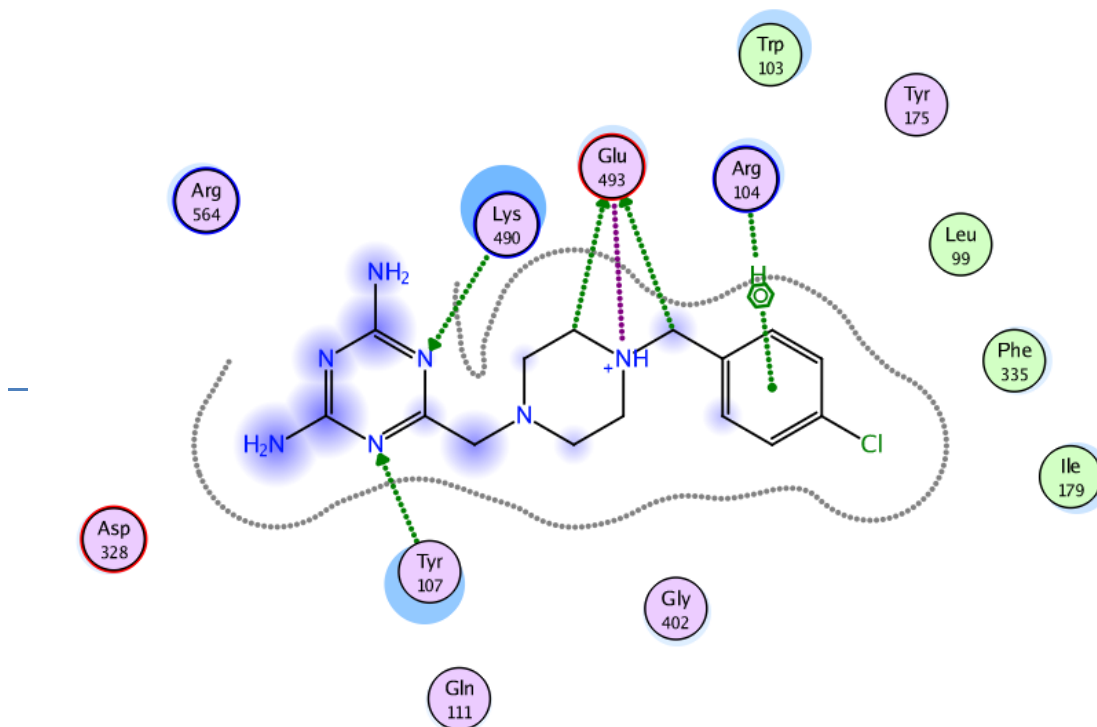


Figure 4.5: 2D ligand interaction map depicting the intermolecular interactions between SM11 and SERT in the proposed S2 binding site based on ABFE calculations (**Table 4.5**).

4.2.4 Relative binding free energy calculations of SM11 analogs

The purpose of SM11 analogs was to elucidate the basis of SERT inhibitor recognition via key modifications to SM11 functional groups and to probe for likely ligand-S2 interactions in general (**Figure 4.5**), toward developing novel allosteric modulators of SERT. FEP calculations were used to assess SM11 analogs and determine which modifications were energetically favorable.

Observation of the intermolecular interactions between SM11 and SERT residues in the S2 site revealed an opportunity to increase intermolecular interactions between SM11 and Glu493 by adding a hydrogen bond donating group to SM11. BJ01 and BJ02 represent SM11 analogs with hydrogen atoms replaced with a hydroxyl group to form intermolecular interactions with Glu493 residue. The S-methanol configuration was measured 2.4 Å away from the closest oxygen atom of the Glu493 carboxylate, and the R-methanol configuration was approximately 3.9 Å away (**Figure 4.6**). The synthesis of these analogs was unviable and was not studied further. Therefore, only analogs that could be synthesized were considered and evaluated using binding free energy calculations.

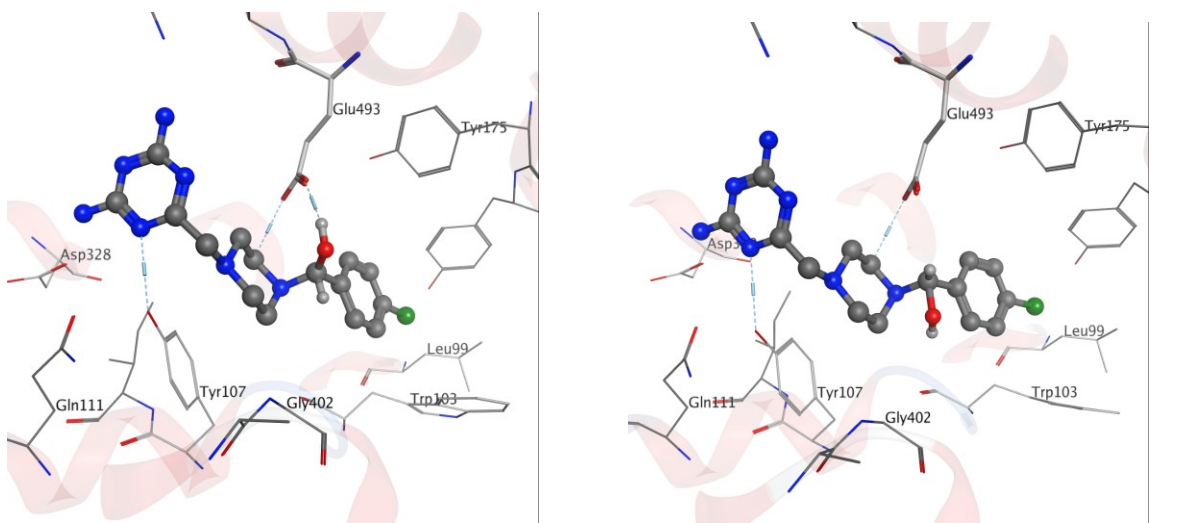


Figure 4.6: SM11 analogs proposed to form a hydrogen bond interaction with Glu493 of the S2 binding site. (Left) S-methanol and (right) R-methanol substitution. These two analogs were unable to be synthesized.

The atoms of the 4-chlorobenzyl group of SM11 was altered to give four analogs (**Figure 4.7**). This hydrophobic ring structure is believed to interact with the hydrophobic, halogen-binding pocket defined by Leu99, Trp103, and Ile179.¹⁴ To validate the binding of this moiety in the halogen binding pocket, several analogs with

modifications to the benzene ring were proposed.^{4, 14} Substitutions included replacement of chlorine with a hydrogen atom (BJ11) or a 3,4-dichloro (BJ12), -CF₃ (BJ13), or -OCH₃ (BJ14) functional group (**Figure 4.7**).

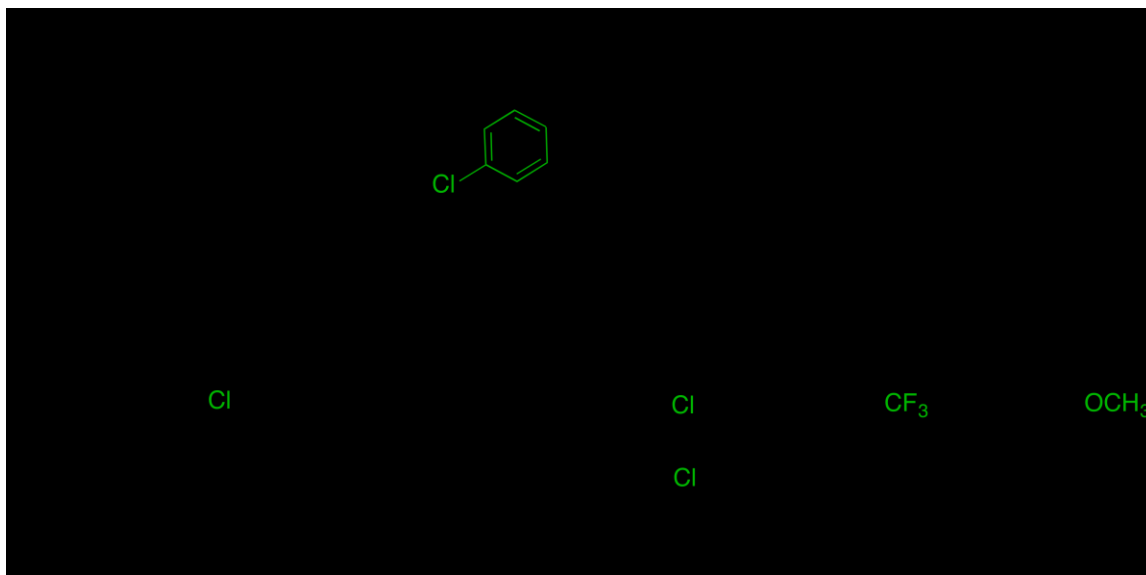


Figure 4.7: Modifications proposed for the 4-chlorobenzyl moiety of SM11: (1) BJ11 (benzene), (2) BJ12 (3,4-dichlorobenzene), (3) BJ13 (4-trifluoromethylbenzene) and (4) BJ14 (4-methoxybenzene).

Dual topology files were generated for each SM11 analog for the relative binding free energy calculations.^{28, 30, 31} At the beginning of the simulation, only the atoms of SM11 is interacting with the environment of the system. Then the interactions of the atoms belonging to SM11 with its environment are gradually reduced while the interactions of the atoms belonging to the analog are introduced. At the end of the simulation, only the atoms of the analog are interacting with the environment of the system. The free energy calculations were applied to the thermodynamic cycle to calculate the relative binding energy of a ligand (*L*) to a protein (*P*) (**Figure 1.11**). ΔG_{hydr} is the calculated difference in ligand hydration energies in bulk solvent, and

ΔG_{site} is the difference in ligand binding energies in a solvated protein-ligand complex ($P:L$). The difference between these two values represents the relative change in binding free energy ($\Delta\Delta G$), which is used to determine if the atomic transformation is energetically favorable.³¹⁻³³

Relative free energy calculations were applied to SM11 to calculate the relative change in free energy based on the modified structural group. Several analogs of SM11 were proposed to improve the interactions of SM11 in S2. The relative binding free energy calculations were performed to determine if the proposed modifications would be energetically favorable. Results from these calculations helped to determine which atom modifications would play a key role in improving the SM11 binding in SERT. SM11 analogs were purchased or synthesized to validate the computational calculations using experimental measurements of the ligand's affinity for SERT. **Table 4.6** summarizes the results of the relative binding free energy calculations.

Table 4.6: RBE ($\Delta\Delta G$) calculation of SM11 analogs in SERT. The change in binding free energy was calculated for modifying SM11 to one of the new ligands in SERT (**Figure 4.7**). ΔG_{site} is the change in binding free energy associated with intermolecular interactions of the ligand in the binding site. ΔG_{hydr} is the change in free energy associated with the ligand in bulk solvent.

<i>Ligand</i>	$\Delta\Delta G = \Delta G_{site} - \Delta G_{hydr}$		
	ΔG_{hydr}	ΔG_{site}	$\Delta\Delta G$
BJ11	2.4 ± 0.2	5.2 ± 0.2	2.8 ± 0.3
BJ12 (pose A)	12.7 ± 0.3	0.6 ± 0.2	-12.1 ± 0.4
BJ12 (pose B)	12.7 ± 0.3	0.4 ± 0.2	-12.3 ± 0.4
BJ13	30.9 ± 0.3	32.5 ± 0.3	-1.6 ± 0.4
BJ14	-7.7 ± 0.2	-5.0 ± 0.3	-12.7 ± 0.4

All energies in kcal/mol

The $\Delta\Delta G$ calculations for BJ11 resulted in a significant reduction in interaction energy at the binding site. The calculated relative binding free energy was supported by

the loss of experimental affinity of BJ11 to SERT (**Figure 4.8**). The lack of 100% radioligand displacement seen in the BJ11 binding curve indicates a profound affinity loss relative to SM11 (**Figure 4.8**). The binding of the benzene ring with the hydrophobic pocket (**Figure 4.8B**, green dashed lines) shows the region previously occupied by the chlorine atom on the benzene ring is now unoccupied with the binding of BJ11 and allows for greater fluctuation of the surrounding SERT residues. These results support the importance of the *para*-halogen atom on the benzene ring.

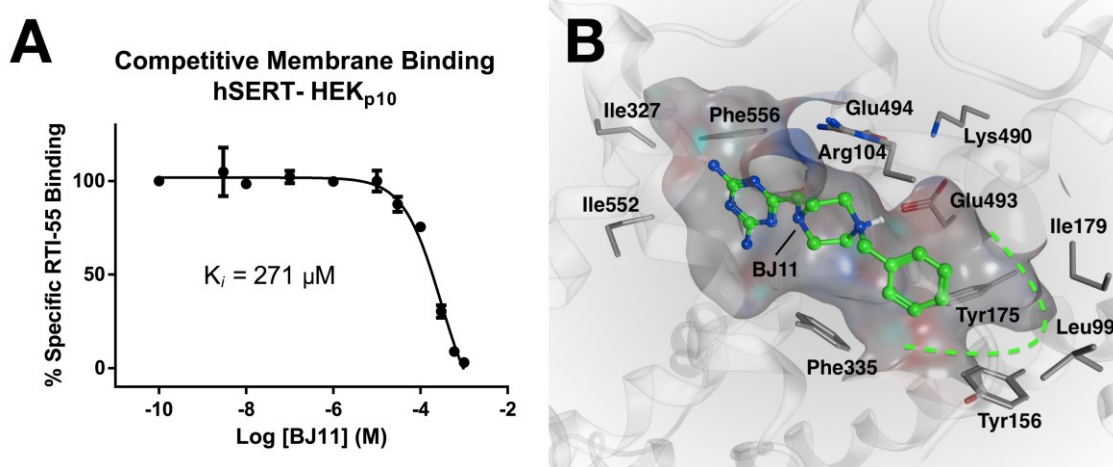


Figure 4.8: A) Competitive SERT membrane binding assay using nonradioactive BJ11 in HEK293-hSERT cell line. The affinity (K_i) was determined by BJ11's ability to competitively bind with SERT against [^{125}I]-RTI-55. B) SERT S2 binding site interactions with BJ11 (green ball-and-stick). The calculated $\Delta\Delta G = 2.8 \pm 0.3$ kcal/mol indicates the removal of the chlorine atom leads to unfavorable SERT binding.

The 3,4-dichlorobenzyl structure was considered, and two poses of the analog were studied, where the placement of the chlorine atom was on either side of the existing chlorine (**Figure 4.9**). This modification was expected to improve SM11 binding interactions in the predicted binding pose with a 3,4-dichlorobenzyl structure because this would make the ring system more reactive with electron-withdrawing halogens. However, BJ12 $\Delta\Delta G_{calc}$ for pose A and pose B indicate there is a minimal impact of a

3,4-dichloro modification in the binding site (pose A, $\Delta G_{hydr} = 0.6 \pm 0.2$ kcal/mol and pose B, $\Delta G_{hydr} = 0.4 \pm 0.2$ kcal/mol). There appears to be a potential driving factor that could force the ligand out of solution and into the binding site. $\Delta\Delta G = -12.1 \pm 0.4$ kcal/mol and -12.3 ± 0.4 kcal/mol indicates BJ12 is an energetically favorable modifications.

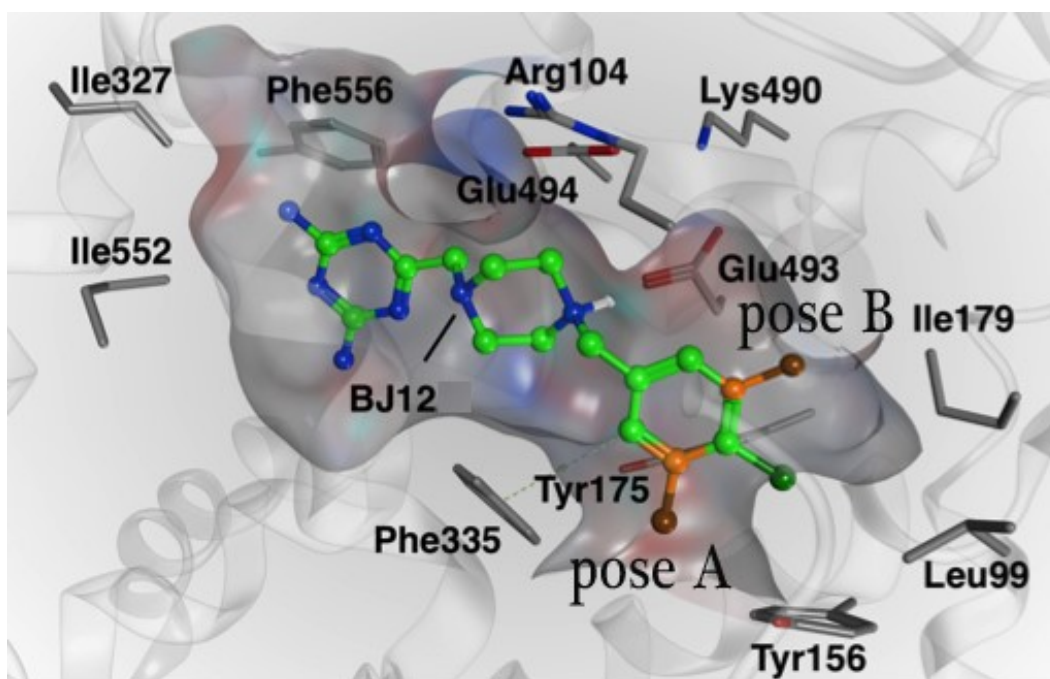


Figure 4.9: SERT S2 binding site interactions with BJ12. The rotation of 3, 4 chlorobenzyl moiety is labeled pose A and B (orange). The calculated $\Delta\Delta G = -12.1 \pm 0.4$ kcal/mol (pose A) and $= -12.3 \pm 0.4$ kcal/mol (pose B).

The trifluoromethyl substitution to the benzene ring has an increased electronegativity and is expected to be more electron withdrawing from the ring. The relative binding free energy change calculated for BJ13 suggested that the trifluoromethyl addition would be a favorable modification. However, the $\Delta\Delta G$ was less favorable than the $\Delta\Delta G$ for BJ12A, BJ12B, and BJ14. The $\Delta\Delta G = -1.6 \pm 0.4$ kcal/mol suggests the trifluoromethyl modification of BJ13 would result in similar binding affinity to SM11.

The large energy values calculated for ΔG_{hydr} and ΔG_{site} may be attributed to potential steric clash of the atoms with the added functional group (**Figure 4.10**). Performing longer MD before the RBE calculation would allow for the sidechains to equilibrate before calculating the binding free energy. Additionally, the force field parameters used to define the atoms of BJ13 may require additional optimization.

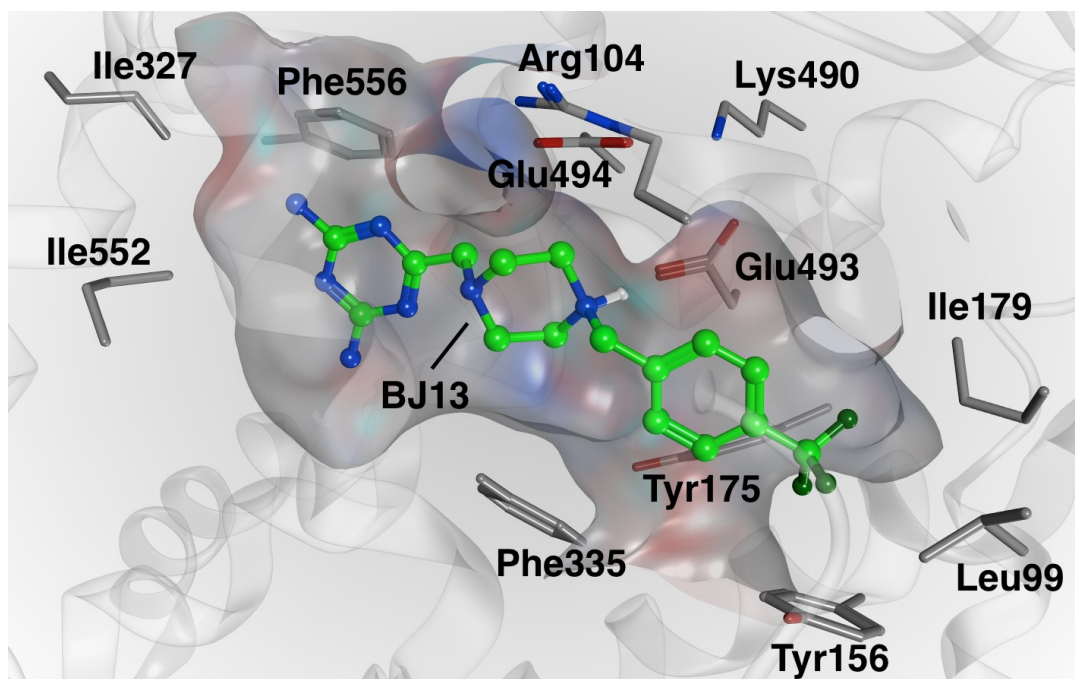


Figure 4.10: Binding site interactions with BJ13 (green ball-and-stick) in S2 site of SERT. The calculated $\Delta\Delta G = -1.6 \pm 0.4$ kcal/mol.

The $-\text{OCH}_3$ (methoxy) substitution to the benzene ring was proposed to favorably interact with the hydrophobic region near Leu99 and Ile179 (**Figure 4.11**). The relative binding free energy change calculated for BJ14 indicated that this is the only modification that results in a favorable change in the hydration free energy (ΔG_{hydr}), possibly because of hydrogen-bond capability of the methoxy functional group added to the benzene ring. Additionally, the relative binding free energy change in the binding site

(ΔG_{site}) was favorable. The methoxy functional group added to the ring is bound to a hydrophobic region near Leu99 and Ile179. The methyl substitution is more hydrophobic and should interact deeper into the pocket and favorably in its hydrophobic area.

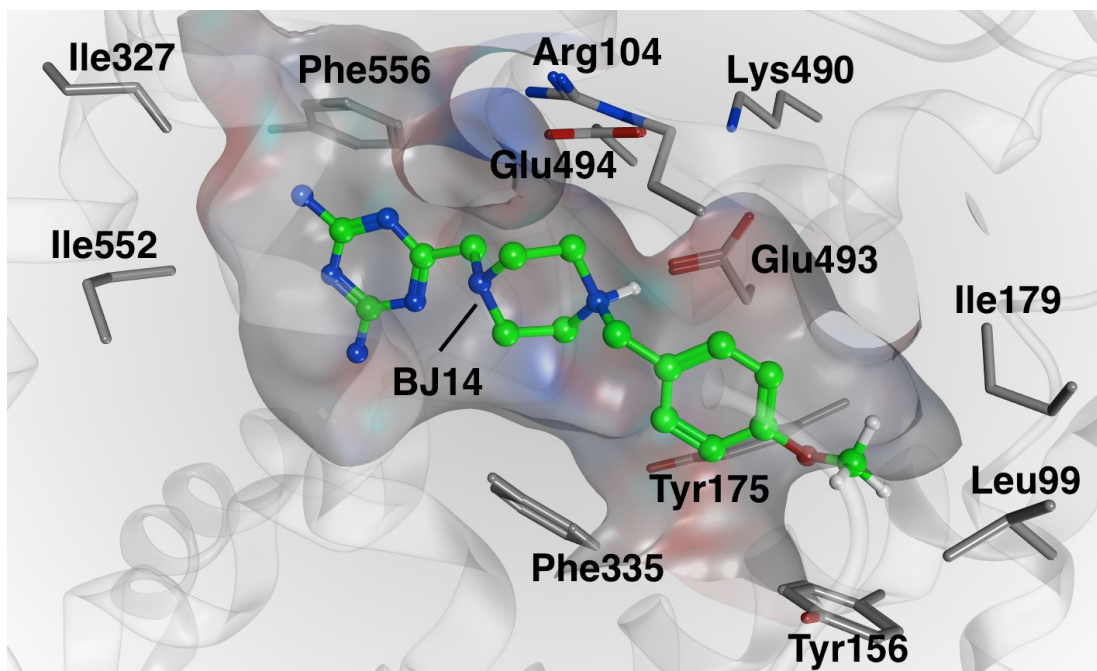


Figure 4.11: Binding site interactions with BJ14 (green ball-and-stick) in S2 site of SERT. The calculated $\Delta\Delta G = -12.7 \pm 0.4$ kcal/mol.

4.3 Conclusions

Modeling the binding of SM11 in SERT revealed the potential to optimize interactions between the ligand and S2 residues. Several analogs were proposed to probe ligand binding and test key interactions with SERT residues. These analogs have been synthesized and are currently available for cell-based assay testing. Once all of the analogs have been pharmacologically tested, and their K_i values have been determined, the structure-activity relationship of SM11 in SERT will be better understood. Furthermore, being that [125 I]-RTI-55 has an affinity for the S1 site of SERT, use of a

radioligand with an affinity for the S2 site of SERT would offer more accurate insight into the ligand's ability to compete for binding in the transporter.

It should be noted that the crystal structure of TCAs and SSRIs in the S2 site of LeuT may not represent similar antidepressant binding in SERT based on later studies.³⁴ However modeling the binding of R-fluoxetine in the S2 site of SERT based on the LeuT crystal structure (PDB entry 3GWV) can offer insight into the allosteric binding site interactions in SERT. Furthermore, the recent crystal structure of SERT with S-citalopram (PDB entry 5I73) shows two inhibitor molecules bound to the S1 and S2 binding sites of SERT, indicating there is a possibility for a second molecule to occupy both the allosteric site and the primary binding site. Additionally, applying the ABFE calculations to S-citalopram in both binding sites would determine if a direct correlation exists between the measured affinity and approach used to calculate ABFE of the inhibitors. For future work, running longer MD equilibration before calculating the binding free energy should be considered to reduce statistical error and improve convergence.

4.4 References

1. Best, J., Nijhout, H. F., and Reed, M. (2011) Bursts and the Efficacy of Selective Serotonin Reuptake Inhibitors. *Pharmacopsychiatry* 44, S76-S83.
2. Lemonde, S., Turecki, G., Bakish, D., Du, L., Hrdina, P. D., Bown, C. D., Sequeira, A., Kushwaha, N., Morris, S. J., Basak, A., Ou, X.-M., and Albert, P. R. (2003) Impaired Repression at a 5-Hydroxytryptamine 1A Receptor Gene Polymorphism Associated with Major Depression and Suicide. *J Neurosci* 23, 8788-8799.
3. von Wolff, A., Holzel, L. P., Westphal, A., Harter, M., and Kriston, L. (2013) Selective serotonin reuptake inhibitors and tricyclic antidepressants in the acute treatment of chronic depression and dysthymia: a systematic review and meta-analysis. *J Affect Disord* 144, 7-15.

4. Zhou, Z., Zhen, J., Karpowich, N. K., Law, C. J., Reith, M. E. a., and Wang, D.-n. N. (2009) Antidepressant specificity of serotonin transporter suggested by three LeuT-SSRI structures. *Nat Struct Mol Biol* 16, 652-657.
5. Hanson, N. D., Owens, M. J., and Nemeroff, C. B. (2011) Depression, antidepressants, and neurogenesis: a critical reappraisal. *Neuropsychopharmacology* 36, 2589-2602.
6. Owens, M. J., Knight, D. L., and Nemeroff, C. B. (2001) Second-generation SSRIs: human monoamine transporter binding profile of escitalopram and R-fluoxetine. *Biol Psychiatry* 50, 345-350.
7. Owens, M. J., Morgan, W. N., Plott, S. J., and Nemeroff, C. B. (1997) Neurotransmitter receptor and transporter binding profile of antidepressants and their metabolites. *J Pharmacol Exp Ther* 283, 1305-1322.
8. Kos, T., Popik, P., Pietraszek, M., Schafer, D., Danysz, W., Dravolina, O., Blokhina, E., Galankin, T., and Bessalov, A. Y. (2006) Effect of 5-HT₃ receptor antagonist MDL 72222 on behaviors induced by ketamine in rats and mice. *Eur Neuropsychopharmacol* 16, 297-310.
9. Kristensen, A. S., Andersen, J., Jorgensen, T. N., Sorensen, L., Eriksen, J., Loland, C. J., Stromgaard, K., and Gether, U. (2011) SLC6 neurotransmitter transporters: structure, function, and regulation. *Pharmacol Rev* 63, 585-640.
10. Pramod, A. B., Foster, J., Carvelli, L., and Henry, L. K. (2013) SLC6 transporters: structure, function, regulation, disease association and therapeutics. *Mol Aspects Med* 34, 197-219.
11. Bisha, I., and Magistrato, A. (2016) The molecular mechanism of secondary sodium symporters elucidated through the lens of the computational microscope. *RSC Adv* 6, 9522-9540.
12. Singh, S. K., Yamashita, A., and Gouaux, E. (2007) Antidepressant binding site in a bacterial homologue of neurotransmitter transporters. *Nature* 448, 952-956.
13. Zhou, Z., Zhen, J., Karpowich, N. K., Goetz, R. M., Law, C. J., Reith, M. E. A., and Wang, D.-N. N. (2007) LeuT-desipramine structure reveals how antidepressants block neurotransmitter reuptake. *Science* 317, 1390-1393.
14. Manepalli, S., Geffert, L. M., Surratt, C. K., and Madura, J. D. (2011) Discovery of novel selective serotonin reuptake inhibitors through development of a protein-based pharmacophore. *J Chem Inf Model* 51, 2417-2426.
15. General, I. J., Dragomirova, R., and Meirovitch, H. (2012) Absolute free energy of binding of avidin/biotin, revisited. *J Phys Chem B* 116, 6628-6636.

16. Genheden, S. (2012) Are homology models sufficiently good for free-energy simulations? *J Chem Inf Model* 52, 3013-3021.
17. Gumbart, J. C., Roux, B., and Chipot, C. (2013) Standard binding free energies from computer simulations: What is the best strategy? *J Chem Theory Comput* 9, 794-802.
18. Jo, S., Jiang, W., Lee, H. S., Roux, B., and Im, W. (2013) CHARMM-GUI Ligand Binder for Absolute Binding Free Energy Calculations and Its Application. *J Chem Inf Model* 53, 267-277.
19. Soderhjelm, P., Tribello, G. A., and Parrinello, M. (2012) Locating binding poses in protein-ligand systems using reconnaissance metadynamics. *Proc Natl Acad Sci U S A* 109, 5170-5175.
20. Singh, S. K., Piscitelli, C. L., Yamashita, A., and Gouaux, E. (2008) A competitive inhibitor traps LeuT in an open-to-out conformation. *Science* 322, 1655-1661.
21. Jorgensen, W. L. (2009) Efficient drug lead discovery and optimization. *Acc Chem Res* 42, 724-733.
22. Kim, J. T., Hamilton, A. D., Bailey, C. M., Domoal, R. a., Domoal, R. a., Wang, L., Anderson, K. S., and Jorgensen, W. L. (2006) FEP-guided selection of bicyclic heterocycles in lead optimization for non-nucleoside inhibitors of HIV-1 reverse transcriptase. *J Am Chem Soc* 128, 15372-15373.
23. Ruiz-Caro, J., Basavapathruni, A., Kim, J. T., Bailey, C. M., Wang, L., Anderson, K. S., Hamilton, A. D., and Jorgensen, W. L. (2006) Optimization of diarylamines as non-nucleoside inhibitors of HIV-1 reverse transcriptase. *Bioorg Med Chem Lett* 16, 668-671.
24. Jorgensen, W. L. (1982) Revised TIPS for simulations of liquid water and aqueous solutions. *J Chem Phys* 77, 4156-4163.
25. Jorgensen, W. L., and Madura, J. D. (1985) Temperature and size dependence for Monte Carlo simulations of TIP4P water. *Mol Phys* 56, 1381-1392.
26. Best, R. B., Zhu, X., Shim, J., Lopes, P. E., Mittal, J., Feig, M., and Mackerell, A. D., Jr. (2012) Optimization of the additive CHARMM all-atom protein force field targeting improved sampling of the backbone phi, psi and side-chain chi(1) and chi(2) dihedral angles. *J Chem Theory Comput* 8, 3257-3273.
27. Liu, P., Dehez, F., Cai, W., and Chipot, C. (2012) A Toolkit for the Analysis of Free-Energy Perturbation Calculations. *J Chem Theory Comput* 8, 2606-2616.
28. Jorgensen, W. L., and Ravimohan, C. (1985) Monte Carlo simulation of differences in free energies of hydration. *J Chem Phys* 83, 3050-3054.

29. Goodman, L. S., Brunton, L., Chabner, B., and Knollman, B. (2011) *Goodman and Gilman's The Pharmacological Basis of Therapeutics*, 12th ed., New York: McGraw-Hill, 2011.
30. Reddy, M. R., Viswanadhan, V. N., and Weinstein, J. N. (1991) Relative differences in the binding free energies of human immunodeficiency virus 1 protease inhibitors: a thermodynamic cycle-perturbation approach. *Proc Natl Acad Sci U S A* 88, 10287-10291.
31. Miyamoto, S., and Kollman, P. A. (1993) Absolute and relative binding free energy calculations of the interaction of biotin and its analogs with streptavidin using molecular dynamics/free energy perturbation approaches. *Proteins* 16, 226-245.
32. Mobley, D. L., Chodera, J. D., and Dill, K. a. (2006) On the use of orientational restraints and symmetry corrections in alchemical free energy calculations. *J Chem Phys* 125, 084902.
33. Mobley, D. L., and Klimovich, P. V. (2012) Perspective: Alchemical free energy calculations for drug discovery. *J Chem Phys* 137, 230901.
34. Sinning, S., Musgaard, M., Jensen, M., Severinsen, K., Celik, L., Koldsø, H., Meyer, T., Bols, M., Jensen, H. H., Schiøtt, B., and Wiborg, O. (2010) Binding and orientation of tricyclic antidepressants within the central substrate site of the human serotonin transporter. *J Biol Chem* 285, 8363-8374.

CHAPTER 5

5 FUTURE DIRECTIONS

5.1 Modeling the binding of DAT inhibitors

All-atom molecular dynamics simulations were previously employed to evaluate the DAT structural changes caused by inhibitor binding. The next step of this project involves applying an enhanced sampling method to capture the distinct conformational changes of DAT that are stabilized by inhibitor binding.¹ This project aims to gain a deeper understanding of DAT structural changes and the interactions responsible for inhibitor binding and disruption of substrate uptake. Results from this study can aid in the development of novel therapeutics to treat, various psychological disorders, such as psychostimulant addiction, Parkinson's disease, and depression.²⁻¹²

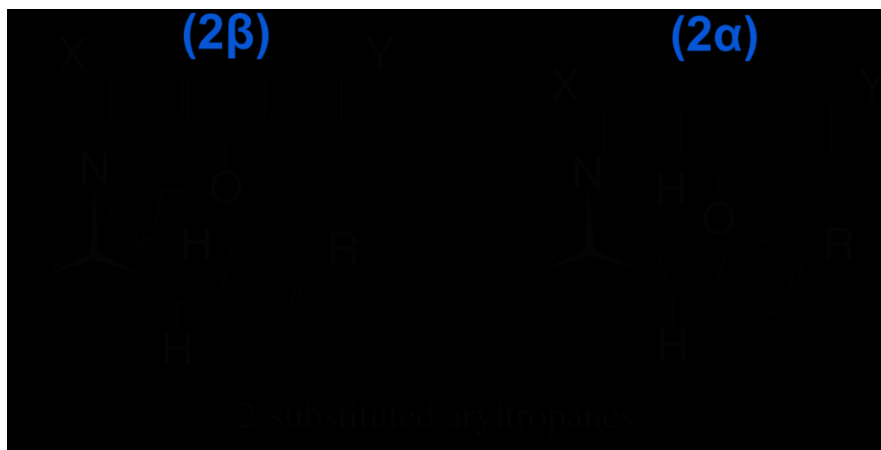


Figure 5.1: 2-substituted aryltropane cocaine analogs to study in future simulations with DAT using an accelerated MD method.^{1, 13} The ligand modifications have been studied *in vitro* and *in vivo* by Hong *et al.* The ligands would be simulated in the OF and IF DAT conformations followed by structural analysis of the transporter.

The next step in this research project can apply an accelerated MD (aMD) method, such as Gaussian accelerated molecular dynamics (GaMD), with additional cocaine analogs $(2\beta\text{-(4-XPh)-(4-YPh)-COCH}_2\text{-3}\beta\text{-4-R-Ph}$ and $2\alpha\text{-(4-XPh)-(4-YPh)-COCH}_2\text{-3}\beta\text{-4-R-Ph}$) of those that were previously tested (**Figure 5.1**).¹³

The advantage of aMD is the ability to run longer timescale simulations that will allow for more sampling of the system's degrees of freedom.^{1, 14} GaMD enhances the conformational sampling by adding a harmonic boost potential to the potential energy surface. The GaMD can be performed with a “dual-boost” to both the dihedral and total potential energetic terms following the protocol outlined by Pang *et al.*¹ The LX10 and LX11 systems can also be subjected to an additional 100 ns of GaMD using NAMD 2.11, starting from the previous coordinates that were simulated for 100 ns using classical molecular dynamics.

In the absence of a DAT co-crystal structure bound to the cocaine analogs, performing GaMD simulations of DAT bound to additional cocaine analogs will reveal details of the discrete conformational changes in DAT and the intermolecular interactions that stabilize either the outward- or inward-facing conformation of DAT (**Figure 5.1**).^{1, 13-15} Applying GaMD for enhanced sampling of DAT will aid to create an accurate reference frame for the protein-ligand systems.¹⁶⁻²¹

Additionally, the coordinates from the GaMD simulations can be used in future binding free energy calculations of cocaine, benzotropine, and the additional cocaine analogs in the DAT homology models. Performing the absolute binding free energy calculations of distinct conformations of the transporter should correlate with the experimental affinity of the inhibitors for DAT if the inhibitors can form the favorable interactions contributing to DAT affinity.²²⁻²⁶ The observed molecular interactions within the transporter can potentially lead to a class of high affinity DAT inhibitors that can bind similarly to cocaine while resulting in behavioral effects that differ from cocaine.^{15, 27}

5.2 Lead optimization of a SERT inhibitor

Performing the competitive membrane binding assay will validate the relative binding free energy calculations for modifications made SM11 (**Figure 5.2**, analogs 1-4). The calculated relative binding free energies can be compared to the experimental affinity measurements of both ligands,

$$\Delta\Delta G(L_x \rightarrow L_y) = RT \ln \left(\frac{K_i^{L_y}}{K_i^{L_x}} \right) \quad (5.1)$$

where K_i^{Lx} and K_i^{Ly} are the respective affinity measurements for each ligand to the target.

The competitive membrane-binding assay will validate the relative binding free energy calculations.

Binding interactions of SM11 can be optimized for the S2 binding site by functional group replacements. The 4-6-piperazine functional and 1,3,5-triazine-2,4-diamine groups of SM11 can be modified to probe the interactions of the ligand in the binding site (**Figure 5.2**).

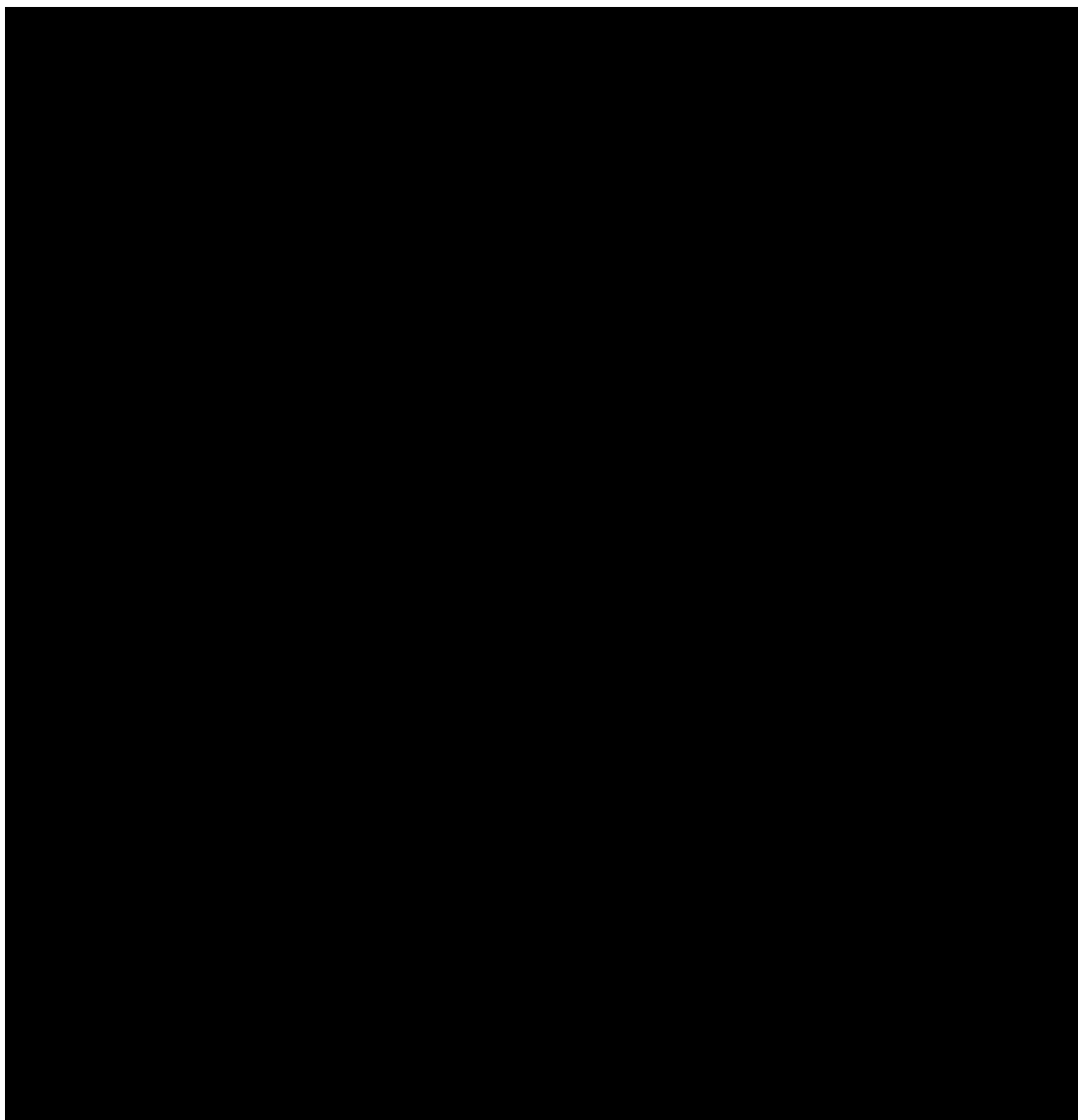


Figure 5.2: Proposed modifications to SM11 for future analogs. 1) benzene; 2) 3,4-dichloro; 3) 4-(trifluoromethyl)benzene; 4) 4-methoxybenzene; 5-6) 4-6-piperidine; 7) benzene-2,4-diamine; 8) pyrimidine-2,4-diamine; 9) pyrimidine-4,6-diamine; 10) 4-(aminomethyl)-1,3,5-triazin-2-amine.

Modifying the 6-4-piperazine (Figure 5.2, analogs 5-6). This structure contains two tertiary amines in its ring system. Only one of the two tertiary amines will be protonated and capable of ionic or ion-dipole interaction with a SERT residue. The ionized amine will be able to interact favorably with the side-chain of Glu493 and will be the most

significant interaction for the ligand binding. To determine which of the tertiary amines should be protonated upon drug binding, the two proposed analogs (5-6) will determine which would be more favorable. The first tertiary amine would be replaced with CH (5) forcing the other amine to become positively charged. Then the second amine will be replaced with CH (6), and comparison of the two binding affinities will help determine which tertiary amine is involved in the ionic interaction. This will increase the concentration of the bioactive molecule, which should result in increased potency. This will also support the ionic interaction with the Glu493 side-chain.

Modifying the 1,3,5-triazine-2,4-diamine (Figure 5.2, analogs 7-10). This structure is capable of forming several hydrogen bond interactions within the S2 binding pocket (Figure 4.5). The proposed binding pose shows that one of the two amine functional groups attached to the ring is interacting as a hydrogen bond donor to the side-chain of the Gln111 residue. This heterocyclic ring also contains π -electrons. One interaction that could occur between SM11 and SERT is the formation of cation- π interactions with the protonated side-chain of Lys490. Additionally, the side-chain of Tyr107, which also contains π -electrons, could form a π - π stacking interaction between the ring systems. A benzene substitution analog (7) could test the π -bonding interactions with these residues. The π - electrons should interact similarly to the lead compound; however, there is a loss of hydrogen bond-accepting capability with the removal of the heterocyclic nitrogen atoms. This change may result in lower binding affinity, which could indicate that one or more the nitrogen atoms are interacting as a hydrogen bond acceptor. To test

if the heterocyclic nitrogen atoms are involved in hydrogen bonding, each nitrogen atom should be replaced with a carbon atom (7-9) in separate analogs to see how binding affinity is affected. With an understanding of the structure-activity relationship of the 1,3,5-triazine-2,4-diamine ring, there is an opportunity to improve the binding of this ring system. By performing a chain extension (10) with the amine functional groups, this will introduce an ionizable functional group. In addition to the interactions that are present, there is an opportunity to introduce new interaction with the ionized side-chain of Asp328. Improved binding affinity of this analog will validate the proposed binding interactions and introduce a new favorable interaction, making SM11 a stronger inhibitor of SERT.

Once the functional groups that are key to SM11 binding in SERT have been determined, the design of new molecules can proceed to find a new candidate with improved binding interactions with SERT residues. The completion of this study will elucidate the S2 binding pocket of SERT and allow for development of new SSRIs with high affinity to inhibit the protein at the allosteric site.

5.3 References

1. Pang, Y. T., Miao, Y., Wang, Y., and Mccammon, J. A. (2016) Gaussian Accelerated Molecular Dynamics in NAMD. *J Chem Theory Comput* 13, 9-19.
2. Wang, C., Jiang, Y., Ma, J., Wu, H., Wacker, D., Katritch, V., Han, G. W., Liu, W., Huang, X. P., Vardy, E., McCorvy, J. D., Gao, X., Zhou, X. E., Melcher, K., Zhang, C., Bai, F., Yang, H., Yang, L., Jiang, H., Roth, B. L., Cherezov, V., Stevens, R. C., and Xu, H. E. (2013) Structural basis for molecular recognition at serotonin receptors. *Science* 340, 610-614.
3. Wang, H., Goehring, A., Wang, K. H., Penmatsa, A., Ressler, R., and Gouaux, E. (2013) Structural basis for action by diverse antidepressants on biogenic amine transporters. *Nature* 503, 141-145.

4. Wang, K. H., Penmatsa, A., and Gouaux, E. (2015) Neurotransmitter and psychostimulant recognition by the dopamine transporter. *Nature* 521, 322-327.
5. Andersen, J., Taboureau, O., Hansen, K. B., Olsen, L., Egebjerg, J., Stromgaard, K., and Kristensen, A. S. (2009) Location of the antidepressant binding site in the serotonin transporter: importance of Ser-438 in recognition of citalopram and tricyclic antidepressants. *J Biol Chem* 284, 10276-10284.
6. Andersen, J., Kristensen, A. S., Bang-Andersen, B., and Stromgaard, K. (2009) Recent advances in the understanding of the interaction of antidepressant drugs with serotonin and norepinephrine transporters. *Chem Commun*, 3677-3692.
7. Andersen, J., Olsen, L., Hansen, K. B., Taboureau, O., Jorgensen, F. S., Jorgensen, A. M., Bang-Andersen, B., Egebjerg, J., Stromgaard, K., and Kristensen, A. S. (2010) Mutational mapping and modeling of the binding site for (S)-citalopram in the human serotonin transporter. *J Biol Chem* 285, 2051-2063.
8. Kristensen, A. S., Andersen, J., Jorgensen, T. N., Sorensen, L., Eriksen, J., Loland, C. J., Stromgaard, K., and Gether, U. (2011) SLC6 neurotransmitter transporters: structure, function, and regulation. *Pharmacol Rev* 63, 585-640.
9. Andersen, J., Stuhr-Hansen, N., Zachariassen, L., Toubro, S., Hansen, S. M. R., Eildal, J. N. N., Bond, A. D., Bogeso, K. P., Bang-Andersen, B., Kristensen, A. S., Stromgaard, K., Bøgesø, K. P., and Strømgaard, K. (2011) Molecular determinants for selective recognition of antidepressants in the human serotonin and norepinephrine transporters. *Proc Natl Acad Sci U S A* 108, 12137-12142.
10. Sørensen, L., Andersen, J., Thomsen, M., Hansen, S. M. R., Zhao, X., Sandelin, A., Strømgaard, K., and Kristensen, A. S. (2012) Interaction of antidepressants with the serotonin and norepinephrine transporters: mutational studies of the S1 substrate binding pocket. *J Biol Chem* 287, 43694-43707.
11. Andersen, J., Stuhr-Hansen, N., Zachariassen, L. G., Koldso, H., Schiott, B., Stromgaard, K., and Kristensen, A. S. (2014) Molecular basis for selective serotonin reuptake inhibition by the antidepressant agent fluoxetine (Prozac). *Mol Pharmacol* 85, 703-714.
12. Andersen, J., Ladefoged, L. K., Wang, D., Kristensen, T. N., Bang-Andersen, B., Kristensen, A. S., Schiott, B., and Stromgaard, K. (2015) Binding of the multimodal antidepressant drug vortioxetine to the human serotonin transporter. *ACS Chem Neurosci* 6, 1892-1900.
13. Hong, W. C., Kopajtic, T. A., Xu, L., Lomenzo, S. A., Jean, B., Madura, J. D., Surratt, C. K., Trudell, M. L., and Katz, J. L. (2016) 2-Substituted 3 β -Aryltropane Cocaine Analogs Produce Atypical DAT Inhibitor Effects Without Inducing Inward-Facing DAT Conformations. *J Pharmacol Exp Ther*, 624-634.

14. Miao, Y., Feher, V. A., and McCammon, J. A. (2015) Gaussian Accelerated Molecular Dynamics: Unconstrained Enhanced Sampling and Free Energy Calculation. *J Chem Theory Comput* 11, 3584-3595.
15. Reith, M. E., Blough, B. E., Hong, W. C., Jones, K. T., Schmitt, K. C., Baumann, M. H., Partilla, J. S., Rothman, R. B., and Katz, J. L. (2015) Behavioral, biological, and chemical perspectives on atypical agents targeting the dopamine transporter. *Drug Alcohol Depend* 147, 1-19.
16. Wang, J., Deng, Y., and Roux, B. (2006) Absolute binding free energy calculations using molecular dynamics simulations with restraining potentials. *Biophys J* 91, 2798-2814.
17. Koldso, H., Autzen, H. E., Grouleff, J., and Schiott, B. (2013) Ligand induced conformational changes of the human serotonin transporter revealed by molecular dynamics simulations. *PLoS One* 8, e63635.
18. Koldso, H., Noer, P., Grouleff, J., Autzen, H. E., Sinning, S., and Schiott, B. (2011) Unbiased simulations reveal the inward-facing conformation of the human serotonin transporter and Na(+) ion release. *PLoS Comput Biol* 7, e1002246.
19. General, I. J., Dragomirova, R., and Meirovitch, H. (2012) Absolute free energy of binding of avidin/biotin, revisited. *J Phys Chem B* 116, 6628-6636.
20. General, I. J., Dragomirova, R., and Meirovitch, H. (2011) Calculation of the Absolute Free Energy of Binding and Related Entropies with the HSMD-TI Method: The FKBP12-L8 Complex. *J Chem Theory Comput* 7, 4196-4207.
21. Ho, B. K., and Agard, D. a. (2009) Probing the flexibility of large conformational changes in protein structures through local perturbations. *PLoS Comput Biol* 5, e1000343.
22. Miyamoto, S., and Kollman, P. A. (1993) Absolute and relative binding free energy calculations of the interaction of biotin and its analogs with streptavidin using molecular dynamics/free energy perturbation approaches. *Proteins* 16, 226-245.
23. Jorgensen, A. M., Tagmose, L., Jorgensen, A. M., Bogeso, K. P., and Peters, G. H. (2007) Molecular dynamics simulations of Na+/Cl(-)-dependent neurotransmitter transporters in a membrane-aqueous system. *ChemMedChem* 2, 827-840.
24. Jorgensen, A. M., Tagmose, L., Jorgensen, A. M., Topiol, S., Sabio, M., Gundertofte, K., Bogeso, K. P., and Peters, G. H. (2007) Homology modeling of the serotonin transporter: insights into the primary escitalopram-binding site. *ChemMedChem* 2, 815-826.

25. Jorgensen, W. L. (1989) Free energy calculations: a breakthrough for modeling organic chemistry in solution. *Acc Chem Res* 22, 184-189.
26. Gumbart, J. C., Roux, B., and Chipot, C. (2013) Standard binding free energies from computer simulations: What is the best strategy? *J Chem Theory Comput* 9, 794-802.
27. Rudnick, G., Kramer, R., Blakely, R. D., Murphy, D. L., and Verrey, F. (2014) The SLC6 transporters: perspectives on structure, functions, regulation, and models for transporter dysfunction. *Pflugers Arch* 466, 25-42.